

## **Copyright Warning & Restrictions**

The copyright law of the United States (Title 17, United States Code) governs the making of photocopies or other reproductions of copyrighted material.

Under certain conditions specified in the law, libraries and archives are authorized to furnish a photocopy or other reproduction. One of these specified conditions is that the photocopy or reproduction is not to be “used for any purpose other than private study, scholarship, or research.” If a user makes a request for, or later uses, a photocopy or reproduction for purposes in excess of “fair use” that user may be liable for copyright infringement,

This institution reserves the right to refuse to accept a copying order if, in its judgment, fulfillment of the order would involve violation of copyright law.

**Please Note: The author retains the copyright while the New Jersey Institute of Technology reserves the right to distribute this thesis or dissertation**

Printing note: If you do not wish to print this page, then select “Pages from: first page # to: last page #” on the print dialog screen

The Van Houten library has removed some of the personal information and all signatures from the approval page and biographical sketches of theses and dissertations in order to protect the identity of NJIT graduates and faculty.

## **ABSTRACT**

### **FEASIBILITY STUDY OF ROTATING FLUIDIZED BED AS A DRY COATER AND A GRANULATOR**

**by  
Manish Sawhney**

This study is directed at enhancing our understanding of the mechanism of dry coating and granulation in a rotating fluidized bed (RFB). The main objective was to study the feasibility of the coating and granulation processes using an RFB, both quantitatively and qualitatively.

A force balance and kinetic model is applied to explain the coating phenomenon and also to investigate why coating takes place in certain particle material systems and not in others. An equation for the resultant velocity with which one particle collides with another has been suggested for the rotating fluidized bed coater. A condition, which predicts whether the colliding particles will stick together, has also been suggested. Experiments show that coating occurs with some host particles while it does not occur with others, in agreement with theoretical analysis.

It has been observed that Geldart Group C particles do not deagglomerate in the rotating fluidized bed. Thus it is assumed that they will collide with the host particle or with themselves to form larger agglomerates. However, experimental observations show a uniform and a fairly good quality of coating, which indicates that the agglomerated particles redistribute after sticking on to a host.

In the granulation studies, the method for binderless granulation using a conventional fluidized bed has been established. A rotating fluidized bed, in principle, operates on the same concept, except that during the forward gas flow, i.e., the fluidization phase, a higher gas throughput is achieved because of higher  $g$  due to the centrifugal force. This should result in better adherence between particles and formation of granules. The reverse flow rate will have no impact on the granulation since the reverse flow rate depends only on supply pressure but will aid in compaction. Hence, the strength of the agglomerate should be the same as that achieved with a conventional fluidized bed granulator using pressure swing.



**FEASIBILITY STUDY OF ROTATING FLUIDIZED BED  
AS A COATER AND A GRANULATOR**

by  
**Manish Sawhney**

**A Masters Thesis  
Submitted to the Faculty of  
New Jersey Institute of Technology  
in Partial Fulfillment of the Requirements for the Degree of  
Master of Science in Chemical Engineering**

**Department of Chemical Engineering, Chemistry and Environmental Science**

**May 2000**

## **APPROVAL PAGE**

### **FEASIBILITY STUDY OF ROTATING FLUIDIZED BED AS A COATER AND A GRANULATOR**

**Manish Sawhney**

---

|  |      |
|--|------|
| Dr. Robert Pfeffer, Thesis Advisor<br>Distinguished Professor, Dept. of Chemical Engineering, NJIT | Date |
|--|------|

---

|   |      |
|---|------|
| Dr. Rajesh Dave, Committee Member<br>Professor, Dept. of Mechanical Engineering, NJIT | Date |
|---|------|

---

|  |      |
|--|------|
| Dr. Henry Shaw, Committee Member<br>Professor, Dept. of Chemical Engineering, NJIT | Date |
|--|------|

## **BIOGRAPHICAL SKETCH**

**Author:** Manish Sawhney  
**Degree:** Master of Science in Chemical Engineering  
**Major:** Chemical Engineering  
**Date:** May 2000

### **Undergraduate and Graduate Education:**

- Master of Science in Chemical Engineering,  
New Jersey Institute of Technology, Newark, NJ, 2000
- Bachelor of Science in Chemical Engineering,  
Panjab University, Chandigarh, India, 1995.

This thesis is dedicated to my beloved mother  
for her love and encouragement to pursue my studies.

## **ACKNOWLEDGMENT**

I start by expressing my sincere appreciation to my advisor, Dr. Robert Pfeffer for his dedication, patience, and wisdom throughout the length of this study and the preparation of this thesis, and without whose guidance this research would not have been possible. I am grateful to Dr. Rajesh Dave, for his inspirational and timely support, technical expertise, and acuity throughout the duration of the project. I am also grateful to Dr. Henry Shaw, who agreed to serve as my committee member.

I deeply appreciate the technical and active support given to me by Dr. Doug Wei who became a good friend during the course of this study. I would also like to thank my fellow students Ajit Mujumdar, Bodhisattwa Chaudhari, Wengliang Chen and Yulu Wang for their continuing support and constructive criticism. A special mention has to be made to Michelle Ramlakhan for all her help and guidance during this project and Gui-Hua Qian for his expertise in the field of rotating fluidized beds. I am also thankful to William Dunphy and Joseph Glaz, who built this equipment, which helped me finish my thesis. And last of all, I thank Dr. Moinuddin Malik and my friends for their support in various ways during this project.

## TABLE OF CONTENTS

| Chapter   | Page |
|---|------|
| 1 INTRODUCTION .....  | 1    |
| 1.1. Wet Processes .....                                    | 2    |
| 1.1.1 Wet Coater .....                                      | 2    |
| 1.1.2 Wet Granulation.....                                  | 3    |
| 1.2 Dry Processes.....                                      | 4    |
| 1.1.1 Dry coating.....                                      | 4    |
| 1.1.2 Dry Granulation .....                                 | 4    |
| 1.3 Objective of the Thesis.....                            | 5    |
| 1.4 Organization of the Thesis .....                        | 5    |
| 2 BACKGROUND STUDIES .....                                  | 6    |
| 2.1 History of Fluidization .....                           | 7    |
| 2.2 Fluidization .....                                      | 8    |
| 2.2.1 Fluidization Regimes .....                            | 8    |
| 2.2.2 Classification of Fluidized Powder .....              | 11   |
| 2.2.3 Predicting Bed Voidage .....                          | 13   |
| 2.3 Different type of Fluidized Bed .....                   | 14   |
| 2.3.1 Dense Phase Fluidized Bed.....                        | 14   |
| 2.3.2 Tumbling Fluidized Bed .....                          | 17   |
| 2.3.3 Spouted Fluidized Bed.....                            | 18   |
| 2.3.4 Rotating Fluidized Bed .....                          | 19   |
| 2.4. Inter-Particle Forces in a Rotating Fluidized Bed..... | 20   |

## TABLE OF CONTENTS (Continued)

| Chapter  | Page   |
|--|--------|
| 2.5. Particle-Particle Interaction in Rotating Fluidized Bed.....                              | 27     |
| 2.6. Kinetics Considerations in Particle Interaction .....                                     | 31     |
| 2.7 Conclusion of Chapter 2.....   | 36     |
| <br>3 EXPERIMENTAL APPROACH SETUP AND PROCEDURE .....  | <br>38 |
| 3.1 Theoretical Analysis of Rotating Fluidized Bed .....                                       | 39     |
| 3.1.1 Theoretical Model.....   | 39     |
| 3.1.2 Graphical representation of Pressure Drop Using Theoretical Model.....                   | 41     |
| 3.2 Apparatus .....  | 43     |
| 3.2.1 Coating Experimental System.....   | 43     |
| 3.2.2 Granulation Experimental System .....  | 47     |
| 3.1 Experimental Procedure.....  | 49     |
| 3.3.2 Coating Experimental Procedure .....   | 50     |
| 3.3.1 Granulation Experimental Procedure.....  | 50     |
| 3.2 Methods to Analyze Coating And Granulation .....   | 51     |
| 3.4.1 Quantitative Analysis For Coating and Granulation- Scanning Electron<br>Microscopy ..... | 51     |
| 3.4.2 Quantitative Analysis for Coating- Ultrasonication .....                                 | 52     |
| 3.4.3 Quantitative Analysis for Coating- Moisture Sorption.....                                | 52     |
| 3.4.4 Quantitative Analysis for Granulation- Size Analysis.....                                | 52     |
| <br>4 RESULTS AND DISCUSSIONS.....   | <br>53 |

## TABLE OF CONTENTS (Continued)

| Chapter   | Page   |
|---|--------|
| 4.1 Discussion of Fluidized State.....                        | 53     |
| 4.1.1 Packed Bed Region .....                                 | 53     |
| 4.1.2 Fluidized Bed Region.....                               | 54     |
| 4.2 Discussion of Rotating Fluidized Bed as a Coater.....     | 60     |
| 4.3 Discussion of Rotating Fluidized bed as a Granulator..... | 76     |
| 5 CONCLUSIONS AND RECOMMENDATIONS FOR FUTURE RESEARCH .....   | 79     |
| 5.1 Conclusions.....  | 79     |
| 5.2 Recommendations for Future Research .....                 | 81     |
| <br><b>Appendix</b>   |        |
| 1 PROGRAM TO COMPUTE THE MINIMUM FLUIDIZATION VELOCITY .....  | 82     |
| 2 PHYSICAL PROPERTIES OF POWDERS .....                        | 88     |
| 3 SAMPLE CALCULATION .....                                    | 89     |
| 4 COATING CRITERIA .....                                      | 94     |
| <br>REFERENCES .....  | <br>97 |



## LIST OF TABLES

| Table   | Page |
|---|------|
| 2.1 Summary of Geldart Group Properties .....   | 12   |
| 2.2 Voidage Vs Sphericity for randomly packed bed and uniformly sized particles<br>larger than 500 microns .....                                | 13   |
| 2.3 Variation of packed bed voidage with particle size for loosely packed spheres ...   | 14   |
| 2.4 Effect of size distribution on packed bed voidage .....   | 14   |
| 4.1 Various forces and energies involved in the collision of host and guest particles<br>during PMMA/Alumina coating.....                       | 73   |
| 4.2 Various forces and energies involved in the collision of guest with another guest<br>particle during PMMA/Alumina coating.....              | 73   |
| 4.3 Various forces and energies involved in the collision of host and guest particles<br>during Fibrous Cellulose/Alumina coating.....          | 74   |
| 4.4 Various forces and energies involved in the collision of guest with another guest<br>particle during Fibrous Cellulose/Alumina coating..... | 74   |
| 4.5 Interpretation of plots of coating criteria versus impact velocity .....  | 75   |
| A1 Physical properties for PMMA, Fibrous Cellulose, Spherical Cellulose, Alumina<br>and Air .....   | 88   |

## LIST OF FIGURES

| Figure  | Page |
|---|------|
| 2.1 Various flow regimes or patterns in dense phase fluidization a) Particulate fluidization b) Bubbling fluidization c) Turbulent fluidization d) Slugging e) Spouting f) Channeling.....  | 10   |
| 2.2 Geldart classification chart of powder .....  | 11   |
| 2.3 Schematic diagram of dense phase fluidized bed .....  | 15   |
| 2.4 Schematic diagram of circulating fluidized bed .....  | 16   |
| 2.5 Schematic diagram of tumbling fluidized bed .....   | 17   |
| 2.6 Schematic diagram of spouted bed .....  | 18   |
| 2.7 Schematic diagram of rotating fluidized bed .....   | 19   |
| 2.8 The influence of surface roughness and geometrical factors on the interaction forces.....   | 22   |
| 2.9 Collision of guest agglomerate and host particle and the redistribution of guest between host particles .....   | 28   |
| 2.10 a) Collision of host with guest particles loosely attached to host particle b) Separated guest gaining momentum, colliding with host and getting coated onto it c) The increase in the size of the agglomerate.....  | 29   |
| 2.11 a) Small agglomerate of Group C particles getting compacted to form a big weak agglomerate b) Attrition of agglomerate during fluidization phase c) Further compaction of agglomerate to form strong agglomerate d) Trimming of agglomerate to form strong agglomerate ..... | 31   |

## LIST OF FIGURES (Continued)

| Figure  | Page |
|---|------|
| 2.12 Various forces, which act on approaching particle during the coating process .....   | 32   |
| 2.13 Resultant momentum with which one particle impact the other particle.....  | 32   |
| 2.14 Criteria for coating to take place.....  | 36   |
| 3.1 Plot of pressure drop versus superficial velocity for cellulose at 100 rpm .....  | 41   |
| 3.2 The schematic diagram of experimental setup of rotating fluidized bed when used<br>as a coater.....   | 43   |
| 3.3 The photographic image of rotating fluidized bed coater .....   | 44   |
| 3.4 Experimental pressure drop versus superficial velocity for slotted distributor .....  | 46   |
| 3.5 Experimental pressure drop versus superficial velocity for a distributor made from<br>sintered metal .....  | 47   |
| 3.6 The schematic diagram of experimental setup of rotating fluidized bed when used<br>as a granulator .....  | 48   |
| 4.1 Plot of pressure drop versus superficial velocity for fibrous microcrystalline<br>cellulose at 800 rpm .....  | 57   |
| 4.2 Plot of pressure drop versus superficial velocity for PMMA at 800 rpm .....   | 57   |
| 4.3 Plot of pressure drop versus superficial velocity for glass beads at 800 rpm .....  | 58   |
| 4.4 Plot of pressure drop versus superficial velocity for fibrous spherical cellulose at<br>800 rpm .....   | 58   |
| 4.5 The relative effect of gravitational force on the particles at the top and bottom of<br>the rotating RFB resulting in the difference in the pressure drop ..... | 59   |

## LIST OF FIGURES (Continued)

| Figure   | Page |
|--|------|
| 4.6 The non-uniform distribution of powders along the axis resulting in the difference in the experimental and theoretical pressure drop ..... | 59   |
| 4.7.1 Uncoated PMMA .....  | 61   |
| 4.7.2 PMMA/Alumina coating at 1500 rpm before ultra-sonication.....  | 61   |
| 4.7.3 Aluminum EDX mapping of RFBC coated alumina at 1500 rpm.....   | 61   |
| 4.7.4 PMMA/Alumina coating at 800 rpm before ultra-sonication.....   | 62   |
| 4.7.5 Aluminum EDX mapping of RFBC coated alumina at 800 rpm.....  | 62   |
| 4.7.6 PMMA/Alumina coating at 1500 rpm after ultra-sonication.....   | 62   |
| 4.8 PMMA/Silica coating .....  | 63   |
| 4.9.1 Uncoated spherical cellulose.....  | 63   |
| 4.9.2 Spherical cellulose/Alumina coating at 1200 rpm before ultra-sonication.....   | 64   |
| 4.9.3 Aluminum EDX mapping of spherical cellulose coating alumina at 1200 rpm ....   | 64   |
| 4.9.4 Spherical cellulose/Alumina coating at 1200 rpm after ultra-sonication.....  | 64   |
| 4.10.1 Uncoated fibrous cellulose.....   | 65   |
| 4.10.2 Fibrous cellulose/Alumina coating at 1500 rpm before ultra-sonication.....  | 65   |
| 4.10.3 Aluminum EDX mapping of fibrous cellulose coating alumina at 1500 rpm .....   | 65   |
| 4.11.1 SEM showing a wide view of coated cellulose with agglomerates of alumina sitting with cellulose .....                                   | 66   |
| 4.11.2 Agglomerates of alumina of size 80 $\mu\text{m}$ .....  | 66   |
| 4.11.3 Aluminum EDX mapping of agglomerated alumina proving the 80 $\mu\text{m}$ particles are of alumina .....                                | 66   |

## LIST OF FIGURES (Continued)

| Figure   | Page |
|--|------|
| 4.11.4 Agglomerates of alumina of size 50 $\mu\text{m}$ .....  | 67   |
| 4.11.5 Aluminum EDX mapping of agglomerated alumina sitting along with the coated cellulose .....  | 67   |
| 4.12 Absorption Isotherms for fibrous cellulose-alumina Coating.....   | 67   |
| 4.13 Absorption Isotherm for spherical cellulose-alumina Coating .....   | 68   |
| 4.14.1 Agglomerates of 10 nm size alumina before running in RFBG .....   | 77   |
| 4.14.2 Granulates of 10 nm size alumina formed after running in RFBG.....  | 77   |
| 4.14.3 Picture showing a single granulate of 10 nm size alumina formed after running in alumina.....   | 78   |
| 4.14.4 Picture showing particles of 25 $\mu\text{m}$ size alumina before running in RFBG.....  | 78   |
| 4.14.5 Picture showing particles of 25 $\mu\text{m}$ size alumina after running in RFBG, with one granulate also present.....  | 78   |
| A1 Plot of difference in Adhesion Energy and Rebound Energy Vs Agglomerate Size for PMMA particles .....   | 94   |
| A2 Plot of difference in Adhesion and Rebound Energy versus the Agglomerate Size for Fibrous Cellulose.....  | 94   |
| A3 Plot of difference in Adhesion Energy and Rebound Energy Vs Impact Velocity for PMMA-Alumina agglomerate of agglomerate sizes 10 $\mu\text{m}$ and 20 $\mu\text{m}$ ..... | 95   |
| A4 Plot of difference in Adhesion Energy and Rebound Energy Vs Impact Velocity for Fibrous Cellulose-Alumina agglomerate of agglomerate size 1 $\mu\text{m}$ .....           | 95   |

## LIST OF FIGURES (Continued)

| Figure  | Page |
|---|------|
| A5 Plot of difference in Adhesion Energy and Rebound Energy Vs Impact Velocity for Fibrous Cellulose-Alumina agglomerate of agglomerate sizes 5 $\mu\text{m}$ , 10 $\mu\text{m}$ and 20 $\mu\text{m}$ ..... | 96   |
| A6 Plot of difference in Adhesion Energy and Rebound Energy as a function of Yield limit, Hamaker Constant and Young's Modulus .....  | 96   |

## LIST OF SYMBOLS

|             |   |   |
|-------------|---|---|
| $F_v$       | = | van der Waal force (N)  |
| $F_e$       | = | Electrostatic force (N)                                       |
| $F_c$       | = | Collision force (N)   |
| $F_y$       | = | Drag force (N)  |
| $F_g$       | = | Centrifugal force (N)   |
| $F_H$       | = | Capillary force (N)   |
| $F_I$       | = | Impact force (N)  |
| $Q_I$       | = | Impact energy (J)   |
| $Q_p$       | = | Plastic deformation energy (J)                                |
| $Q_A$       | = | Total adhesive energy (J)                                     |
| $U_M$       | = | Mechanical energy (J)   |
| $U_S$       | = | Surface energy (J)  |
| $N$         | = | External load on the interacting particle (N)                 |
| $Q$         | = | Charge of the particle (C)                                    |
| $q_1$       | = | Charge of particle 1 (C)                                      |
| $q_2$       | = | Charge of particle 1 (C)                                      |
| $H$         | = | Separation distance between charge and uncharged particle (m) |
| $m_1$       | = | Mass of particle 1 (kg)                                       |
| $m_2$       | = | Mass of particle 1 (kg)                                       |
| $V$         | = | Volume of powder in the bed (m <sup>3</sup> )                 |
| $P_0$       | = | External load applied on the particle (N)                     |
| $A, A_{12}$ | = | Hamaker constant (J)  |

## LIST OF SYMBOLS (Continued)

|            |   |   |
|------------|---|---|
| $v$        | = | Impact velocity (m/s)                                       |
| $r$        | = | Radius of distributor or radial co-ordinate (m)             |
| $r_0$      | = | Outer radius of the powder bed (m)                          |
| $r_i$      | = | Inner radius of the packed bed (m)                          |
| $r_{pf}$   | = | Radius of the interface of fluidized bed and packed bed (m) |
| $l$        | = | length of the distributor (m)                               |
| $s$        | = | Distance between two species (m)                            |
| $T$        | = | Radius of particle on which forces are acting (m)           |
| $V$        | = | Relative velocity of the between two particles (m/sec)      |
| $R$        | = | Radius of the particle                                      |
| $d_1$      | = | Diameter of the colliding particle 1 (m)                    |
| $d_2$      | = | Diameter of the colliding particle 2 (m)                    |
| $d_g$      | = | Granular diameter (m)                                       |
| $D_b$      | = | Bubble diameter (m)   |
| $E$        | = | Young's modulus of elasticity (MPa)                         |
| $y$        | = | Elastic yield limit (MPa)                                   |
| $Re$       | = | Reynolds number   |
| $Ga$       | = | Galileo number  |
| $N$        | = | Rotating speed (rpm)  |
| $F$        | = | Pressure drop factor  |
| $L$        | = | Bed thickness (m)   |
| $\Delta P$ | = | Total pressure drop across the bed (Pa)                     |



## LIST OF SYMBOLS (Continued)

|                |   |  |
|----------------|---|--|
| $\Delta P_f$   | = | Pressure drop across the fluidized bed region (Pa)       |
| $\Delta P_p$   | = | Pressure drop across the packed bed region (Pa)          |
| $U_{avg}$      | = | Average minimum fluidization velocity (m/s)              |
| $U_{mfs}$      | = | Surface minimum fluidization velocity (m/s)              |
| $U_{mf}$       | = | Critical minimum fluidization velocity (m/s)             |
| $U_o, u_o, u$  | = | Superficial gas velocity (m/s).                          |
| $\omega$       | = | Angular velocity (rad/s).                                |
| $\varepsilon$  | = | Voidage or void fraction                                 |
| $\rho_p$       | = | Particle density or granule density (kg/m <sup>3</sup> ) |
| $\rho_g$       | = | Bulk density (kg/m <sup>3</sup> )                        |
| $\rho_f$       | = | Fluidization gas density (kg/m <sup>3</sup> )            |
| $\rho$         | = | Density of particle colliding (kg/m <sup>3</sup> )       |
| $\mu$          | = | Fluidization gas viscosity in (kg/m-s)                   |
| $\phi_s$       | = | Sphericity   |
| $\varphi$      | = | Limiting velocity (m/s)                                  |
| $\alpha$       | = | Displacement of maximum compression coefficient          |
| $\nu$          | = | Poisson ratio  |
| $\gamma$       | = | Surface tension  |
| $\Delta\gamma$ | = | Surface adhesive energy (J/m <sup>3</sup> )              |
| $\sigma$       | = | Size spread (m)  |

# **CHAPTER 1**

## **INTRODUCTION**

Engineered particulates are the norm of the day. Particulates tailored to need are important in many industrial applications. Two such types are "composite particles" and "granulates". Composite particles are obtained when one type of particle is coated onto another type. The particles being coated are referred to as guest particles and adhere to the surface of larger particles, referred to as host particles. Granulates are obtained when similar particles collide with each other to form large particles called agglomerates. Various inter-particle forces such as van der Waals, electrostatic and capillary forces are involved in adhesion of one particle to the surface of another particle. In actual applications the size of the particles also plays an important role. For example, in coating applications the ratio of the size of the host to guest particles is at least 10: 1 for good results. In granulation applications, nano-size particles exist only as agglomerates and are most difficult to granulate.

Engineered particulates have applications in various industries, which include pharmaceuticals, ceramics, food and agricultural products. For application in these industries we have to incorporate properties suitable to the need of the application such as enhanced flowability, wettability, conductivity, higher or lower sintering temperature or easy handling, etc. This is achieved by either coating a particle with suitable properties on to the core or host particle or changing the size of the particle. The product obtained is

engineered specific to the need of the application. Thus engineered particulates are very important and present a revolutionary concept and should have a major impact on the field of particle technology [11].

Engineered particulates can be accomplished by both dry and wet processes. Both dry and wet processes are described briefly below while dry processes are dealt with in detail later.

## **1.1 Wet Processes**

### **1.1.1 Wet Coating**

A wet coating process involves adding a liquid forming a suspension or solubilizing the small guest particles. In a conventional process, the host to be coated is first dispersed in a fluid medium, and the guest particles also dispersed in liquid are added where they are precipitated onto the surface of the host particles. The forces involved here are capillary, electrostatic and van der Waals forces. Binders can be used to improve the adherence of guest to host. [11].

In a fluidized bed wet process, the coating material usually consists of a polymeric binder, solvents (organic or water) and pigments. Here the host/guest particles or host alone forms the fluidized bed and air or guest dispersed in air is used to fluidize the bed. Binders or solvents are sprayed into the medium to enhance the coating efficiency. To

avoid the use of organic solvents in coating processes, some investigators [11] proposed the use of supercritical fluids as a substitute to fast-evaporating solvents to minimize harmful environmental effects. The use of supercritical coating is still in its infancy. Dry coating is an excellent solution to the above problem; it is expected to be environmental friendly and cost effective.

### 1.1.2 Wet Granulation

Wet Granulation of powders is widely used as an industrial process to engineer the size of powders. Granulation is done to improve the flow properties and reduce dust formation. Agglomerates can form in two types of processes: forming type processes such as a pellet mill, roll compaction and tableting. In this process, individual properties of particles such as size, shape, composition, density are carefully controlled. The second type is bulk material type processing such as high shear granulation, fluid bed granulation and prilling. In all the wet granulation processes, liquid is added or sprayed onto a moving bed of particles and thus the liquid forms a bridge between the particles. A binder compound can be dissolved in the spraying liquid or premixed in the powder bed. As a result of evaporation of the binder, liquid bridges solidify between particles. Due to rupture forces in the apparatus, the bond between particles may be broken. The growth rate of particles depends upon the rate of bond formation and bond rupture, which is dependent on the amount of binder used for the granulation.

## **1.2. Dry Processes**

### **1.2.1 Dry Coating**

Dry coating has received much attention because it is ecological and requires no binder or solvent. In a dry method, the particles are subjected to a mixture of large shear and compressive stress or impact forces. Dry coating of fine particles (guest) onto large particles (host) by various methods is presently investigated as an alternative solution to solvent-based processes. The dry coating method being studied are mechanofusion, hybridizer, theta composer and MAIC (Mechanically assisted impaction coating) and fluidized bed- sprouted and rotating. The process of dry coating is dealt with in detail in Chapter 3 and 4.

### **1.2.2 Dry Granulation**

To date, in most granulation processes binders are used to generate cohesiveness to agglomerate particles. Binders will definitely have an effect on granule properties. For example granules with higher binder content are stronger and harder to break and consequently require higher compaction pressure to break or form them. Nishii et al [17] has made some progress with binderless granulation in fluidized bed by pressure swing granulation, cyclic fluidization and gas flow compaction. The dry granulation process is described in detail in chapter 5.

### **1.3 Objective of the Thesis**

The objective of this research is to study the feasibility of a rotating fluidized bed as a dry coating device and adding pressure swing to produce granulation. Dry coating technique was examined by using different host/guest particles such as PMMA/ALUMINA, CELLULOSE/ALUMINA and PMMA/SILICA. Properties such as moisture absorption were examined to evaluate the feasibility and SEM-EDX for characterization. A force and kinetic model is suggested for the coating phenomenon, which is examined in the light of observation based on SEM-EDX characterization. The dry granulation technique was examined using Alumina and Titanium dioxide as the powder medium to be granulated.

### **1.4 Organization of the Thesis**

A brief account of the main topics of this thesis is given in this chapter. In Chapter 2, we discuss fluidization and various types of fluidized beds with emphasis on the mechanism involved in fluidization of powders in a rotating fluidized bed. We also provide an overview of inter-particulate forces and how these forces act on particles in a rotating fluidized bed. In chapter 3, we present our theoretical analysis of the RFB, the experimental setup and procedure for both coating and granulation experiments. We also attempt to explain the fluidized state in a rotating fluidized bed. In chapter 4, we present the experimental results and provide an interpretation of these results. In Chapter 5, we present the conclusions of this work and make recommendations for future research.

## CHAPTER 2

### BACKGROUND STUDIES

Fluidized beds have been around for a long time and have been found advantageous as gas solid reactors, dust filters, dryers etc. The basic components required for a gas fluidized bed consist of a vessel, gas source, powder, and distributor. The provision of other elements depends on the particular application at hand. As a result, there are many types of fluidized beds encountered in commercial operations. The rotating fluidized bed (RFB) is an extension of fluidized bed technology in which a fluidized bed operates against centrifugal force instead of normal gravitational force, and uses a cylindrical distributor instead of a flat distributor. RFB's are used when high gas throughput is required, since in a conventional fluidized bed, a very large cross-sectional area is required to maintain a high gas throughput. A rotating fluidized bed seems to be promising in many industrial applications and engineered particulate matter is one such application. The offshoot of this application is engineered composites (dry particle coating) and granulates.

In this chapter, we discuss fluidization regimes and forces acting on particles in a fluidized bed. In particular, we try to gather information on the various studies done using a rotating fluidized bed, and what can

possibly be achieved with rotating fluidized bed in future. We also discuss inter-particle forces and how they affect the fluidization and coating and granulation processes that we want to achieve. We would also like to discuss what we mean by good or poor coating quality. A brief account of other type of processes, which are used for coating and granulation purposes is also given.

### **2.1. History of Fluidization**

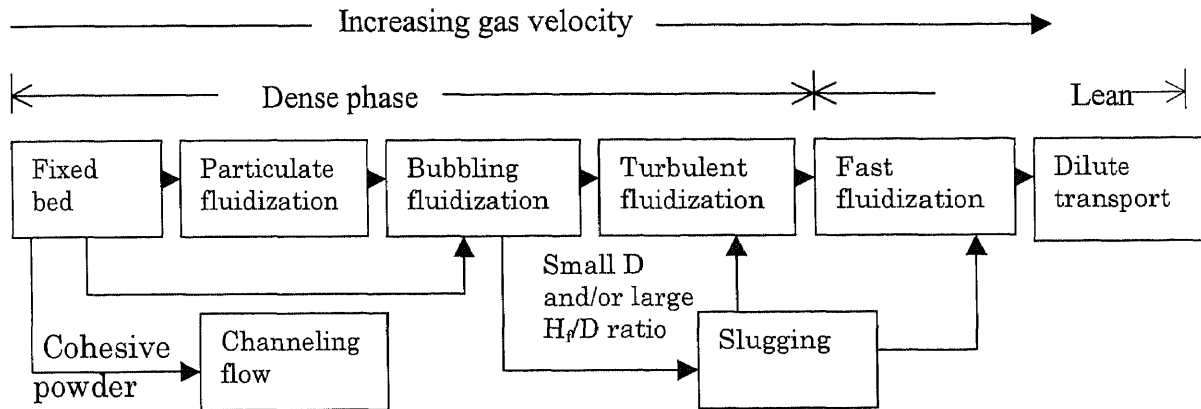
The first commercial use of a fluidized bed was in 1926 for the gasification of coal, but it was only in the early 1940's that its widespread use began with the construction of the fluidized bed catalytic cracker (FCC). In the late 1940's, the Dorr Oliver Company used the fluidized bed to roast sulfide ores. Fluidized bed dryers were successfully developed in 1950's. The Sohio process for making acrylonitrile in a fluidized bed was highly successful and therefore since 1960 virtually all acrylonitrile plants have used fluidized beds. In the late 1970's fluidized bed were used by Union Carbide for the synthesis of polyethylene, which ensured the demise of all its competitors. In the 1970's and 1980's fluidized bed combustion attracted much attention due to its relatively low temperature operation (800 – 900°C) and its ability to absorb SO<sub>2</sub> through the use of limestone and dolomite. The history of fluidization contains examples of processes which were built but never used commercially or used only for a very short period of time. Examples of processes that did not progress beyond the pilot plant scale include ethylene oxide production and ethanol dehydration [6].



## 2.2 Fluidization

### 2.2.1. Fluidization Regimes:

Fluidization regime classification is shown in the diagram below:



The diagram above shows the interrelationship between dense phase fluidization and lean phase fluidization. The dense phase is distinguished from the lean phase, since in the dense phase the bubbles and the upper surface of bed is distinguishable. But as the gas velocity increases, the void/bubble become indistinguishable and the particle entrainment rate suddenly increases. This is called lean phase fluidization.

The fundamental distinction between regimes and condition of operation is described below and shown schematically in Figure 2.1.

- 1) **Particulate fluidization:** This regime is bounded by the minimum fluidization and minimum bubbling velocity and all the gas passes through the interstitial spaces without forming bubbles. This regime exists in a bed with only Geldart Group A particles [7] and in a very narrow operating range.

- 2) **Bubbling fluidization:** Bubbling fluidization is achieved when the gas velocity is increased beyond the bubbling velocity. Bubbles form and induce vigorous motion of the particles. In the bubbling regime particle coalescence and breakup takes place, which is enhanced by increasing gas velocity and hence two distinct phases- bubble and emulsion phases are present.
- 3) **Turbulent fluidization regime:** When the gas velocity is increased beyond the bubbling fluidization regime, it is difficult to distinguish between the bubble and emulsion phase. The suspension is more uniform and bubble breakup is enhanced as the gas velocity is increased and turbulent fluidization is achieved.
- 4) **Slugging:** Bubbles or slugs characterize this regime whose sizes are comparable to the bed diameter. This occurs only in beds with small diameter or large height/diameter ratio. It is formed by the coalescence of bubbles. When the gas velocity is increased, the slugging regime turns into the turbulent or fast fluidization regime.
- 5) **Spouting:** Spouting occurs when the gas is injected at a high velocity through a small opening into the bed containing typically Geldart Group D particles. At the center of the bed, the gas penetrates the whole bed and carries some particles upward thus forming a dilute flow core region. Particles reaching the top move to the dense region between the core and the wall and particles in the annular region move downward in a moving bed mode and recirculate to the core region forming a solid circulatory pattern. Thus particle mixing in the spouted regime is more regular and cyclic than in the turbulent or bubbling regime.

- 6) **Channeling:** As shown in the Figure 2.1, channeling is due to aggregation effects of the cohesive particles. Group C particles, due to inter-particle contact forces, remain as aggregates and do not fluidize in a conventional fluidized bed.

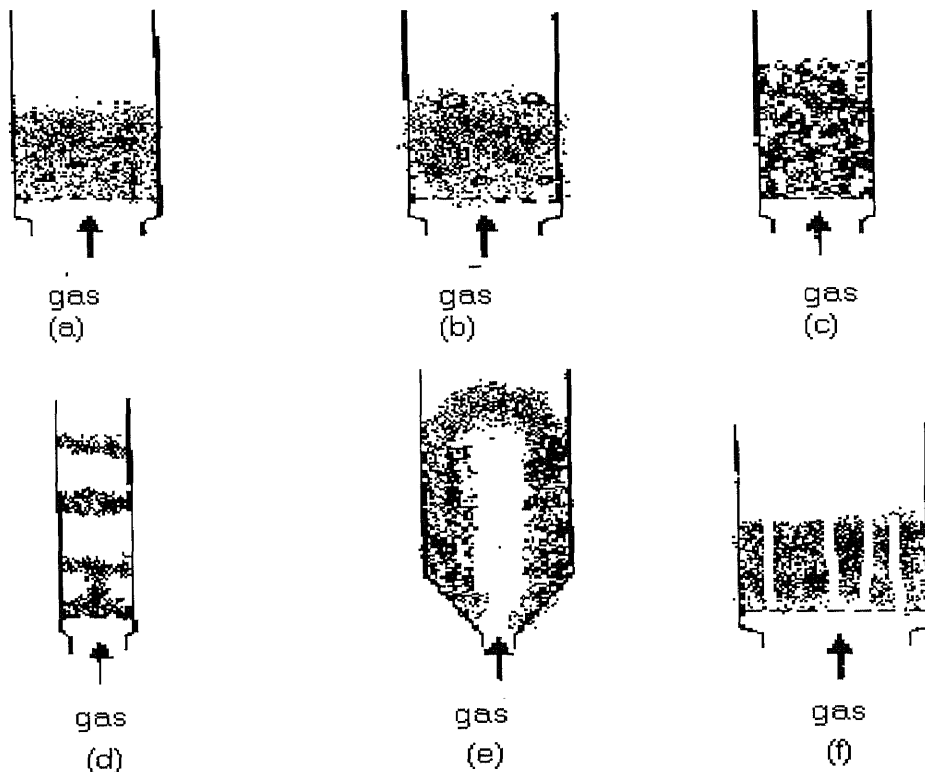


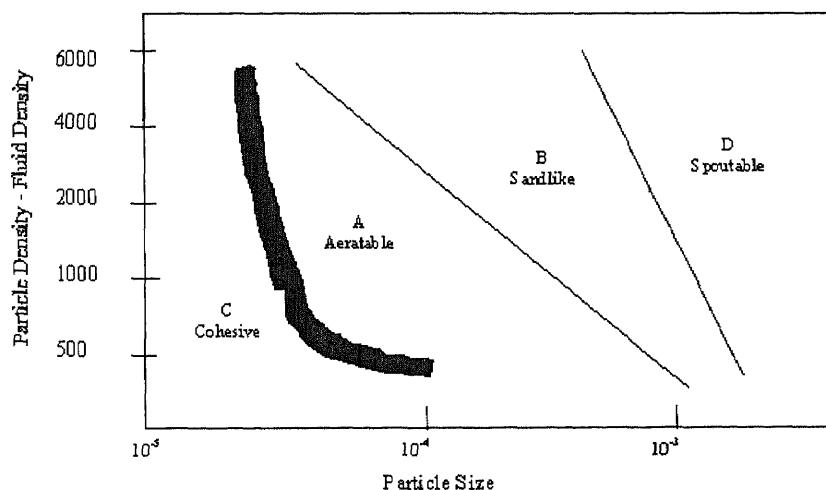
**Figure 2.1:** Various flow regimes or patterns in dense phase fluidization: (a) Particulate fluidization (b) Bubbling fluidization (c) Turbulent fluidization (d) Slugging (e) Spouting (f) Channeling

In addition to the size and density, shape also has an effect on cohesiveness. Channeling can also form in non-cohesive particles when the gas distribution is not uniform throughout the bed.

### 2.2.2. Classification of Fluidized Powders:

Powders have been grouped together based on their fluidization behavior [7]. They basically are grouped as Group C, A, B and D in the order of increasing particle size. The Group C particles are generally  $< 20 \mu\text{m}$ . In Group C particles, the inter-particle forces dominate the hydrodynamic forces and therefore are difficult to fluidize. Group A particles, with a typical size range of  $30\text{-}100 \mu\text{m}$ , are readily fluidized. A bed with Group A particles can be operated in both the particulate and bubbling regime. Group B particles, do not show a particulate fluidization regime and are particles less than  $1 \text{ mm}$  in size but larger than group A particles. Group D particles are larger than  $1 \text{ mm}$  and are commonly processed by spouting.

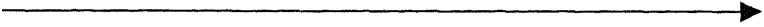
The sizes are only correct for a given density difference. If the density difference changes to higher or lower value, the sizes will also change.



**Figure 2.2:** Geldart classification chart for powder [7]

**Table 2.1:** Summary of Group properties [7]

Increasing size and density

|  |                   |  |  |                                      |   |
|--|-------------------|--|--|--------------------------------------|---|
| Group  |                   | C  | A  | B                                    | D   |
| Most obvious characteristic                            |                   | cohesive, difficult to fluidize  | Bubble free range of fluidization                                    | start bubbling at $U_{mf}$           | coarse solids                             |
| Property/Solid<br>↓                                    |                   | flour, cement  | Cracking catalyst  | building sand                        | table salt                                |
| 1)   | Bed Expansion     | low when bed channels, high when fluidized   | High   | moderate                             | low                                       |
| 2)   | Deaeration Rate   | initially fast, exponential  | Slow, Linear   | fast                                 | fast                                      |
| 3)   | Bubble Properties | no bubble channels and cracks  | Splitting / recoalescence, predominate; max. size exists; large wake | no limit on size                     | no known upper size, small wake           |
| 4)   | Solid mixing      | very low   | High   | moderate                             | low                                       |
| 5)   | Gas back mixing   | very low   | High   | moderate                             | low                                       |
| 6)   | Slug properties   | solid slugs  | Axisymmetric   | axisymmetric, asymmetric             | horizontal voids, solid slugs, wall slugs |
| 7)   | Spouting          | no   | No except in very shallow beds                                       | shallow beds only                    | yes even in deep beds                     |
| Effect on properties 1 to 7 of                         |                   |  |  |                                      |   |
| Mean particle size within group                        |                   | cohesiveness increases as $d_p$ increases  | properties improve as size increases                                 | properties improve as size increases | not known                                 |
| Particle size distribution                             |                   | not known  | increasing $<45\mu\text{m}$ fraction improves properties             | none                                 | segregation                               |
| Increasing, pressure, temp., viscosity, density of gas |                   | probably improves  | definitely improves  | uncertain, some possibly             | uncertain, some possibly                  |

### 2.2.3. Predicting Bed Voidage:

If at all possible, the voidage of the packed bed should be measured in the condition it will be used. For particles of group B and D, an estimate can be made. The reference points are loose packing and dense packing, which are the two extremes for the packing. There are various factors that affect voidage and these are defined as below:

1) **Particle shape:** The sphericity tells how much the particle deviates from a perfect sphere and is given as  $\psi = \frac{\text{surface area of equivalent volume sphere}}{\text{surface area of particle}}$

As shown in Table 2.2, the voidage decreases with increase in sphericity.

**Table 2.2:** Voidage versus sphericity for randomly packed bed uniformly sized particles larger than 500  $\mu\text{m}$  [7]

| $\phi_s$ | $\epsilon$    |               |
|----------|---------------|---------------|
|          | Loose packing | Dense Packing |
| 0.25     | 0.85          | 0.80          |
| 0.30     | 0.80          | 0.75          |
| 0.35     | 0.75          | 0.70          |
| 0.40     | 0.72          | 0.67          |
| 0.45     | 0.68          | 0.63          |
| 0.50     | 0.64          | 0.59          |
| 0.55     | 0.61          | 0.55          |
| 0.60     | 0.58          | 0.51          |
| 0.65     | 0.55          | 0.48          |
| 0.70     | 0.53          | 0.45          |
| 0.75     | 0.51          | 0.42          |
| 0.80     | 0.49          | 0.40          |
| 0.85     | 0.47          | 0.38          |
| 0.90     | 0.45          | 0.36          |
| 0.95     | 0.43          | 0.34          |
| 1.00     | 0.41          | 0.32          |

**2) Particle size:** As shown in Table 2.3, the smaller the particle size, the looser is the packing.

**Table 2.3:** Variation of packed bed voidage with size for loosely packed sphere [7]

|                    |       |       |       |       |       |       |       |       |
|--------------------|-------|-------|-------|-------|-------|-------|-------|-------|
| $d_p, \mu\text{m}$ | 2890  | 551   | 284   | 207   | 101   | 89    | 72    | 55    |
| $\varepsilon$      | 0.422 | 0.432 | 0.440 | 0.437 | 0.507 | 0.563 | 0.590 | 0.602 |

**3) Size distribution:** Table 2.4 shows that when two sand powders with different size distribution, were taken, a wider size spread gave lower voidage.

**Table 2.4:** Effect of size distribution on packed bed voidage [7]

|        | $d_p (\mu\text{m})$ | $\sigma (\mu\text{m})$ | $\varepsilon$ |
|--------|---------------------|------------------------|---------------|
| Sand 1 | 195                 | 75                     | 0.432         |
| Sand 2 | 197                 | 7                      | 0.469         |

**4) Particle and wall roughness:** The rougher the surface, the higher is the voidage.

## 2.3. Different type of fluidized beds

**2.3.1. Dense Phase Fluidized Beds:** The components of a dense phase fluidized bed consist of a gas distributor, cyclone, dipleg, heat exchanger, expanded section and baffles [6]. A schematic diagram is given in Figure 2.3. The purpose of the gas distributor is to support the particles and provide uniform gas distribution. The cyclone

is used to separate solid particles from the outlet gas. The dipleg returns the particle separated by the cyclone into the dense bed. The heat exchanger removes generated heat

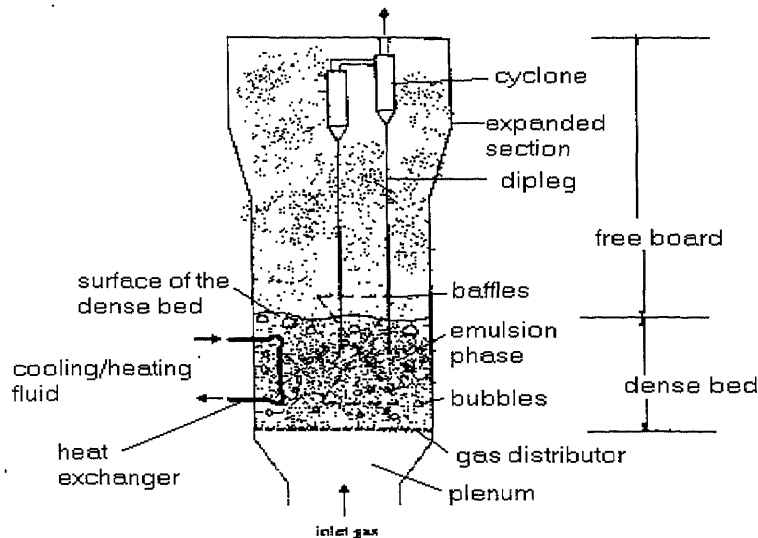


**Figure 2.3:** Schematic diagram of dense phase fluidization

or adds required heat. The expanded section reduces the gas velocity in the freeboard so that the settling of the particles, carried by the fluidization gas, can be efficiently achieved. The baffles restrict flow, enhance the breakup of bubbles, promote gas-solid contact and reduce particle entrainment.

Dense phase fluidization can also be conducted in the presence of various force fields other than a gravitational field. Such force fields include vibration, acoustic, magnetic and centrifugal forces. Operations with applications of these fields are known as vibrofluidized beds, acoustic fluidized beds, magneto-fluidized beds, and rotating fluidized beds, respectively. Also based on the state of fluidization, it can be a particulate fluidized bed, bubbling fluidized bed, turbulent fluidized bed, slugged bed or spouted



bed. Of all the above-mentioned beds, dry particle coating has been tried in the spouted and the rotating fluidized bed. Apart from these, a tumbling bed has also been used for coating purposes. But in this discussion we will describe briefly the spouted and tumbling fluidized bed and elaborate on the rotating fluidized bed as we feel that forces involved in the rotating fluidized bed are much higher in order to achieve better coating. In the lean phase fluidization regime we have circulating fluidized beds (CFB). CFB is a fluidized bed in which solid particles circulate between the riser and the downcomer and the fast fluidization regime is the principal regime under which circulating fluidized beds operate. A CFB, potentially can be used as a dry coater since it operates in the regime where gas velocity is even more than in a spouted bed. It includes a riser, a gas solid separator, a downcomer and the solid particles. A schematic diagram is shown in Figure 2.4.

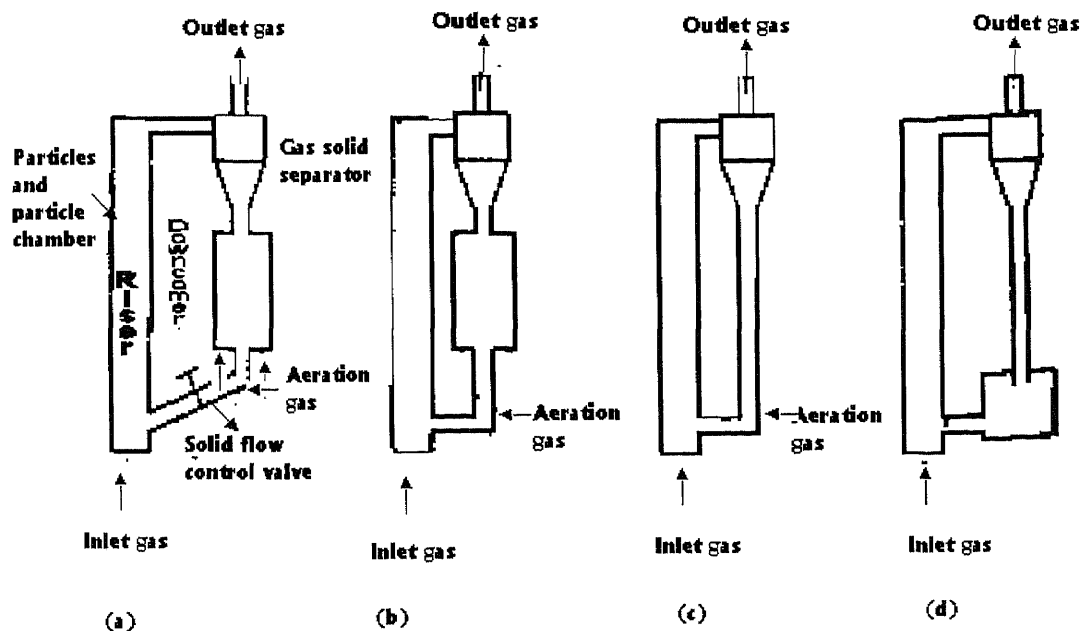
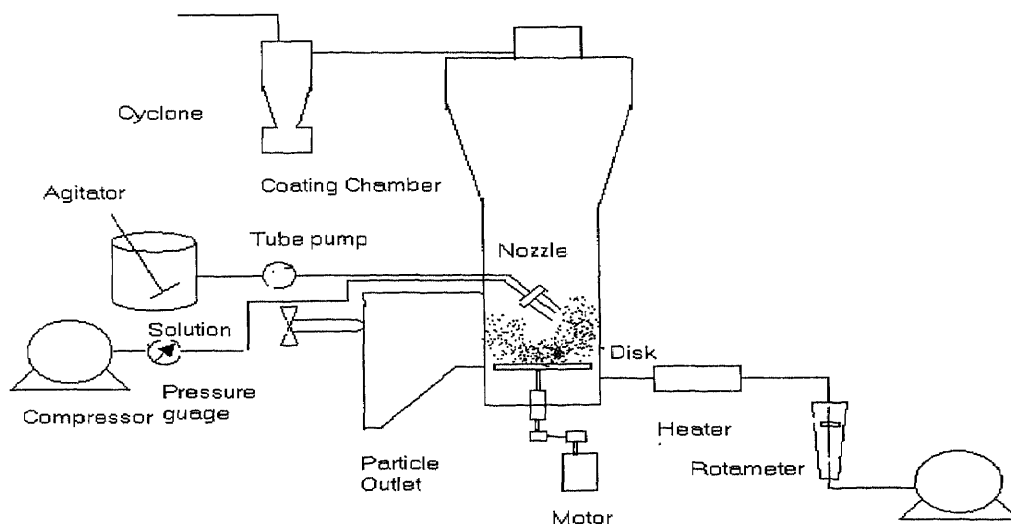


Figure 2.4: Schematic diagram of a circulating fluidized bed

In the operation of a circulating fluidized bed the fluidization gas is introduced at the bottom of the riser, where solid particles from the downcomer are fed via a control device and carried upward in the riser. Particles exit at the top of the riser to a gas solid separator. Separated particles then flow through the downcomer and return to the riser.

### 2.3.2. Tumbling Fluidized Bed:

A schematic diagram of the tumbling fluidized bed is shown in Figure 2.5 as described by Abe et al [20]. This bed operates on gravitational as well as on centrifugal force in the dense fluidization regime. A rotary disk is placed at the base with the clearance between the outer perimeter and wall. A mesh is fixed in this clearance. An external mixing type pneumatic nozzle for liquid outlet is placed at some distance above the disk and directed away from the middle of the disk surface. Air flows into the fluidization chamber through the clearance. Particles on the rotary disk are tumbled and forced to move to the outer portion of the disk by centrifugal force. In the vicinity of the wall, particles are lifted by fluidization air.



**Figure 2.5:** Schematic Diagram of Tumbling Fluidized bed

### 2.3.3. Spouted Fluidized Bed:

This is another type of conventional fluidized bed that operates in the spouted regime. The gas enters through a jet of diameter  $D_i$ , forming a spout of diameter  $D_s$  in the center of bed, as shown in Figure 2.6. The surrounding annular region forms a downward moving bed. Particles are entrained into the spout from the bottom or the sidewall of the spout. Part of the gas seeps into the annular region while the rest leaves the bed from the

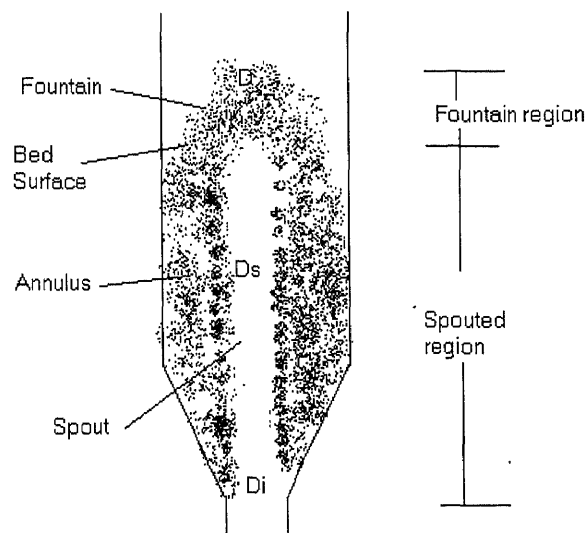


**Figure 2.6:** Schematic Diagram of Spouted Bed

top of the spout. The particles carried with the gas disengage just above the bed and then return to the top of the annular region. Geldart Group D particles are generally used for spouted bed operations. Geldart Group B particles can also be used for spouting, if the nozzle diameter does not exceed by more than 25 times the particle diameter.

### 2.3.4. Rotating Fluidized Bed:

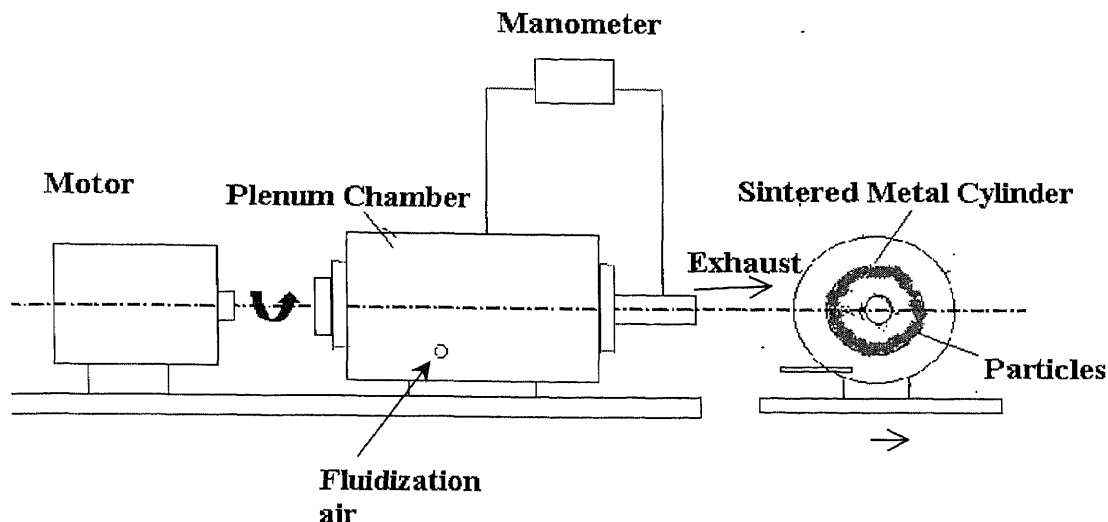


**Figure 2.7:** Schematic Diagram of Rotating Fluidized Bed

In a fluidized bed, high heat and mass transfer rate, temperature homogeneity, and high flowability of particles are obtained. These conditions are all useful for continuous large scale gas-solid reaction systems. Hence the fluidized bed is used in FCC cracking, fluid chocking, drying, dust filtration and coal combustion. In all these operations vertical gravity driven fluidized bed is used. However in some of these applications a centrifugal or rotating fluidized bed can be used. A RFB will reduce the bed size and achieve a high gas throughput and for greater process efficiency. We are trying to develop a new application for the rotating fluidized bed, where it can be used to create unique engineered particulates. For studies on a lab scale, a horizontal rotating fluidized bed will be used for this research.

The working principle of a rotating fluidized bed is the same as of conventional fluidized bed with the difference that the fluidization takes place under a centrifugal force field rather than in a gravitational force field. The bed is a porous cylinder rotating about its axis with aeration introduced radially inward to fluidize the particles. The force field is an adjustable parameter that is determined by the rotational speed and radius of the cylinder. The granules also are not fluidized as a whole but layer by layer with the inner most layer fluidizing first and fluidization moving radially outward to the distributor wall as the gas velocity is increased. The gas-solid contact at high aeration rate is improved since fluidization occurs at much higher gas velocities than in conventional fluidized bed. This characteristic is useful for our application where the particles are required to have sufficient force to impact each other so that particles will adhere to one another. Here it is immaterial whether the other particle is a different particle (coating application) or a similar particle (granulation). In the granulation experiment, a reverse gas flow is also used so that the forward flow fluidizes the bed and the reverse flow compacts the bed. The compaction during the reverse flow compacts the powder into agglomerates and attrition during the forward flow makes the agglomerate spherical thus forming granules. This cyclic phenomenon forms the concept of dry granulation.

#### **2.4. Inter-Particle Forces in a Rotating Fluidized Bed**

In a conventional fluidized bed, powder fluidization is a result of the balance between fluid-dynamic and gravitational forces. The powder is assumed, more or less free flowing and inter-particle interaction forces are minimum [9].

The interaction forces for gas fluidized beds are van der Waal forces, electrostatic, capillary and adsorption forces. The van der Waals forces are noticeable when particle come sufficiently close together, of the order of the size of a molecule, e.g., 0.2 to 1 nm. However their magnitude becomes negligible compared with that of the gravitational force above a certain diameter as gravitational force is proportional to cube of the diameter and van der Waals forces are proportional to the diameter. This diameter has been approximated to be around 50  $\mu\text{m}$  [8]. Inter-particle forces are more pronounced in Geldart Group C particles, which have an average diameter less than 20  $\mu\text{m}$  and density larger than 1  $\text{g}/\text{cm}^3$ .

The transition between Group C and Group A is also of importance. Fan et al [6] pointed out that boundary between Group C and Group A is strongly influenced by inter-particle forces, such as van der Waals, capillary, electrostatic and magnetic forces. It is also influenced by the size of surface asperities, hardness of solid material, humidity, melting or softening point, electric conductivity and magnetic susceptibility. The guest particles used in the present study are sub-micron size silica and alumina, and hence fall under this category, i.e., Group C behavior. The coating of the guest particles onto the surface of host particles generally depends upon whether the forces involved are strong enough to overcome the inter-particle forces between the guest particles, for only then can the guest be deagglomerated and coated on to the host. The various inter-particle forces for two interacting spherical bodies are briefly described below [6-8].

### 1) van der Waal forces:

The van der Waal forces are the result of attraction between particles [21]. According to Israelachvili [8], the van der Waal force between two spherical particles of diameter  $d_1$  and  $d_2$  is given by

$$F_v = \frac{A_{12}}{12s^2} \frac{d_1 d_2}{d_1 + d_2} \quad (2.1)$$

where  $A_{12}$  is Hamaker Constant and  $s$  is the distance between the centers of the two particles. For real particles, which are almost always non-spherical, the interaction forces depend on surface roughness and actual area of contact [9]. As illustrated in Figure 2.8, the van der Waal forces will be approximately zero for the case (a) and (b), because the surface is rough which limit the approach of two particles and hence low contact area. However for cases (c), (d) and (e), van der Waal forces are high, as there is large contact area between the particles.

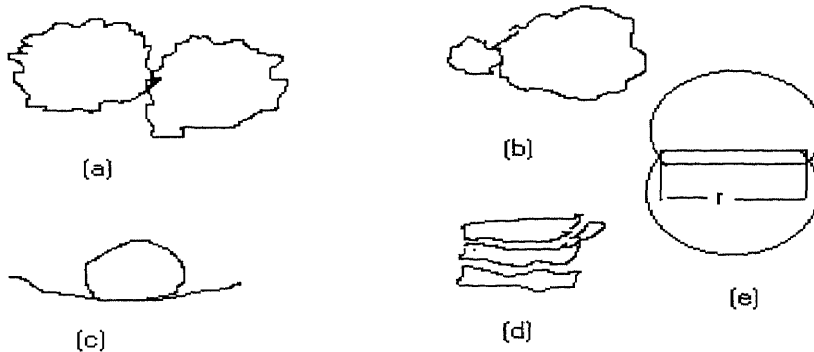


**Figure 2.8:** The influence of surface roughness and geometrical factors on interaction forces [9]

## 2) Electrostatic forces:

Particles become charged by surface contact during collision and the motion of a charged particle in a gas-solid flow is affected by a nearby charged particle. The force acting on one charged particle having charge  $q_1$  by another charged particle having charge  $q_2$  is given by Coulomb's law as

$$F_e = \frac{1}{4\pi\epsilon_0} \frac{q_1 q_2}{s^2} \quad (2.2)$$

where  $\epsilon_0$  is the permittivity of vacuum. The force of interaction between a spherical particle of radius  $R$  and charge  $Q$ , interacting with an adjacent uncharged particle with a separation distance  $H$  due to its own image charge is given by

$$F_e = \frac{Q^2 \left[ 1 - \frac{H}{(R^2 + H^2)^{1/2}} \right]}{16\pi\epsilon_0 H^2} \quad (2.3)$$

The latter case is between the particle and the wall of the fluidized bed. However if the air is not dry, Coulomb interaction does not come into play as the charges are annihilated [9].

## 3) Capillary forces:

Capillary forces come into play in an environment of humidity greater than 65% [9]. The capillary force between two spherical particles of radius  $R$  and surface tension  $\gamma$ , is given by

$$F_H = 2\pi\gamma R \quad (2.4)$$



#### 4) Collision force:

The equations derived here are taken from Timoshenko and Goodier [15], who consider the central impact of two spheres with a velocity of approach  $V$ . The relative displacement  $\alpha$  of the centers of two spheres at the instant of maximum compression is given by

$$\alpha = \left( \frac{5V^2}{4nn_1} \right)^{2/5} \quad (2.5)$$

where  $n$  and  $n_1$  are given by

$$n = \sqrt{\frac{8}{9\pi^2(k_1 + k_2)^2} \frac{d_1 d_2}{d_1 + d_2}} \quad (2.6)$$

$$n_1 = \frac{m_1 + m_2}{m_1 m_2} \quad (2.7)$$

In the above equation,  $m_1$  and  $m_2$  are the mass of spheres 1 and 2 respectively.

$k_1$  and  $k_2$  are the  $k$  factor for sphere 1 and 2.  $k$  is given by equation

$$k = \frac{1 - \nu^2}{\pi E} \quad (2.8)$$

where  $E$  and  $\nu$  are Young's Modulus and Poisson's ratio respectively.

The approach velocity  $V$  is given as

$$V = \left( 1.5 P_{s,n} D_b r \omega^2 \epsilon \right)^{1/2} \quad (2.9)$$

where  $D_b$  is the bubble diameter. Although no information is available in the literature to calculate the bubble diameter in a rotating fluidized bed, it has been observed that bubble sizes in an RFB are very small. Hence the bubble size in an RFB can be approximated by the bubble diameter at the start of bubbling fluidization in conventional fluidized bed. Thus, we assume that the equation to calculate the initial bubble diameter in a bubbling fluidized bed can be used to calculate the bubble diameter in an RFB and is given by [22]

$$D_b = \frac{3.77}{r\omega^2} [(u - u_{mf})]^2 \quad (2.10)$$

$P_{s,n}$  is average dimensionless particle pressure of a non-sticky system. The value of  $P_{s,n}$  is taken to be 0.077 [22]. The collision force is given as

$$F_c = n\alpha^{3/2} \quad (2.11)$$

### 5) Kinetic or Drag force:

The drag force depends on the value of Reynolds number. The Reynolds number  $Re$ , for a particle of diameter  $d_2$  at a superficial velocity  $u_0$  is calculated using the equation 2.10 to determine in which region the particle is. The equation for  $Re$  is given as:

$$Re = \frac{\rho_f u_0 d_2}{\mu} \quad (2.12)$$

If the particle is in the Newton's law region (i.e., low  $d/D$  and Reynolds number  $Re > 500$ ), the drag force is given by [10, 14],

$$F_y = 0.055\pi\rho_f d_2^2 u_0^2 \epsilon^{-4.8} \quad (2.13)$$

where  $\rho_f$  is the density of fluid,  $u$  is the superficial velocity and  $\epsilon$  is the bed voidage. For Stokes' law region (i.e. low  $d/D$  and  $Re < 0.2$ ), the drag force is given by

$$F_y = 3\pi\mu d_2 u_0 \epsilon^{-4.8} \quad (2.14)$$

For a particle in the range  $0.2 < Re < 500$ , the above equations are not valid and a complex equation follows. Even the factor of  $\epsilon^{-4.8}$  if used would give unrealistic results. Hence the equation for drag force  $F_y$  in this region is given as [14]

$$F_y = \left[ 2.25 + 0.36 (Re \epsilon^{-n})^{0.37} \right]^{3.45} \frac{\pi}{8} \rho u_0^2 d_2^2 \epsilon^{-2n} \quad (2.15)$$

where  $n$  is related to Galileo Number by the following equation

$$\frac{4.8 - n}{n - 2.4} = 0.043 Ga^{0.57} \quad (2.16)$$

and the Galileo Number  $Ga$  is given as

$$Ga = \frac{(\rho_p - \rho_f) \rho_f d_2^3 r \omega^2}{\mu^2} \quad (2.17)$$

where  $\rho_p$  and  $\rho_f$  are the particle and fluid density, respectively.

In the case of a rotating fluidized bed, the bed is operated at superficial velocities between 1.5 to 2 times the minimum fluidization velocity. Therefore at 1.5 times the minimum fluidization velocity for all the particles, the superficial velocity is in the range of 0.45 to 0.8 m/s. The diameter of the guest particle, alumina, can vary from 700 nm for

individual alumina particles to 30  $\mu\text{m}$  for agglomerate of alumina. Hence the Reynolds Number can vary from 0.02 to 20. Thus the particle is in the Stokes' law region or a little above the Stokes' law region. The drag force in the Stokes' law region is calculated using equation (2.12). If the particle is above the Stokes' law region, the drag force is calculated using equation (2.13). The factor  $\varepsilon^n$  is calculated by determining Ga first and then putting it into the equation for n. Since the value of d is small, none of our particle fall into the Newton's law region.

#### 6) Field forces:

Field forces are external forces such as an electric field and/or a magnetic field, which can influence the motion of the particle. In the case of a rotating fluidized bed, the external forces acting on the particle are the centrifugal-buoyant force and the gravitational-buoyant force. The bed is operated at 1200 to 1500 rpm for most of the particles. At these rotational speeds the centrifugal force is 2 orders of magnitude larger than the gravitational force. Thus the gravitational force is negligible compared to centrifugal force. Hence the only external force considered is the centrifugal-buoyant force.

The equation for the centrifugal-buoyant force is given as [10]

$$F_g = \frac{\pi}{6} (\rho_p - \rho_f) d_p^2 r \omega^2 \varepsilon \quad (2.18)$$

where r is the distributor radius,  $\omega$  is angular velocity and  $\varepsilon$  is the voidage in the fluidized state.

## 2.5. Particle-Particle Interaction in Rotating Fluidized Bed

The particles used in the rotating fluidized bed for coating are guest and host particles with a minimum size ratio of 1:10. Since granulation involves one type of particle, they are of the same average size. We will first consider particle-particle interaction during the coating process. The particle-particle interaction in the rotating fluidized bed coater is a complex phenomena, as guest particles fall under the Geldart Group C category, which are sub-micron and highly cohesive with strong intermolecular forces.

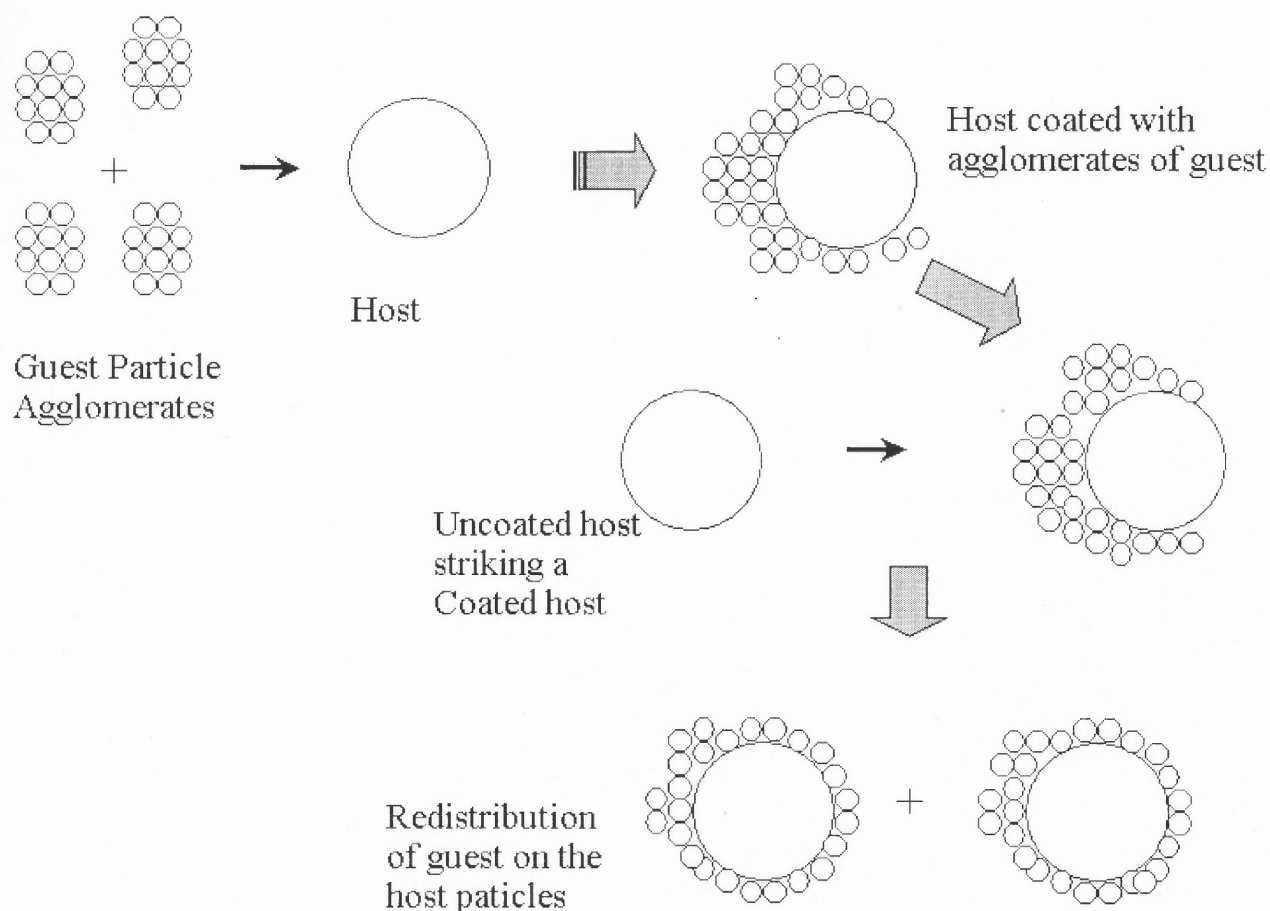
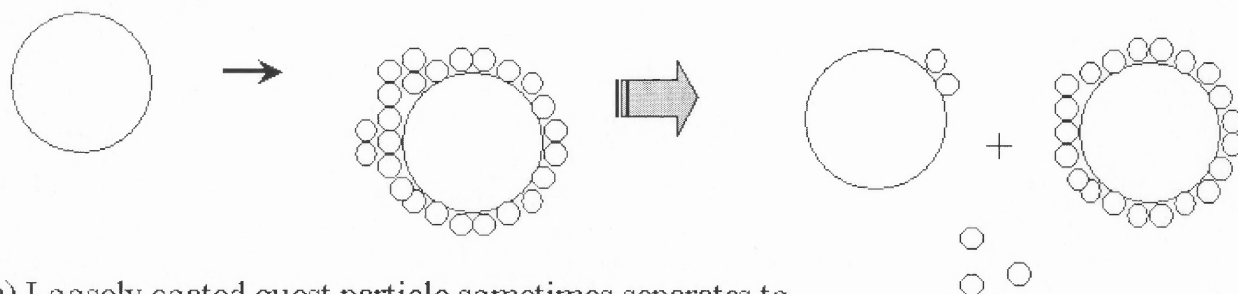
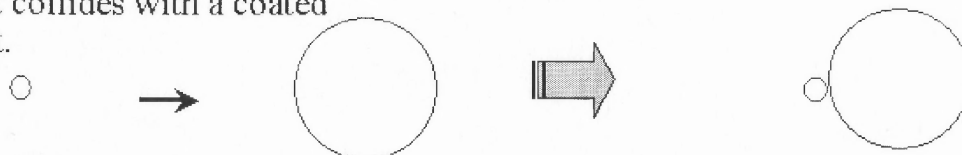


**Figure 2.9:** Collision of guest agglomerate and host and the redistribution of guest particles onto the host particles.

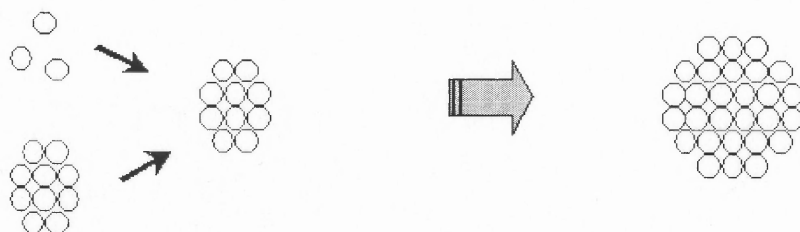
As a result, they do not exist as individual particles, but as agglomerates. When we run the rotating fluidized bed as a coater the fluidization air does not provide enough energy to break the agglomerates. Therefore the guest particles collide with the host particles as agglomerates as depicted in Figure 2.9 and Figure 2.10. When another host particle collides with a host particle coated with agglomerates of guest particles, the guest particles redistribute and some of the guest particles get transferred onto the new host particles.



(a) Loosely coated guest particle sometimes separates to exist as an individual guest particle when an uncoated host collides with a coated host.



(b) Individual guest particle colliding with a host and is coated onto it.



(c) Agglomerates colliding to form bigger agglomerates

**Figure 2.10:** Part (a) shows the collision of host with guest particles loosely attached to host particles Part (b) shows an individual guest gaining momentum, colliding with host and becoming coated onto the host and part (c) shows the increase in size of the agglomerate.

When the host particles collide with one of those guest particles that are loosely coated onto the host particles, some get coated on to the new host and some for an instance exist as individual particles. Some of these individual particles gain momentum and collide with host particles. Others collide with similar individual particles and get agglomerated since they cannot exist as individual particles. Hence the process of coating and agglomeration takes place simultaneously and the extent of each phenomenon depends upon the size of particle used, size ratio, type of material and magnitude of the forces generated on the coater.

In the case of granulation, all of the particles used are Group C particles, which are highly cohesive. The granulation phenomenon is shown schematically in Figure 2.11. It is caused by cyclic fluidization and reverse gas flow compaction. Thus the powder is densified during the reverse flow and agglomerated into spherical granules during the forward flow. The weak agglomerate get attrited during the fluidization and then reagglomerate during the compaction, hence the process is called granulation because the final particles are actually granules and not agglomerates.

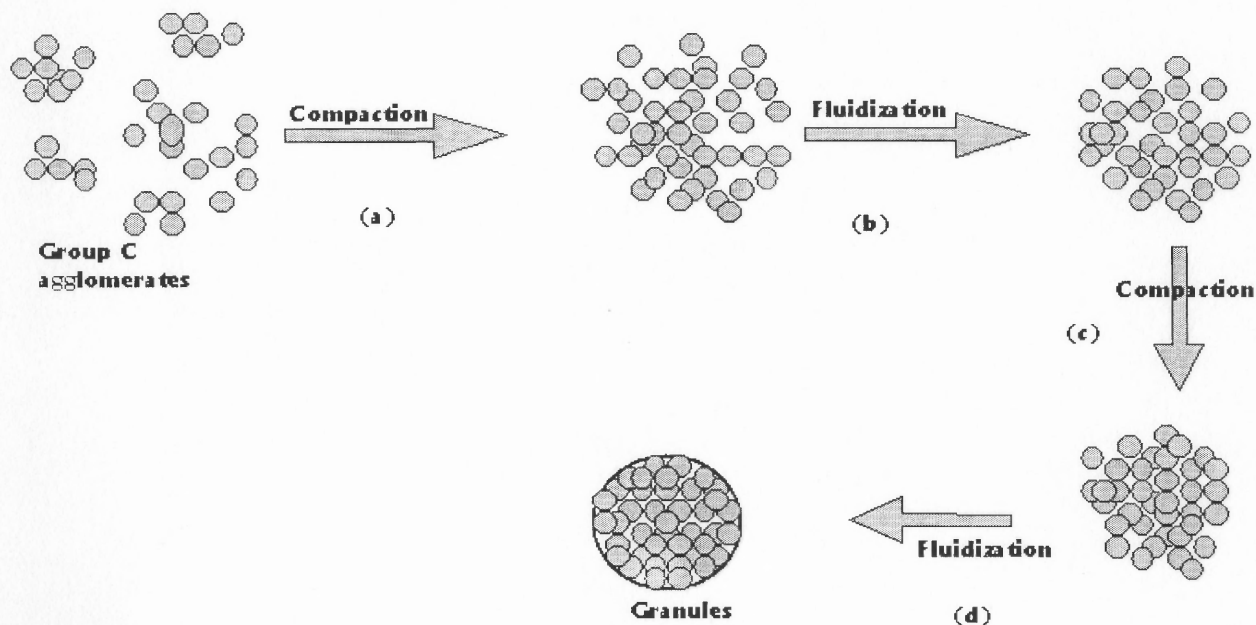


**Figure 2.11:** (a) Small agglomerates of Geldart Group C particles get compacted to form big weak agglomerate. (b) Attrition of agglomerate during the fluidization phase and (c) Further compaction of agglomerate to form strong agglomerate (d) Trimming of the agglomerate to take the shape of a spherical granule.

## 2.6. Kinetics Considerations in Particle Interaction

The kinetics of the system is a function of force and momentum transfer. The purpose of discussing the kinetics is to understand the various forces, (Figure 2.12) which are acting on the particle in a RFB.



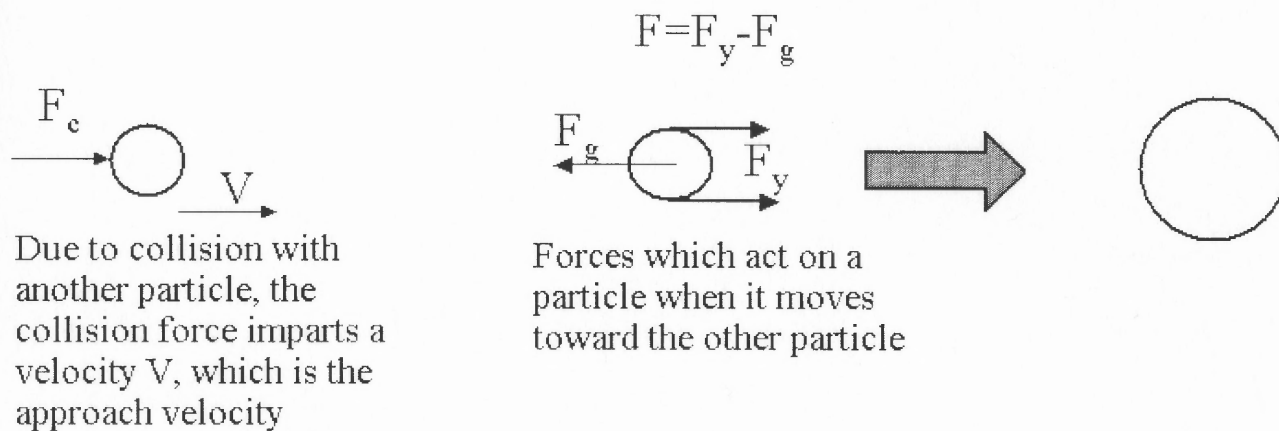


**Figure 2.12:** Various forces acting on an approaching particle during the coating process.

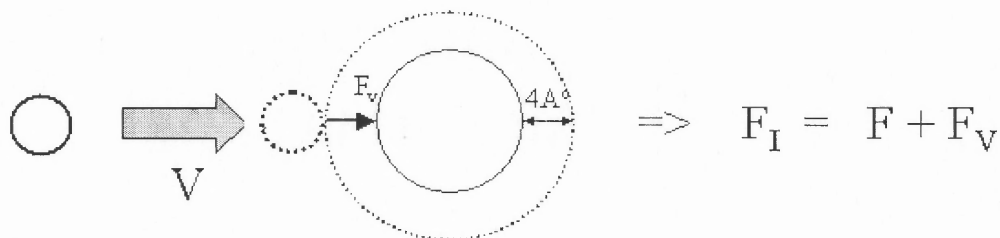


**Figure 2.13:** The resultant momentum with which the guest particle agglomerate impacts the host particle during the fluidization.

This study will also help to determine the criterion for coating, since we achieve a good coating with some particles and a poor coating with others. In this study we have made the following assumptions. First, the particles are considered to be spherical. Second, the collision can be both elastic and plastic. Third, in a rotating fluidized bed, the force due to gravity is considered negligible compared to the centrifugal force for the reason discussed in Section 2.3. Thus the forces, which can act on the particle, are binding, drag, collision, centrifugal-buoyant and field forces. The binding forces are electrostatic, capillary and/or van der Waal forces. Since the air is neither dry nor humid, the electrostatic and capillary forces are neglected as was discussed in Section 2.3. The drag force and collision force will be used in the resultant force equation. The equations for drag force, collision force and centrifugal- buoyant force are also defined in Section 2.3.

The momentum with which one particle hits the other particle is dependent on various forces like  $F_c$ ,  $F_y$  and  $F_g$  as illustrated in Figure 2.12. Figure 2.12 and 2.13 depict, how the particle attains the impact velocity. Due to the collision force, the particle attains an approach velocity  $V$  and travels some distance before colliding with the other particle. During this distance traveled, the drag force and centrifugal force are continuously acting on the particle. When the particle reaches within an annular distance of the other particle of around  $4 A^0$  [8], the van der Waal force of attraction acts in the direction in which the particle is moving and gives it an acceleration. Thus the particle collides with the resultant velocity, say  $v$ , at the time of impact and is the impact velocity. The resultant force acting on the particle at the time of impact is given as

$$F_I = F_y + F_v - F_g \quad (2.19)$$

When the particle strikes with an impact velocity  $v$ , whether the coating takes place is examined on the basis of the Roger and Reed theory [18].

According to Roger and Reed, the velocity with which one particle strike another particle should be greater than limiting elastic velocity  $\phi$ , for coating to take place. The limiting velocity  $\phi$  is given by following equation

$$\phi = \left( \frac{2\pi}{3K} \right)^2 \left( \frac{2}{5\rho} \right)^{\frac{1}{2}} y^{\frac{5}{2}} \quad (2.20)$$

where  $y$  is elastic yield limit and

$$K = \frac{4}{3\pi(k_1 + k_2)} \quad (2.21)$$

where  $k_1$  and  $k_2$  are the  $k$  values for particle 1 and 2 derived using equation 2.8.

If the impact velocity is less than the limiting elastic velocity, the particle will rebound back without getting coated onto the other particle, and the rebound velocity is slightly less than the impact velocity as some fraction,  $f$ , of the total energy will be dissipated. If the velocity is greater than the limiting elastic velocity, plastic deformation will take place in softer of the two bodies. Here it is assumed that elastic yield limit remains constant, i.e., work- hardening effects are assumed to be negligible. Therefore some energy,  $Q_p$ , will be dissipated due to plastic deformation, which is given by

$$Q_p = \left( \frac{\left( 2mv^2 - \frac{1}{8}m\phi^2 \right)^{\frac{1}{2}} - \left( \frac{15}{8}m\phi^2 \right)^{\frac{1}{2}}}{2} \right)^2 \quad (2.22)$$

where  $v$  is impact velocity,  $\phi$  is limiting elastic velocity and  $m$  is mass of particle.

The energy with which the particle will rebound back is the difference of impact energy and energy due to plastic deformation i.e.  $Q = Q_I - Q_p$ . If this rebound energy  $Q$ , is less than the total adhesive energy  $Q_A$  the particle will get coated otherwise the two particles will separate. According Johnson et al (21), the total adhesive energy  $Q_A$  is composed of mechanical energy  $U_M$  and surface energy  $U_S$ , i.e.  $Q_A = U_M + U_S$ . The two energy components are given by expression

$$U_M = P_0 \frac{\left( P_1^{2/3} + 2P_0P_1^{-1/3} \right)}{3K^{2/3}R_c^{1/3}} \quad (2.23)$$

and

$$U_S = \Delta\gamma\pi \left( \frac{R_cP_1}{K} \right)^{2/3} \quad (2.24)$$

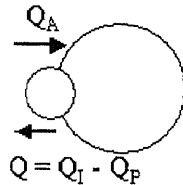
where  $P_0$  is the external force applied between contacting bodies. (Note the external force applied in our case is a centrifugal force due to the mass of the particle and is equal to  $m\omega^2$ ).  $P_1$  is given by

$$P_1 = P_0 + 3\Delta\gamma\pi R_c + \left[ (P_0 + 3\Delta\gamma\pi R_c)^2 - P_0^2 \right]^{1/2} \quad (2.25)$$

and for spherical bodies,  $R_c$  is given by

$$\frac{1}{R_c} = \frac{1}{R_1} + \frac{1}{R_2} \quad (2.26)$$

In equation 2.23 and 2.24,  $\Delta\gamma$  is surface adhesive energy per unit area of contact and is related to Hamaker constant as  $A=2.1*10^{-18}\Delta\gamma$ .



For Coating  $Q < Q_A$

For coating to occur, after satisfying the condition that the impact velocity is greater than the limiting velocity, the condition  $Q < Q_A$  should also be satisfied. A sample calculation is shown in Appendix 3. The values which were obtained by putting the experimental parameters in the equations 2.1 to 2.26, and calculated as per the sample calculations done in appendix 3 are tabulated in chapter 4. Their agreement with the experimental observation is also discussed in chapter 4. The values of the impact velocities, which are most suitable for coating to occur, are also calculated in chapter 4.

## 2.7. Conclusion to Chapter 2

- 1) In the coating studies, since the guest particles are Group C particles they are highly cohesive so it is very difficult to deagglomerate them in the RFB.

- 2) The forces i.e. drag force, collision force and centrifugal-buoyant force, involved in the rotating fluidized bed are more than in a conventional fluidized bed, so it is more suitable for coating and granulation purposes.
- 3) The guest particles have not been deagglomerated by any other process before entering the RFB and the RFB doesn't provide enough force to deagglomerate them, so they collide with the host particles as agglomerates and get redistributed onto the host. Thus we get a very soft coating with the RFB.
- 4) In the granulation studies also, we also start with Group C particles. But here the agglomerates get compacted during the compaction run and then subject to attrition during the fluidization run. Thus the powder take the shape of granules. Therefore the fluidization energy will define the sphericity of the granule and the compaction energy due to the reverse flow will define the size of the granule.
- 5) During coating, the resultant momentum with which the particle collides with the other particle is dependent on forces  $F_c$ ,  $F_y$ ,  $F_g$ , and  $F_v$  i.e. collision force, drag force, centrifugal force and van der Waal force. The final impact velocity  $v$  is the resultant of all these forces, which has to be more than the limiting elastic velocity for coating to take place. When the impact velocity is more than the limiting elastic velocity, plastic deformation will take place and some energy will be lost due to elastic deformation. The difference of elastic and energy loss due to deformation has to be less than the total adhesive energy for particles to stay together.

## CHAPTER 3

### EXPERIMENTAL APPROACH, SETUP AND PROCEDURE

In this study, the apparatus used is a rotating fluidized bed (RFB). Fluidized beds have been used successfully as gas-solid reactors, highly efficient dust filters, etc. In conventional fluidized beds, the bed operates under its own weight. The drag force is working against the gravitational force of 1 g, so the forces involved in this type of fluidized bed are small. In a rotating fluidized bed, the bed rotates around its axis and gas flow is radial so the drag force is working against a centrifugal force which varies anywhere from 0 to several hundred g's depending on the size of the distributor and rotating speed of the device. The rotating fluidized bed can be best described as a rotating porous cylinder whose walls act as a distributor within a fixed cylindrical drum. The porous cylinder is filled with powder and gas is passed radially through the distributor. Fluidization occurs when the drag force is equal to or exceeds the centrifugal force.

In a conventional fluidized bed, all the layers of the bed fluidize at the same time whereas in the rotating fluidized bed, the bed fluidizes layer by layer with the inner most layer fluidizing first and then moving outwards till the outermost layer, next to the distributor wall, gets fluidized. At this point the bed is completely fluidized. The velocity corresponding to the point where the innermost layer fluidizes is called *surface minimum fluidization velocity*. The velocity corresponding to the point where the outer most layer,

next to the distributor wall, fluidizes is called the *critical minimum fluidization velocity*.

The average over this range of velocity is called *average minimum fluidization velocity*.

### 3.1 Theoretical Analysis of the Rotating Fluidized Bed

#### 3.1.1 Theoretical model

The theoretical analysis of pressure drop and fluidization velocity is based on semiempirical equations of Chen (1986) [1] and further modified by Kao, Pfeffer and Tardos (1987) [2]. The final equations are as follows:

1) For the fixed bed region, the pressure drop is given by

$$\frac{dP}{dr} = \phi_1 \left( U_0 \frac{r_0}{r} \right)^2 + \phi_2 \left( U_0 \frac{r_0}{r} \right)^2 \quad (3.1)$$

where

$$\phi_1 = \frac{150(1-\varepsilon)^2 \mu}{\varepsilon^3 (\phi_s d_g)^2} \quad \phi_2 = \frac{1.75(1-\varepsilon) \rho_f}{\varepsilon^3 \phi_s d_g}$$

2) For the fluidized bed region, the pressure drop is given by

$$\frac{dP}{dr} = (\rho_g - \rho_f)(1-\varepsilon)r\omega^2 \quad (3.2)$$

The average minimum fluidization velocity is given by the equation

$$U_{avg} = \frac{\sqrt{(\phi_1 C_2)^2 + 4\phi_2 C_1 \omega^2 C_3 (1-\varepsilon)(\rho_g - \rho_f)} - \phi_1 C_2}{2\phi_2 C_1} \quad (3.3)$$

where

$$C_1 = r_0^2 \left( \frac{1}{r_i} - \frac{1}{r_0} \right) \quad C_2 = r_0 \ln \left( \frac{r_0}{r_i} \right) \quad C_3 = \frac{(r_0^2 - r_i^2)}{2}$$



Equation (3.3) has been obtained by equating the total pressure drop across the fixed bed with that across the fluidized bed. Similarly, we can also obtain the surface and critical minimum fluidization velocity. The surface minimum fluidization velocity  $U_{mfs}$  is defined as the point where the inner most layer of the bed fluidizes and the critical minimum fluidization velocity is the point where the outer most layer fluidizes. The surface minimum fluidization velocity is obtained by equating the local pressure drop across the packed and fluidized bed at the inner radius of the bed. Similarly the critical fluidization velocity can be obtained by equating the local pressure drops at the outer radius, i.e., at  $r = r_0$ .

$$U_{mfs} \frac{r_0}{r_i} = \frac{\sqrt{(\phi_2)^2 + 4\phi_1\omega^2(1-\varepsilon)(\rho_g - \rho_f)r_i} - \phi_2}{2\phi_1} \quad (3.4)$$

and

$$U_{mf} = \frac{\sqrt{(\phi_2)^2 + 4\phi_1\omega^2(1-\varepsilon)(\rho_g - \rho_f)r_0} - \phi_2}{2\phi_1} \quad (3.5)$$

From the above relationships, we observe that pressure drop across the bed will depend on  $U_0$ , i.e., depending in what region  $U_0$  falls under. The three regions are  $U_0 \leq U_{mfs}$ ,

$$U_{mfs} \leq U_0 \leq U_{mf}, \quad U_0 > U_{mf}.$$

In the region  $U_0 \leq U_{mfs}$ , the bed is completely packed and the pressure drop is given by

$$\Delta P = \left[ \left\{ (\phi_1 U_0 r_0) \ln \left( \frac{r_0}{r_i} \right) \right\} + \left\{ \phi_2 U_0^2 r_0^2 \left( \frac{1}{r_i} - \frac{1}{r_0} \right) \right\} \right] \quad (3.6)$$

In the region  $U_{mfs} < U_0 < U_{mf}$ , the resulting pressure drop is a combination of the pressure drop across the fluidized and the packed bed and is given by

$$\Delta P = (1 - \varepsilon)(\rho_g - \rho_f)\omega^2(r_{pf}^2 - r_i^2) + \left[ \left\{ (\phi_1 U_0 r_0) \ln \left( \frac{r_0}{r_{pf}} \right) \right\} + \left\{ \phi_2 U_0^2 r_0^2 \left( \frac{1}{r_{pf}} - \frac{1}{r_0} \right) \right\} \right] \quad (3.7)$$

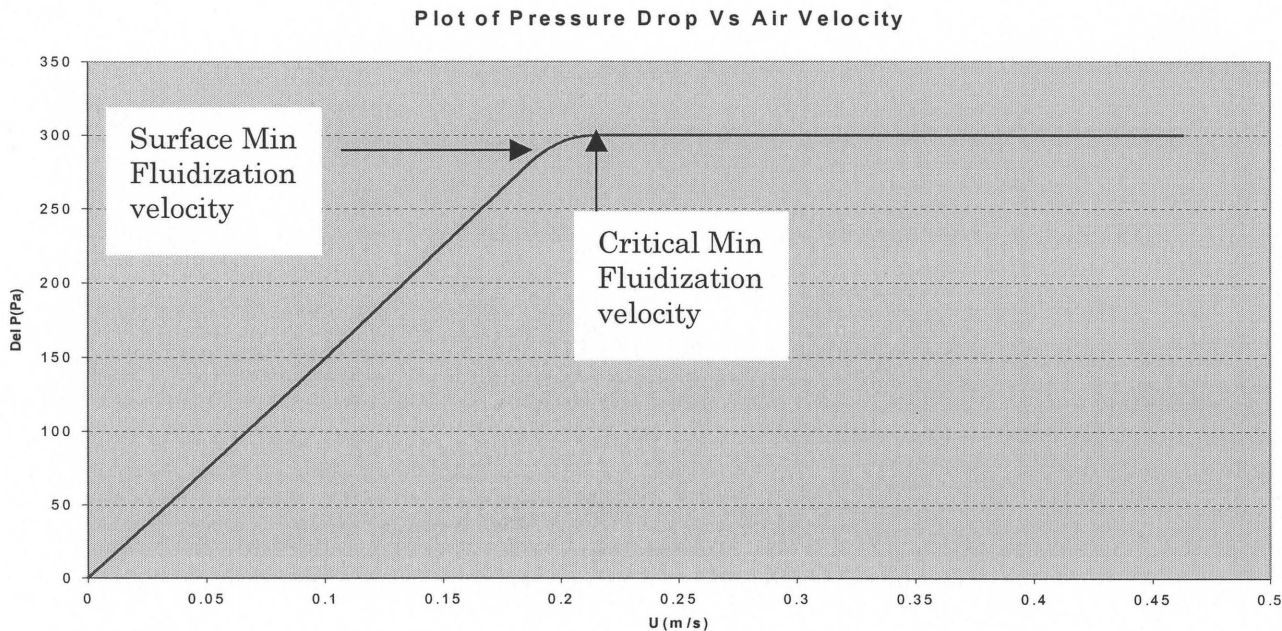
In the region  $U_0 \geq U_{mf}$ , the bed is completely fluidized and pressure drop is given by

$$\Delta P = (1 - \varepsilon)(\rho_g - \rho_f)\omega^2(r_0^2 - r_i^2) \quad (3.8)$$

We observe that beyond the critical fluidization velocity the pressure drop across the bed is dependent only three factors, the rotating speed, the mass of the bed and the length of the bed.

### 3.1.2 Graphical Representation of Pressure Drop Using the Theoretical Model

When we plot the curve for pressure drop versus superficial velocity  $U_0$ , we obtain a graph as obtained in Figure 3.1. From the graph, we observe that the pressure drop



increases linearly till it reaches the surface minimum fluidization velocity and then rises more slowly along a curve till it reaches the critical fluidization velocity. The slope for the linear portion of the pressure drop depends on various factors such as the voidage, the density of the powder, the rotating speed, the size of the distributor and the superficial velocity. But after the critical fluidization velocity, a flat portion represents a constant pressure. Since the powder is in a fluidized state, the pressure drop is dependent only on the mass of powder and the length of distributor, which is fixed. This can be explained using equation 3.8. According to equation 3.8,

$$\Delta P = (1 - \varepsilon)(\rho_g - \rho_f)\omega^2(r_0^2 - r_i^2) \quad (3.8)$$

Since  $\rho_f \ll \rho_g$ ,

$$(\rho_g - \rho_f)(1 - \varepsilon) = \rho_p$$

and,

$$(r_0^2 - r_i^2) = \frac{V}{\pi l}$$

Hence

$$\Delta P = \rho_p \frac{V}{\pi l} \omega^2 = \frac{m \omega^2}{\pi l} \quad (3.9)$$

where  $m$  is the mass of the particles in the bed.

At a given rotating speed, with the distributor dimensions fixed, the pressure drop will only depend on the mass of powder in the bed. Since we do not add powder after the bed start running, and if we assume that powder is not lost during the operation, then the pressure will remain constant after the critical fluidization velocity is reached.

## 3.2 Apparatus

### 3.2.1 Coating Experimental System

The schematic diagram of the apparatus used for the coating experiments is shown in Figure 3.2 and Figure 3.3.

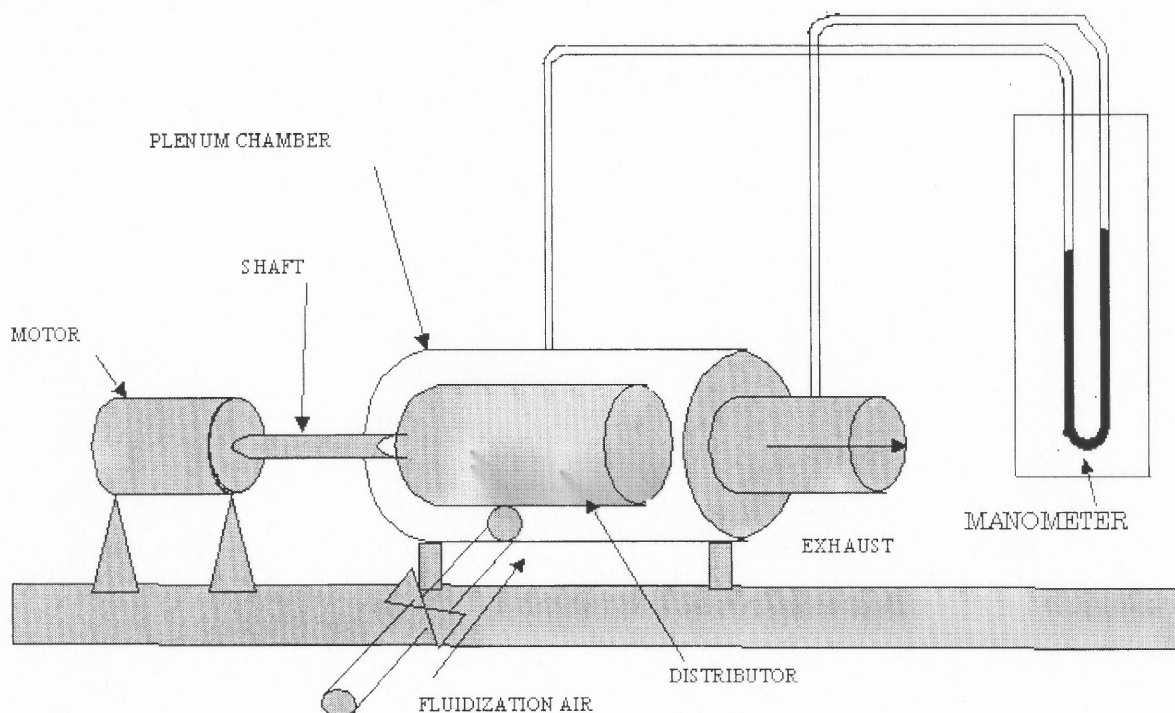


**Figure 3.2:** Schematic diagram of experimental setup of rotating fluidized bed for coating purposes.

In this setup, the rotating fluidized bed comprises of an outer chamber, a gas distributor, a motor connected to the distributor through a shaft, a manometer to read the pressure,

rotameters to measure the flow rate and an exhaust connected to a hood. The outer chamber has a radius of 5.5 cm and a length of 15 cm. The air is sent into the chamber

Photograph of Rotating Fluidized Bed Coater

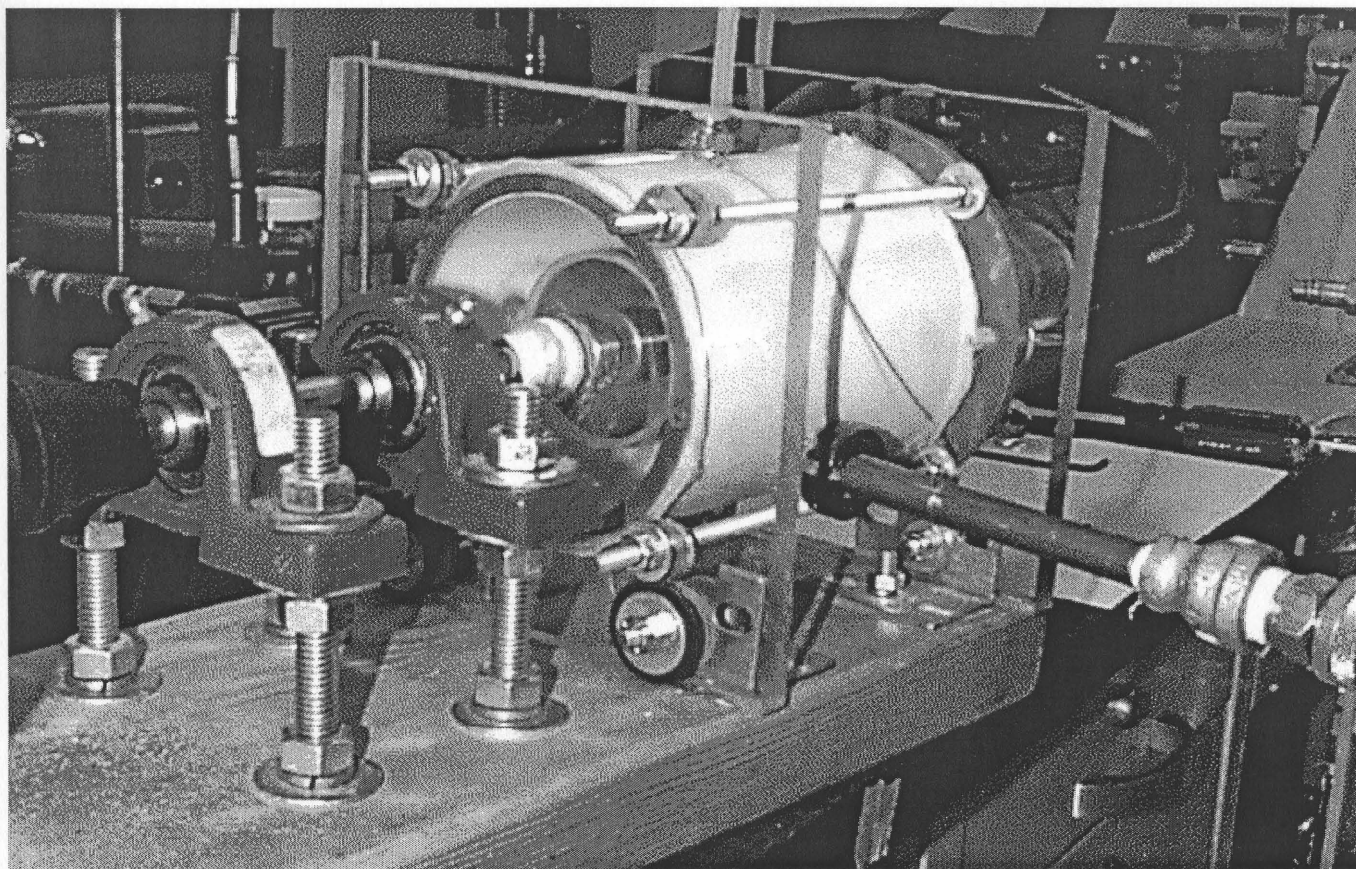


Figure 3.3: Photographic image of rotating fluidized bed coater

tangentially such that the fluidization air enters the distributor radially. The distributor has a radius of 2.9 cm and a length of 8.7 cm. Both slotted and sintered metal distributors were used, but the fluidization curves achieved were better with the sintered metal distributor, which is also substantiated by Quin et al [3]. The slotted distributor is

4.9 square cm, resulting in an open area of 93.1 square cm. The sintered metal distributor is a cylinder made from type 316 low carbon stainless steel powder, which is sintered together in an inert environment. The average pore size of the sintered metal distributor is 55  $\mu\text{m}$ . In the slotted distributor only a fraction of the particles get fluidized because of the metal webs, so the experimental superficial minimum fluidization velocity is much lower than the theoretical minimum fluidization velocity. Also, the experimental pressure drop is lower than the theoretical pressure drop. The open area of the slotted distributor is 93.1 square cm whereas the total area is 151.3 square cm, i.e., 60% of the total particles are fluidized. This is also quantified by Figure 3.4 and 3.5 where it can easily be observed that using the slotted distributor we have a lower pressure drop than with the sintered metal distributor. It can also be observed from the figures, that the minimum fluidization velocity for the slotted distributor is lower than that for the sintered metal under the same conditions of operation.

Qain et al [3] have also observed a hysteresis loop using a slotted distributor, with increasing and then decreasing gas velocity. A sudden fall in the pressure drop after the critical fluidization velocity is reached at high rpm was also observed with the slotted distributor. So considering all the above factors, the use of a slotted distributor was ruled out. The sintered metal distributor is placed within the chamber and rotates on its horizontal axis with the help of a variable DC motor. The distributor is connected to the motor with a solid shaft. The motor runs at speeds between 0 to 1725 rpm creating a centrifugal force in the range of 0 to 1000g.

The pressure drop is measured with a U-tube manometer in mm H<sub>2</sub>O. At low rotating speeds, when it is practically impossible to measure the pressure drop at low gas velocities, a micro manometer is used to measure the pressure drop. The micro manometer uses alcohol with a specific gravity of 0.8 as the manometer fluid, to give the pressure drop in terms of mm H<sub>2</sub>O. The manometer has one line inside the chamber and one attached to the exhaust area. The powder is weighed and added to the distributor manually. The exhaust system is made of acrylic and connected to the hood.

Plot of  $\delta P$  versus  $U$  with slotted distributor for cellulose at 1000 rpm and  $F=0.5$

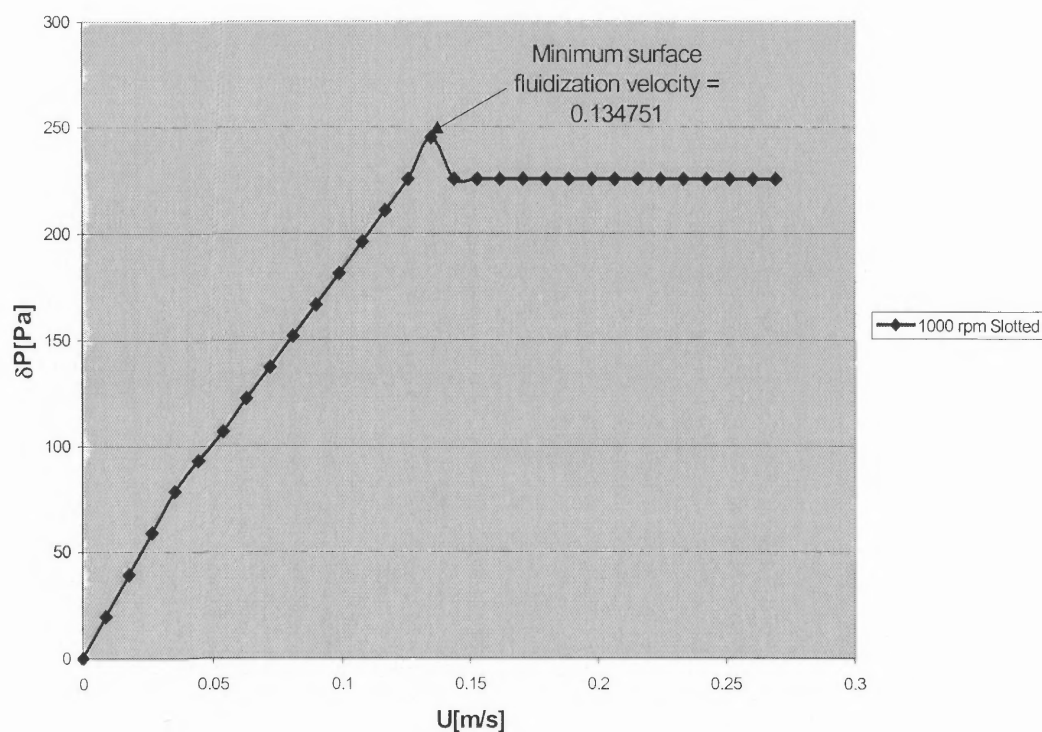


**Figure 3.4:** Experimental plot of pressure drop versus superficial velocity for slotted distributor



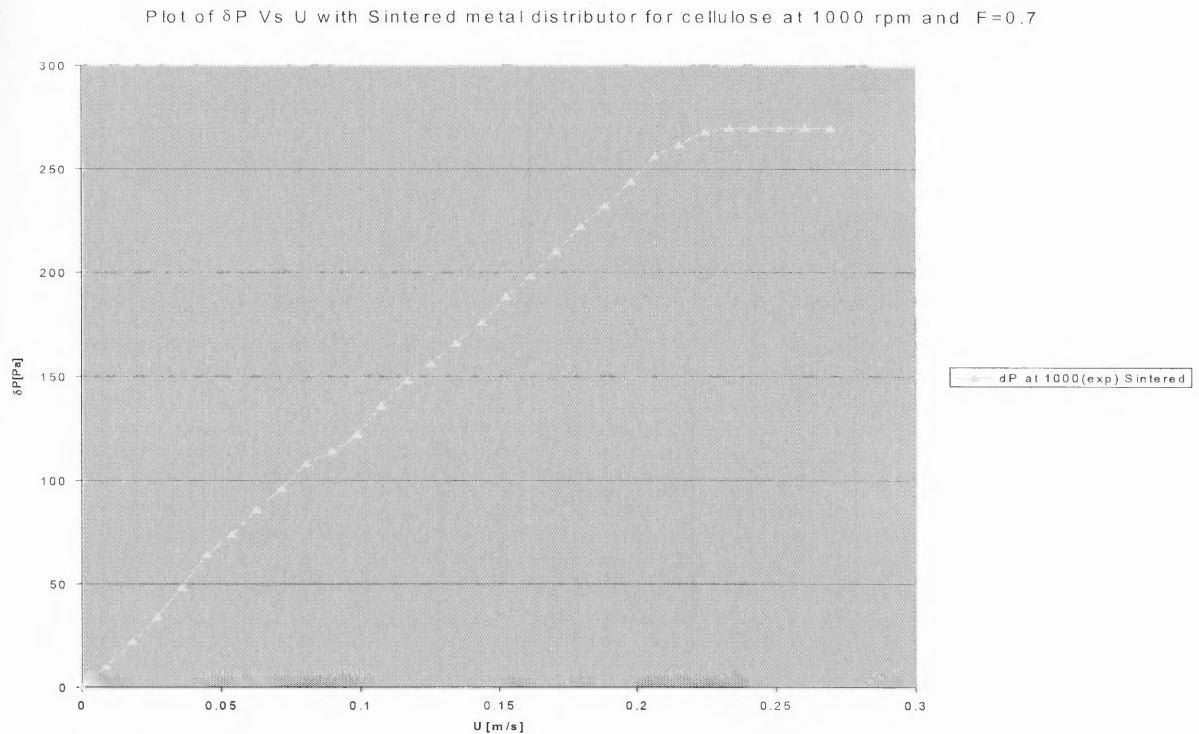


**Figure 3.5:** Experimental plot of pressure drop versus superficial velocity for sintered metal distributor

### 3.2.2 Granulation Experimental System

The schematic diagram of the experimental apparatus is shown in Figure 3.6. Here again we have a rotating fluidized bed, which is comprised of an outer chamber with a radius of 15 cm. and a length of 25 cm. The air is sent into the chamber tangentially and the fluidization air enters the distributor radially. The distributor was chosen as sintered metal because of the reasons mentioned above. The dimensions of the distributor are 5.08 cm in radius and 15.24 cm in length. The distributor is connected to a motor with a hollow shaft, which is connected to a source of a high-pressure air supply. A reverse puff



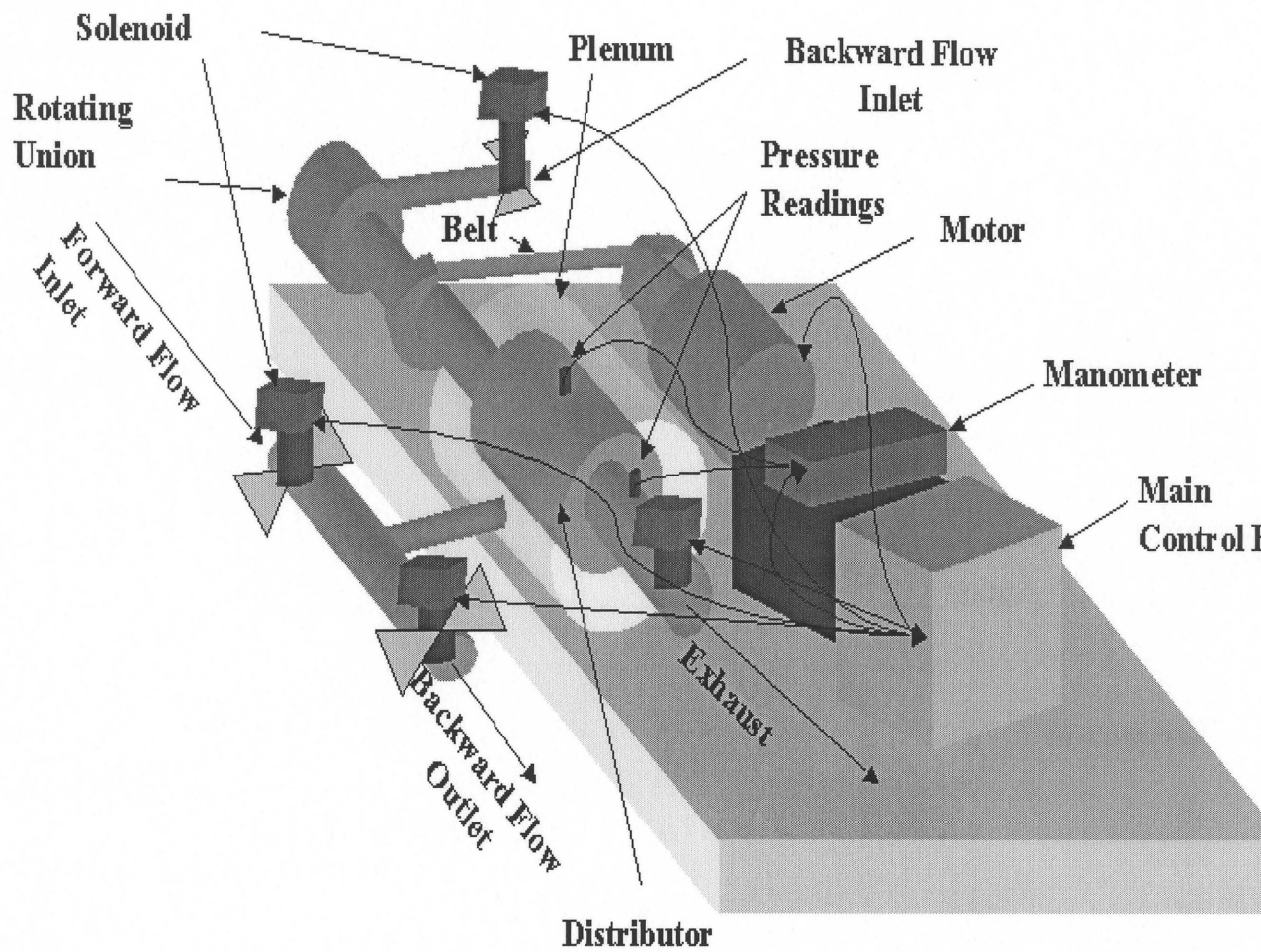


**Figure 3.6:** Schematic diagram of rotating fluidized bed granulator

of air is sent through the shaft radially into the distributor at very high pressure. An AC inverter motor, which can run from 0 to 1520 rpm, is used as it allows running high forward fluidization air velocities. Here we have pressure sensors and rotameters connected to the equipment. These sensors are connected to the exhaust area and into the plenum chamber to measure the pressure drop across the bed. The rotameters are connected to the inlet of the fluidization air. The solenoids are connected to the inlet and outlet of both the forward fluidization air and the reverse pulse to obtain cyclic fluidization.

### **3.3 Experimental Procedure**

The first requirement for working with any powder/powder system is to calibrate the bed for that specific powder, whether it is being used as a coater or a granulator. To calibrate the RFB, a manometer was used to measure the pressure drop and a rotameter was used to measure the gas flow rate.

The calibration was done by first running the empty distributor at the rotating speed at which the experiment is to be performed, with the pressure drop being measured at different flow rates. This speed was referenced as the calibration speed. The amount of powder was then weighed, with this weight being referenced as the calibration weight. This powder was then added to the distributor and the motor was run at the calibration speed. The pressure drop was measured for increasing gas flow rate. The difference

between the pressure drops of the filled and the empty distributors was recorded and this difference was plotted against the superficial gas velocity, which was obtained by dividing the gas flow rate by the area of the distributor. The graphs obtained are similar to that, shown in Figures 3.4 and 3.5.

### **3.3.1 Coating Experimental Procedure:**

From the calibration graphs, the value of average minimum fluidization velocity was determined. A weighed amount of host particles equal in weight to the calibration weight was added to the distributor. Guest particles equivalent to around 5% of the calibration weight are added to the distributor. The exhaust was fitted onto the bed, and the motor was then run for 2-3 minutes. The gas flow rate was set to 1.5-2 times the average minimum fluidization velocity until the powder starts flowing out. The experiment was run at this flow rate for some time (optimum time: 40 minutes). The motor was stopped and the powder was taken out and weighed. The difference in the weight before the run (sum of host and guest weight) and after the run (total weight of the coated material) gives the loss in powder, which averaged between 0-15% depending on the fines in the powder and the density of the powder.

### **3.3.2 Granulation Experimental Procedure:**

As in the coating procedure, the RFBG was calibrated for a specific powder, and then the value of the average minimum fluidization velocity was determined from the graph obtained in the calibration. Powder weighing the same as the calibration weight was put into the distributor. The exhaust was fitted and the motor was run at the calibrated speed

for 1-2 minutes. The forward gas flow rate was set to 1.5 times the average minimum fluidization velocity. The forward pulse rate was set at 15 seconds, which fluidizes the bed while the reverse pulse rate was set at 5 seconds, which compacts the powder. When the forward pulse was on, the reverse pulse shuts down and when the reverse pulse was on, the forward pulse shuts down. There is a gap of 1 second between the two pulses of air supply to depressurize the bed. This cyclic procedure is used until granules are obtained. The granules are then taken out and their weight was measured. The difference between the weights before the run and after the run gives the powder loss, which should be as small as possible.

### **3.5 Methods to Analyze Coating and Granulation**

#### **3.5.1 Qualitative Analysis for Coating and Granulation– Scanning Electron Microscopy:**

The coating morphology was studied using Scanning Electron Microscopy (back scattering detector was used). The charging strength was 20 kV and the distance from which the beam was focused was 8 mm. Both coating and granulation was interpreted by observing the photographs obtained through SEM. For coating, photographs were taken both before and after the ultrasonication was done.

### **3.5.2 Qualitative Analysis for Coating–Ultrasonication:**

This test determines the strength of the coating. It is a very strong physical test to determine the coating strength. In this test, the coated material is placed in a mesh basket and the basket was dipped in water in an ultrasonic bath. The bath used was run at a frequency of 60 Hz for 1 min. The basket was then dried in an oven at 60°C for 48 hours and the powder taken for SEM again.

### **3.5.3 Quantitative Analysis for Coating- Moisture Sorption:**

This moisture absorption method [19] is used for cellulose only since cellulose has a tendency to absorb moisture. A weighed quantity of cellulose (1 gm) was converted into a tablet using a Universal Testing Machine, at a force of 100 kN. These tablets were then dried in an oven for 48 hours at 80°C and weighed. They were then kept in a dessicator maintained at a relative humidity of 100%. To achieve 100% relative humidity, water was poured in the dessicator below the plate on which cellulose tablets were kept. Then the dessicator was put under vacuum for 60 minutes. The change in weight was measured every 24 hours and was plotted against time.

## **CHAPTER 4**

### **RESULTS AND DISCUSSIONS**

In this chapter, the results of fluidization, dry coating and granulation in the rotating fluidized bed is presented and an interpretation of these results, in light of the forces and kinetics discussed in chapter 2, is done. The discussion includes elaboration of the results obtained on fluidization, coating and granulation in the rotating fluidized bed. In Section 4.1, the topic of fluidization deals with the deviation of the pressure drop from theoretical values, based on the theoretical analysis by Kao et al [2] discussed in Section 4.1. Results of dry coating are shown in Section 4.2, wherein the system in which coating is achieved is shown and explained. Results of dry granulation are presented and discussed in Section 4.3, wherein the most suitable conditions for granulation are studied.

#### **4.1. Discussion of Fluidized States**

##### **4.1.1 Packed Bed Region**

In the plot of pressure drop versus gas flow velocity, the packed bed region is shown by the linear part of the curve. This region depends on various factors such as the type of distributor, radius of the distributor, length of distributor, sphericity, voidage and mass of particles inside the distributor. Generally, radius and length of the distributor and

mass of the particles is fixed for a particular system, so the packed regime is dependent on voidage and particle shape, e.g., sphericity, which are also interrelated. The value of voidage is between 0.41 to 0.44 for most of the particle systems studied in the rotating fluidized bed. The point where the packed bed regime ends is known as the *surface minimum fluidization velocity*. At this point, the first layer of bed fluidizes.

#### 4.1.2. Fluidized Bed Region

As the air pressure is increased beyond the minimum surface fluidization velocity, the next layer gets fluidized until a point is reached at which the whole bed is fluidized. This point is the *critical fluidization velocity*. Beyond this point, the whole bed is fluidized and the pressure drop across the bed is dependent on the mass of the bed and the length of the bed. Since the length of the distributor is fixed, hence the only factor that affects the pressure drop in this region is the mass of the bed. But it has been observed that the experimental pressure drop in this region is less than the theoretical pressure drop calculated from Equation 3.8. The bed was calibrated for cellulose, PMMA and glass beads. An error of 30% for fibrous cellulose (see Figure 4.1), 24 % for PMMA (see Figure 4.2), 20% for spherical cellulose (see Figure 4.4) and 13-15% for glass beads (see Figure 4.3) was observed. This behavior is accounted for by introducing a factor,  $F$ , such that:

$$\text{Experimental Drop} = \text{Theoretical Drop} * F$$

The factor  $F$  is dependent on various other factors, such as the loss of particles during the operation of the experiment. The loss noted is as follows:

1. 11% for fibrous cellulose (Grade: AVICEL PH 200)

2. 2-3% for PMMA (Grade: Polysciences Mol wt 75000, 200  $\mu\text{m}$ )
3. 2% for spherical cellulose (Grade: AVICEL CP 230)
4. 5% for glass beads (Grade:).

This loss could be due to spillover while the bed was filled or due to powder lost with the fluidization air.

The second factor that  $F$  is dependent on is gravity. As we see in Figure 4.5, the force of gravity on the particles at the top of the bed act against the centrifugal force whereas at the bottom it acts towards the centrifugal force. This can affect the pressure drop by 5%. The third factor is non-uniformity of the bed along the axis as seen in Figure 4.6. There are more particles near the back plate as the bed is tilted while the powder is filled in, so we have a thicker bed at the back than in front. Moreover, the bed is non-uniform overall, and this can affect the pressure drop by 10 %.

The type of particles also affects the pressure drop. The type of particle includes the number of fines present, the shape of the particle and the size distribution (For example, in the case of cellulose, we have two types of cellulose. One type is fiber shaped of size 180  $\mu\text{m}$  with an aspect ratio of 4 to 5, bulk density 350  $\text{Kg/m}^3$  and of wide size distribution, thus giving an  $F$  factor of 0.7. The other type is spherical of size 230  $\mu\text{m}$ , density 750  $\text{Kg/m}^3$  and of narrow size distribution, thus giving an  $F$  factor of 0.8).



Together these four factors account for an average drop of around 20% in pressure compared to theoretical value giving an F factor of 0.8. So to match the theoretical value with the experimental value, the weight of the particles is multiplied by the correction factor, F. The theoretical graph was obtained by writing a C++ program (See Appendix 1) and taking the output in Microsoft Excel (See Figures 4.1, 4.2, 4.3, 4.4). The voidage  $\varepsilon$  in the figures was obtained comparing the theoretical graphs with the experimental graph, by the method of trial and error.

For cellulose, it has been observed that there is a reduction in the moisture content of the cellulose particles after running the particles in the bed. Cellulose has a tendency to absorb moisture, and unprocessed cellulose has moisture content of approximately 5%. The reduction in moisture content is dependent on the operating condition. For example, the reduction when the bed was run at 1500 rpm for 40 minutes in the fluidized state was 3.2%. After processing any particles in the bed, an increase in density was observed. But the density change with cellulose was nil, which can be attributed to the loss of water, which has a higher density than cellulose and compensated for the increase in the density which took place after processing the cellulose in the bed. This explains to some extent, a greater loss of weight in case of cellulose. Other reasons can be wide size distribution and a large aspect ratio, which can result in the powder moving out of the bed when the bed is completely fluidized.

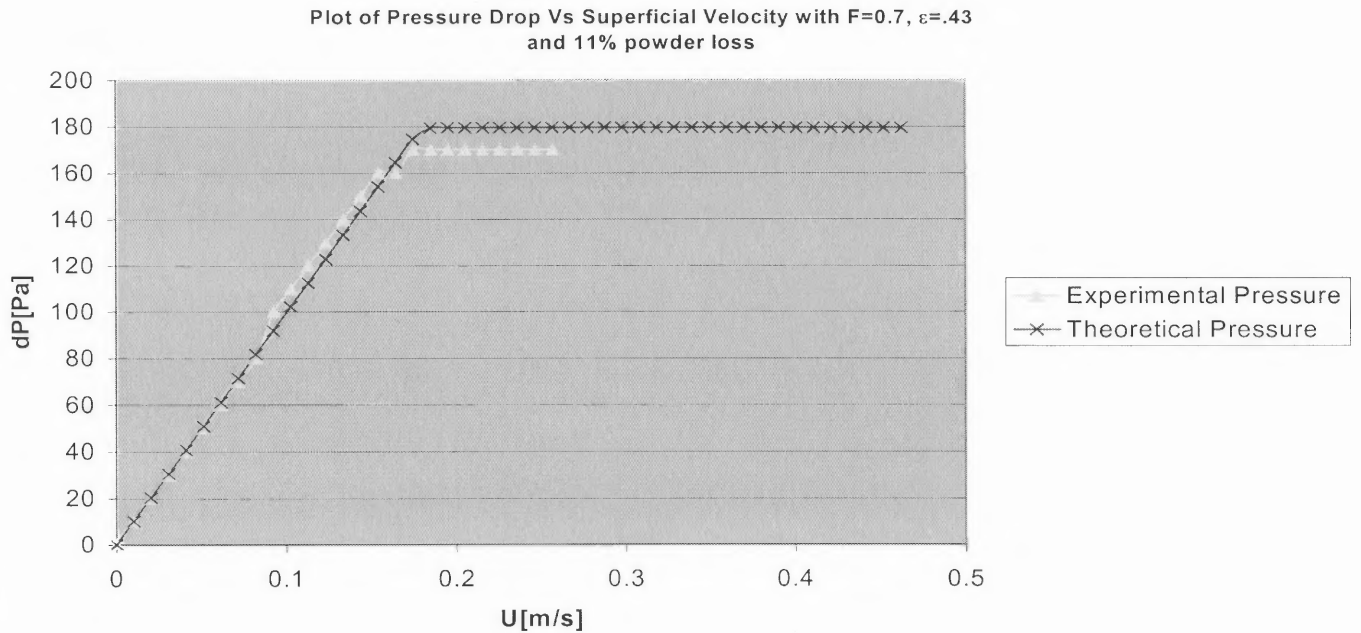


**Figure 4.1:** Plot of Pressure Drop versus Superficial Velocity for fibrous microcrystalline cellulose at 800 rpm.

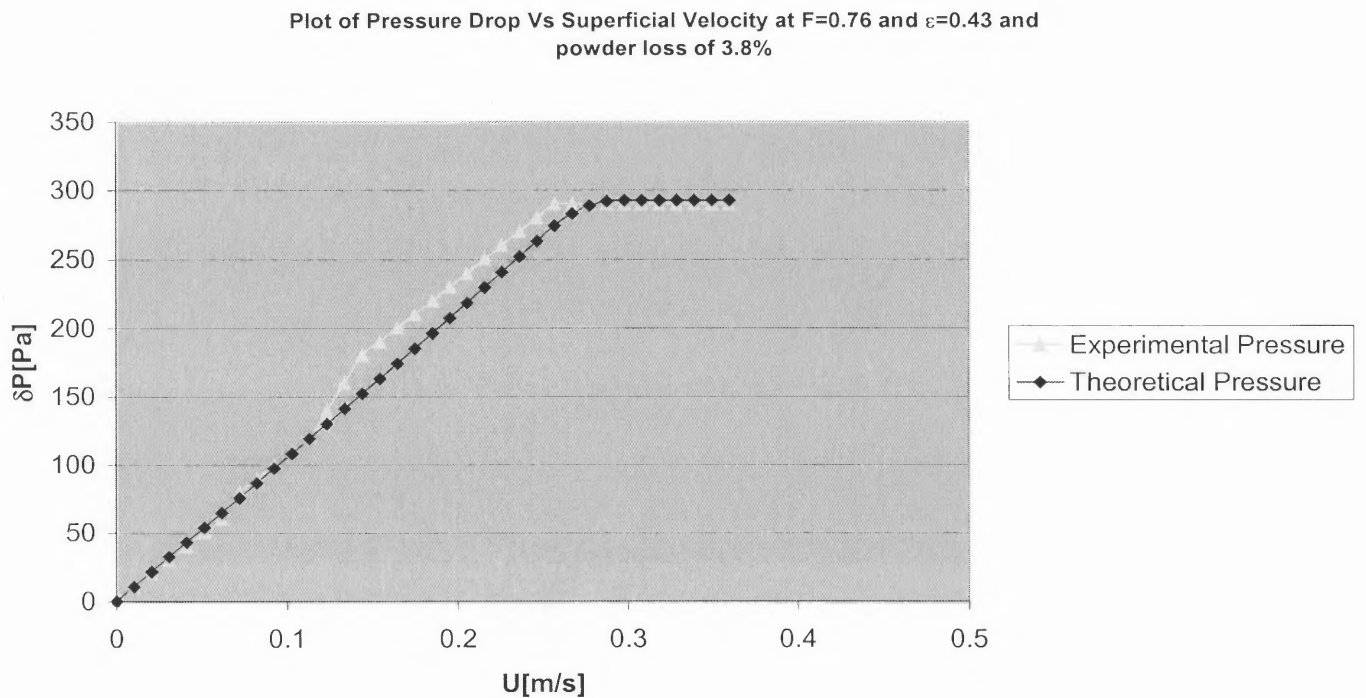


**Figure 4.2:** Plot of Pressure Drop versus Superficial Velocity for PMMA at 800 rpm.

Plot of Pressure drop Vs Superficial velocity at  $\varepsilon=0.43$ ,  $F=0.87$  and powder loss of 3 %.

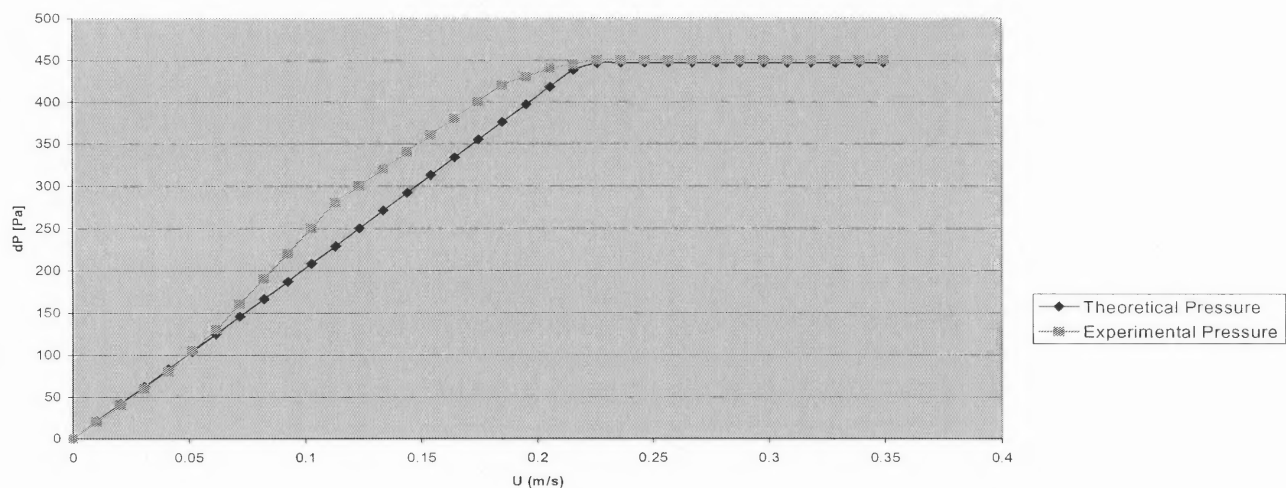


**Figure 4.3:** Plot of Pressure Drop versus Superficial Velocity for Glass beads at 800 rpm

Plot of Pressure Drop Vs Superficial Velocity at  $e=0.43$ ,  $f=0.8$  and 2% powder loss

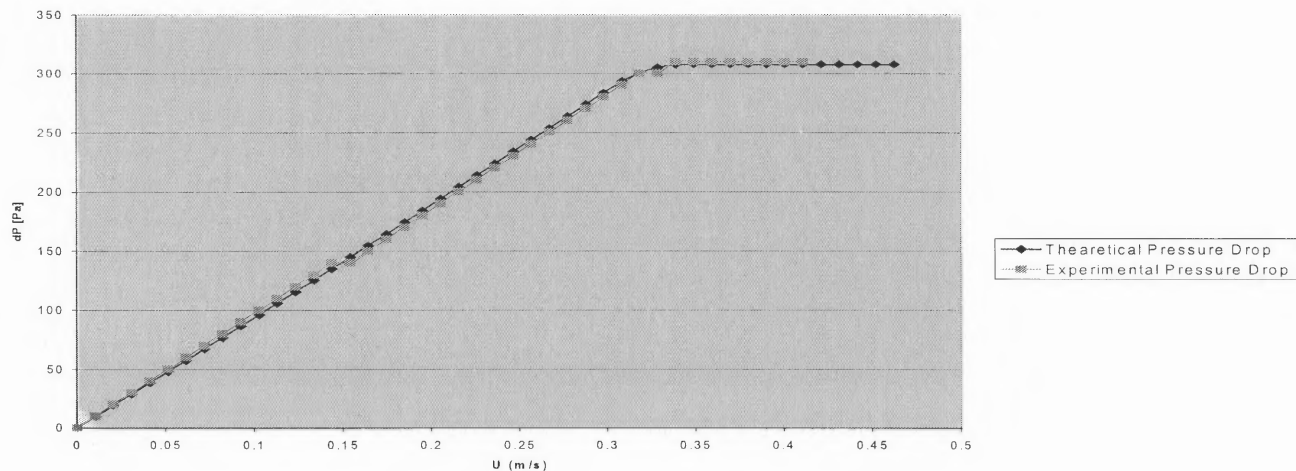


**Figure 4.4:** Plot of Pressure Drop versus Superficial Velocity for Spherical Cellulose at 800 rpm

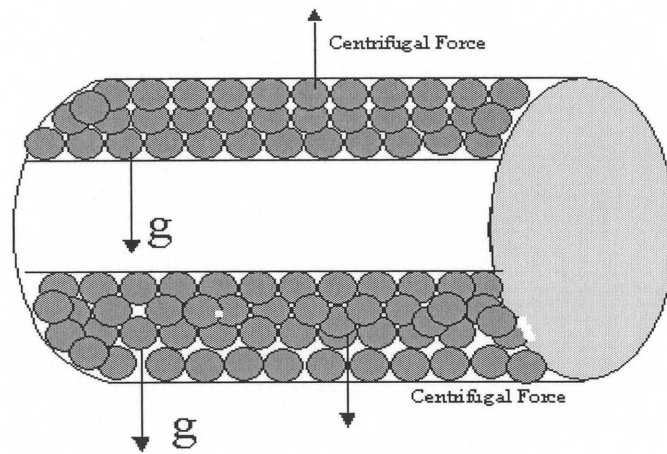
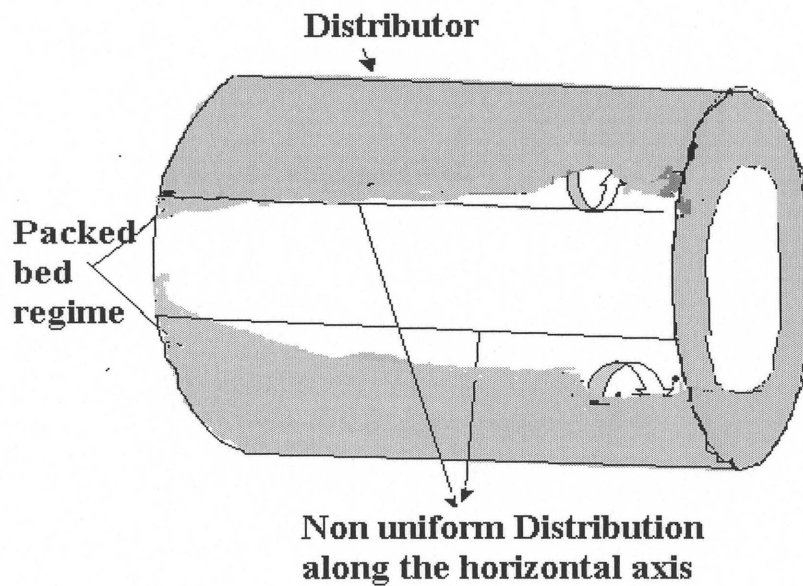


**Figure 4.5:** The relative effect of gravitational force on the particles at top and bottom resulting in the difference in the pressure drop



## 4.2 Discussion of Rotating Fluidized Bed as a Coater

In previous studies, it has been established that the coater deagglomerates the guest particles for coating to take place. It has been observed that the rotating fluidized bed cannot deagglomerate the guest particles by itself, and no additional method was employed to deagglomerate the particles before entering into the rotating fluidized bed. So very little or no coating was achieved with FIBROUS CELLULOSE/ALUMINA. But still some good quality coating was achieved in the rotating fluidized bed with some systems like PMMA/ALUMINA or SPHERICAL CELLULOSE/ALUMINA, which has made the rotating fluidized bed as a coater, an interesting topic for research. An attempt has been made to explain this phenomenon using the force and kinetic model discussed in Chapter 2. It is clear, from the above, that forces involved in the RFB are not very strong so the RFB can be adjudged as a soft coater and will find applications where the coating can easily be removed after its job is done. It can also be used with polymeric materials where strong forces can change the structural integrity.

Most of the experimental study for RFBC has been qualitative, since it was very difficult to quantify the results because of the inherent limitations of the system. In a rotating fluidized bed, some of the particles were lost with the fluidization air. It was very difficult to determine which particles, whether guest or host, were lost since the percentage of particles lost was more than the percentage of guest particles added and hence it was difficult to keep track of the remaining guest particles in the system. This made quantitative study very difficult. The test of ultra-sonication is a good

representation of the strength of the coating. In this test, we observe the coated particles under the SEM, before and after performing the ultra-sonication on the coating.

The results from the rotating fluidized bed coating device are in the form of SEM pictures, EDX mapping, moisture absorption curves for cellulose and are as follows:

### PMMA/ALUMINA

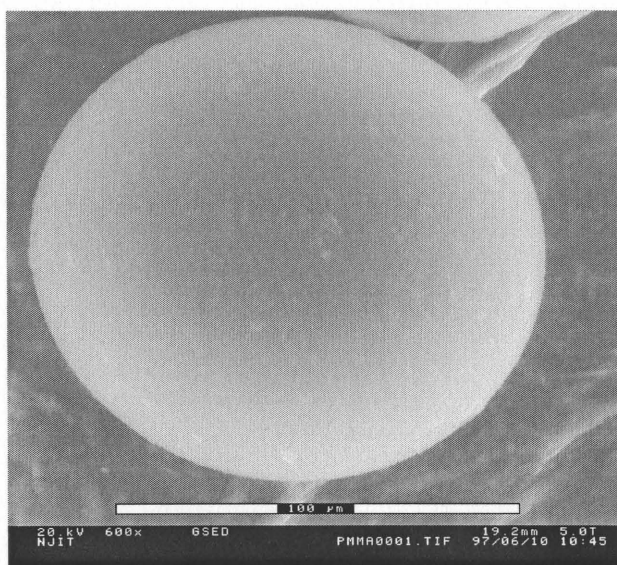


**Figure 4.7.1:** Uncoated PMMA

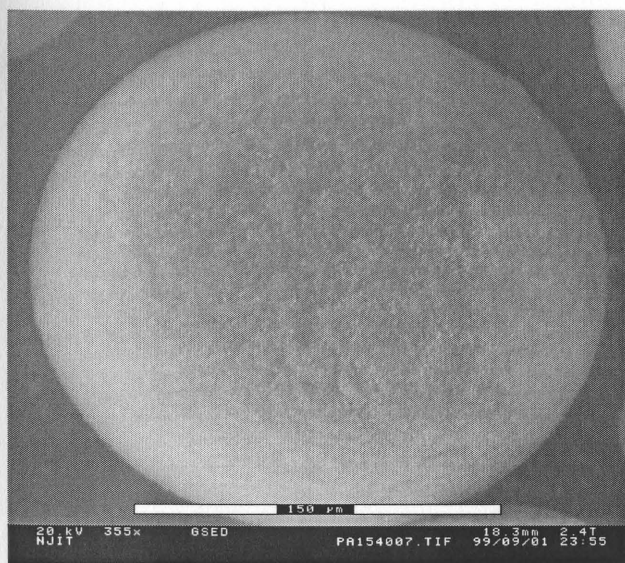


**Figure 4.7.2:** PMMA/Alumina Coating

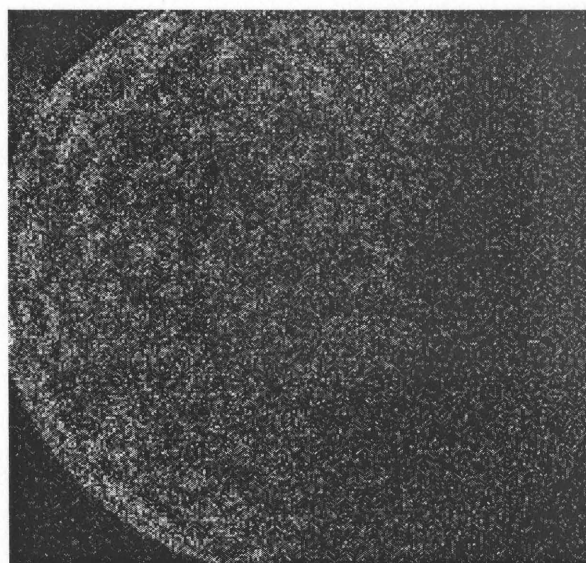


**Figure 4.7.3:** Aluminum EDX Mapping



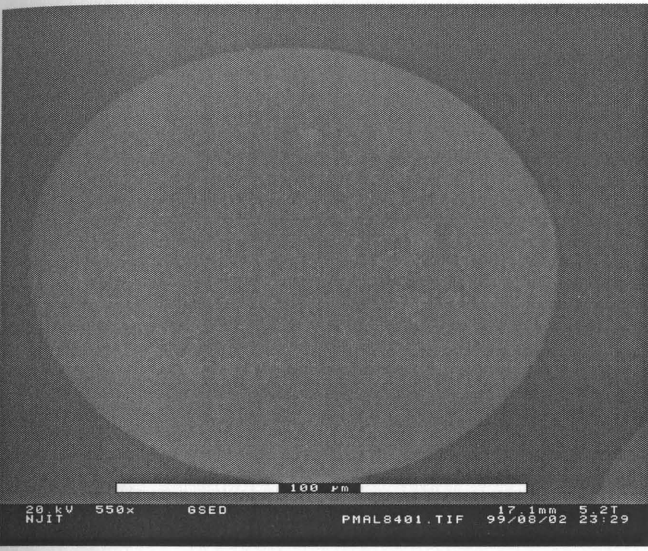


**Figure 4.7.4:** PMMA/Alumina Coating at 800 rpm before Ultrasonication

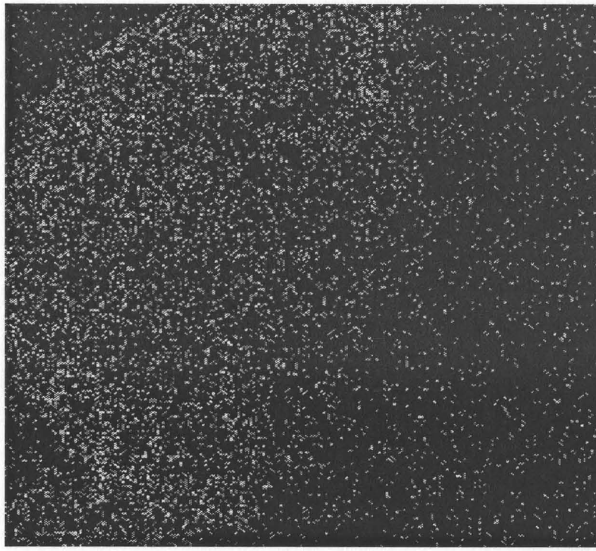


**Figure 4.7.5:** Aluminum EDX Mapping of RFBC Coated PMMA/Alumina at 800 rpm

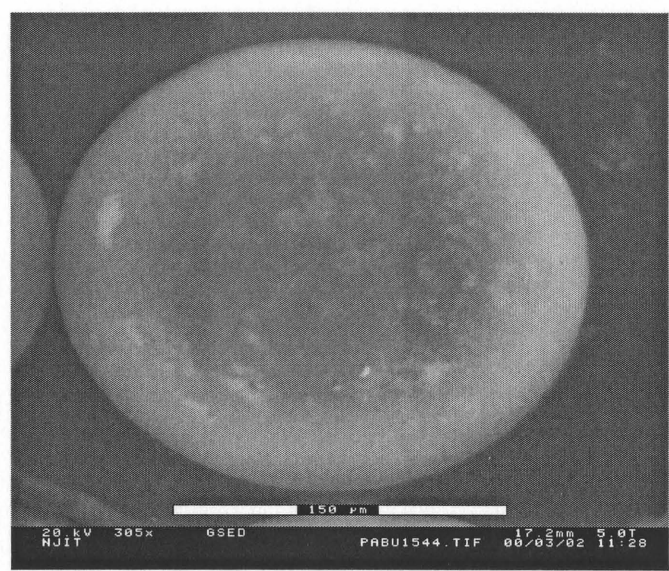


**Figure 4.7.6:** PMMA/Alumina Coated at 1500 rpm after Ultrasonication

## PMMA/SILICA

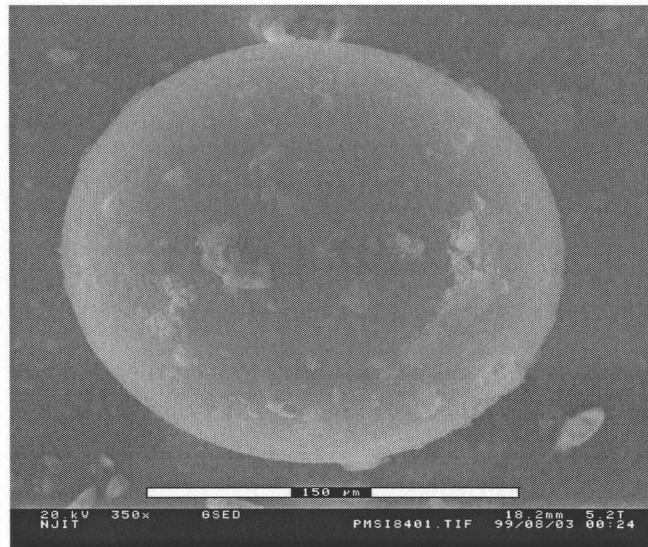


Figure 4.8: PMMA/Silica

## SPHERICAL CELLULOSE/ALUMINA

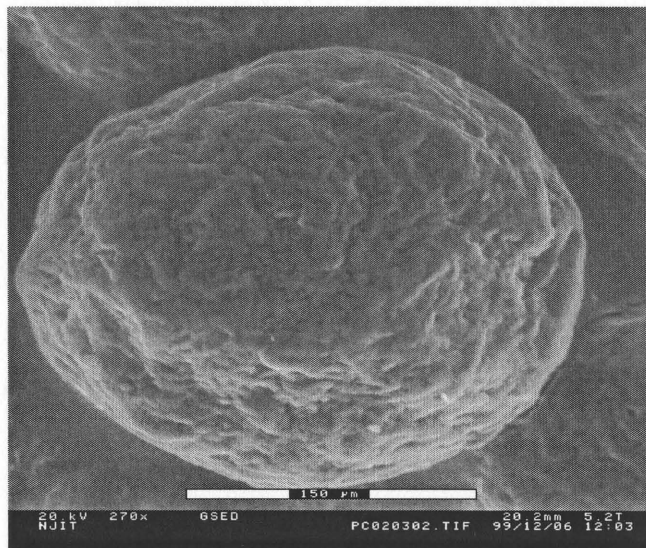
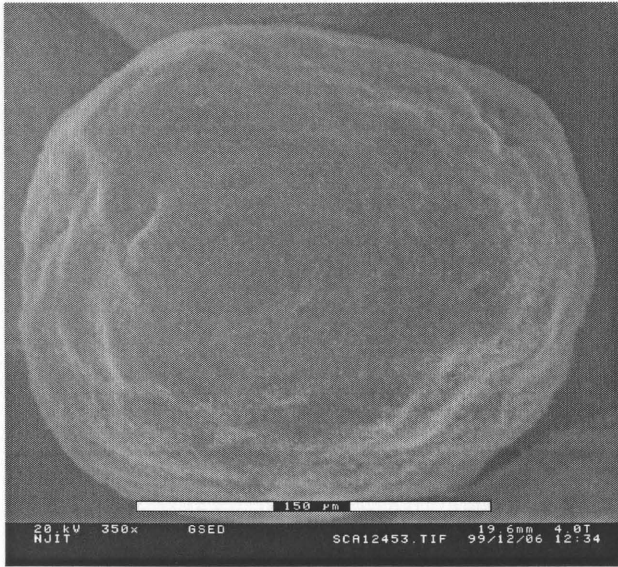
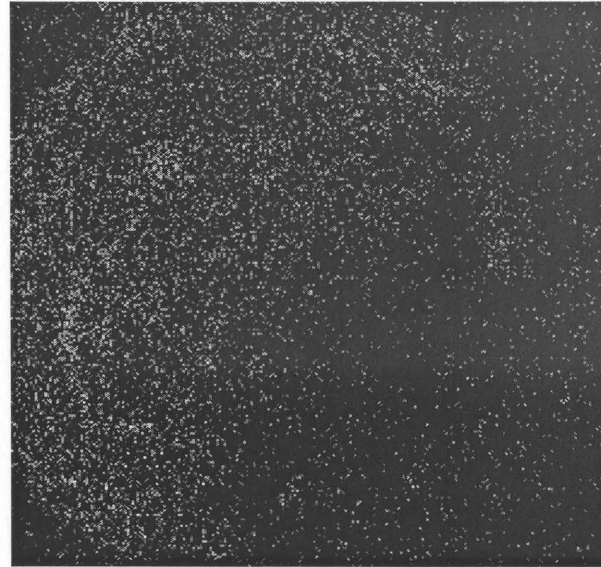


Figure 4.9.1: Uncoated Spherical Cellulose





**Figure 4.9.2:** Spherical Cellulose/Alumina Coated at 1200 rpm before Ultrasonication



**Figure 4.9.3:** Aluminum EDX Mapping of Spherical Cellulose/Alumina at 1200 rpm

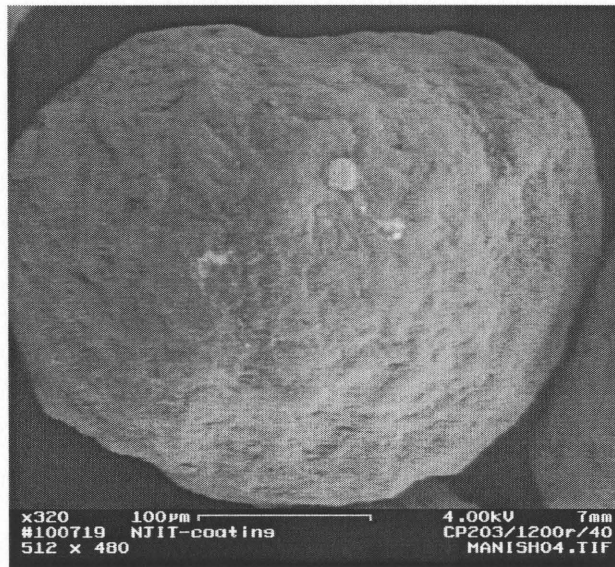


**Figure 4.9.4:** Spherical Cellulose/Alumina Coating at 1200 rpm after Ultrasonication

## FIBROUS CELLULOSE/ALUMINA

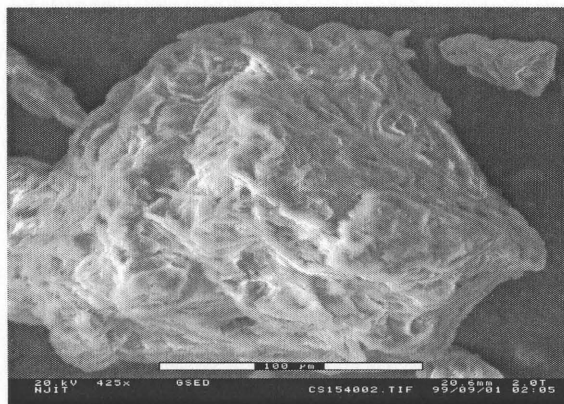


**Figure 4.10.1:** Uncoated Fibrous Cellulose

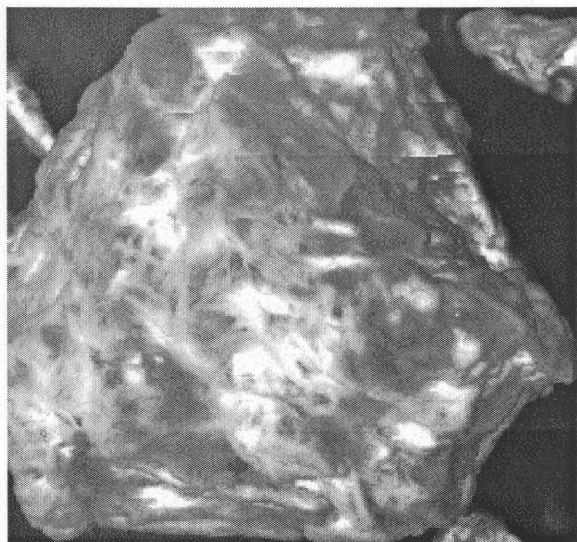


**Figure 4.10.2:** Fibrous Cellulose/Alumina Coated at 1500 rpm before Ultrasonication



**Figure 4.10.3:** Aluminum EDX Map of Fibrous Cellulose/Alumina at 1500 rpm

## AGGLOMERATION OF ALUMINA DURING COATING PROCESS

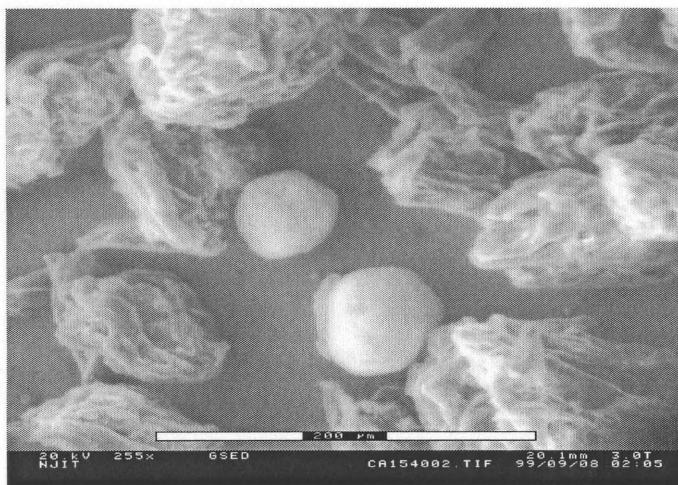


**Figure 4.11.1:** SEM showing a wide view of coated cellulose with agglomerates of alumina sitting with cellulose.



**Figure 4.11.2:** Agglomerates of Alumina of size 80 μm.



**Figure 4.11.3:** Aluminum EDX mapping of agglomerated alumina showing 80 μm particles in adjoining picture of alumina.





**Figure 4.11.4:** Agglomerates of Alumina of average size 50  $\mu\text{m}$ .

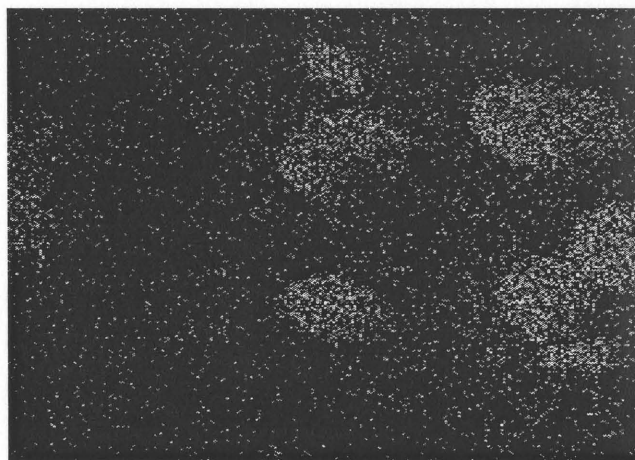


**Figure 4.11.5:** Aluminum EDX mapping agglomerated alumina sitting along with coated cellulose

## MOISTURE ABSORPTION CURVE FOR CELLULOSE

**Absorption Isotherm for Fibrous Cellulose as a function of time elapsed for Uncoated Cellulose and the cellulose coated with alumina after running in RFB for different times.**

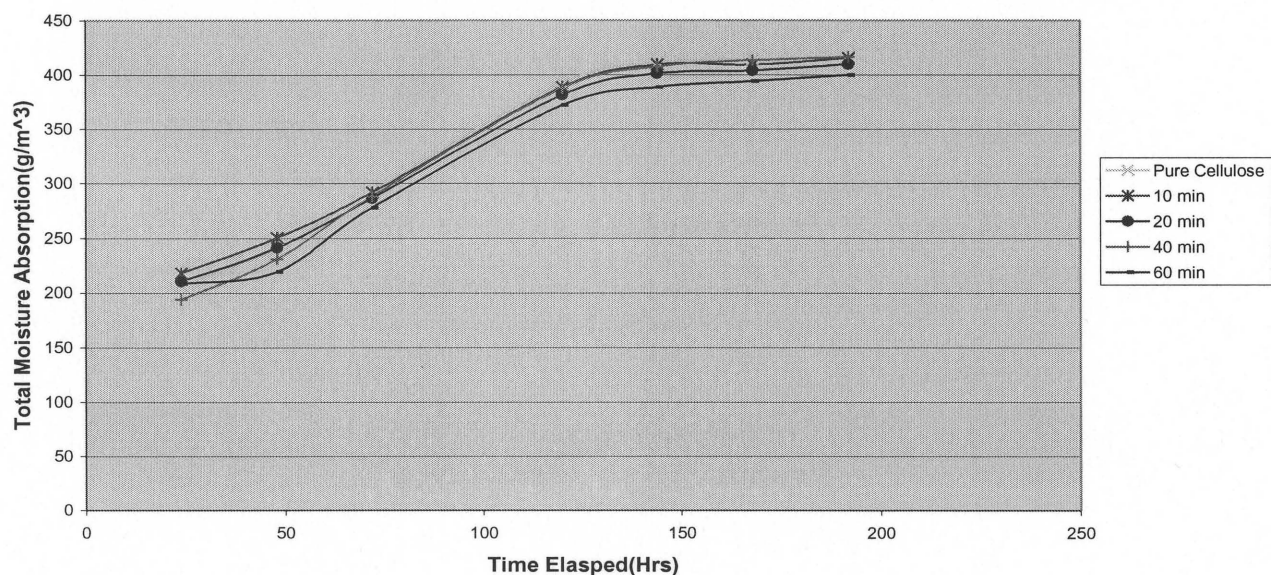


**Figure 4.12:** Absorption Isotherm for Fibrous Cellulose after Alumina Coating

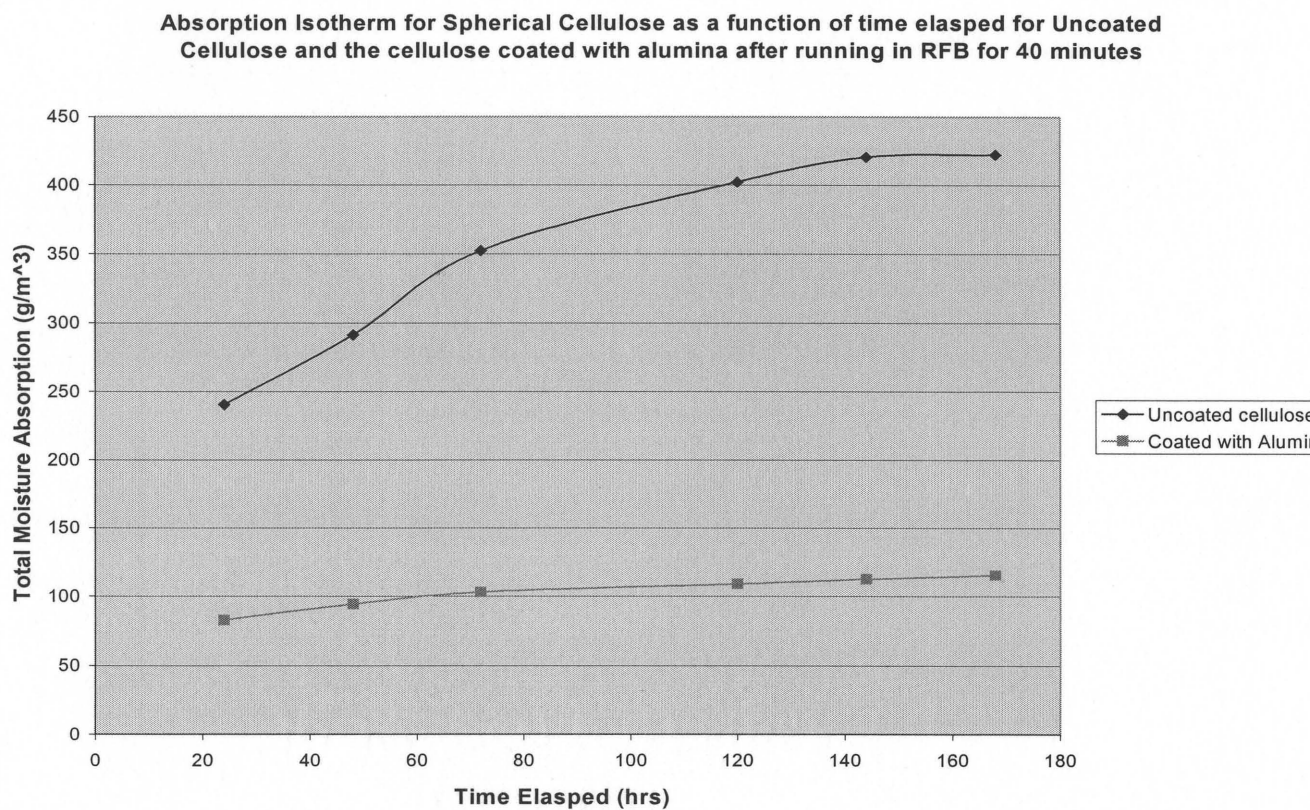


**Figure 4.13:** Absorption Isotherms for Spherical Cellulose - Alumina coating.

**The following observations have been made from the above figures:**

- ◆ Good and uniform coating was observed with the PMMA-Alumina system as shown in Figure 4.7.2. This is proved by EDX mapping which shows a very dense mapping of aluminum in Figure 4.7.3. Also, Figure 4.7.6 shows that the strength of the coating was good because even after sonication at 60 Hz for one minute, some Alumina was left on the PMMA particle. Typical properties of PMMA particles are 200  $\mu\text{m}$  size, 750  $\text{kg/m}^3$  density.
- ◆ Good but discrete coating was observed with the spherical cellulose-alumina system as shown in Figure 4.9.2. The aluminum mapping in Figure 4.9.4 shows a moderately dense mapping of aluminum for spherical cellulose. The strength of coating on spherical cellulose was poor as is observed from SEM pictures taken after sonication and shown in Figure 4.9.4. Typical properties of spherical cellulose are 230  $\mu\text{m}$  size, 900  $\text{kg/m}^3$  density.
- ◆ Very poor coating was observed with the fibrous cellulose-alumina system. As is observed in Figure 4.10.2 and 4.10.3, both the SEM and EDX indicate that the coating was poor and much below expectation. The reason for the phenomenon is explained later using the kinetic model discussed in Chapter 2. Typical properties of fibrous cellulose are 180  $\mu\text{m}$  size, 1:4 aspect ratio and 350  $\text{kg/m}^3$  density.
- ◆ Absorption Isotherms for Fibrous Cellulose-Alumina shown in Figure 4.12 also show a very poor coating. A good coating will show a sizable reduction in moisture absorption, which was not observed. The reason for reduction in the absorption is that the area of the cellulose that is coated with alumina will not

absorb moisture, and if poor coating takes place, no sizable reduction in absorption is observed.

- ◆ Absorption Isotherms also justify the observation that some coating is achieved with spherical cellulose whereas negligible coating was achieved with fibrous cellulose. From Figure 4.13, it is obvious that there is sizable reduction in moisture absorption when spherical cellulose is processed in the RFB for 40 minutes. This indicates that the spherical cellulose is coated with alumina.
- ◆ PMMA/Silica system (Figure 4.8) gave a very poor coating, so use of silica as a guest for other host particles was ruled out.
- ◆ Agglomerates of guest particles were observed along with the coated host. Figure 4.11.1 shows that big agglomerates are sitting with the host particles. This is further proved by EDX mapping in figure 4.11.5.
- ◆ Agglomerates of alumina were more pronounced with fibrous cellulose-alumina than with spherical cellulose-alumina or PMMA-alumina system. The reason for this could be the fact that since the coating is not taking place in fibrous cellulose-alumina system, the alumina particles must be colliding among themselves and agglomerating.
- ◆ An increase in the size of agglomerates was also observed. For example, alumina particles of size up to 80 $\mu$ m were observed as shown in Figures 4.11.2 and 4.11.3 but the most agglomerates observed were of average size of 50  $\mu$ m.

The above observations are in accordance with the model for particle-particle interaction in coating, described in Section 2.5. Based on these observations, it can be said that although the guest particles are not de-agglomerating, a good coating is still achieved in some cases, which means that the agglomerates of guest particles strike either the host or other guest particles as agglomerates only. A uniform coating in the case of PMMA means that when another host particle strikes the coated host, the guest particles redistribute. A discrete coating in the case of spherical cellulose-alumina means that if the coating is difficult, some agglomerates get coated onto the host and others collide among themselves to form bigger agglomerates. But negligible coating and formation of big agglomerates in the case of fibrous cellulose-alumina coating means that the only phenomenon taking place is agglomeration of guest particles.

An attempt has also been made to understand and find the resultant velocity with which one particle strikes the other particle and also the impact velocity range required for the coating to take place. This attempt is based on the kinetic model described in Section 2.6. In this model, first, the forces involved are calculated from the experimental values for different parameters like the rotating speed of 1500 rpm for PMMA and fibrous cellulose and 1200 rpm for spherical cellulose. The superficial air velocity was taken as 1.5 times the minimum fluidization velocity. The above values of rotating speed and superficial velocity factor were used because they were the maximum possible values. Various physical properties and experimental values of the parameters used for different material are given in Appendix 2. A sample calculation is given in Appendix 3. The graph for the agglomerate size range and the velocity range, which



satisfies the condition for coating in the case of both PMMA and fibrous cellulose, is given in Appendix 4. The graph showing the plot of coating criteria as a function of  $E$ ,  $\gamma$  and  $A_{12}$  is also given in Figure A6 in Appendix 4.

The mechanical properties like Young's modulus, Poisson's ratio, Yield strength and Hamaker constant of spherical cellulose were not available either from the manufacturer or in the literature. So no calculations have been done for spherical cellulose.

The values for various forces and energies calculated as per the sample calculations done in Appendix 3 are tabulated below. In Table 4.1, the case of Alumina colliding with PMMA, both as an individual or agglomerate, and also, two PMMA particles colliding with each other, is considered. Table 4.2 considers the case of individual Alumina particles colliding with each other, or an agglomerate of Alumina colliding with another agglomerate during the PMMA coating. In Table 4.3, the case of Alumina colliding with Fibrous Cellulose, both as an individual particle or agglomerate, is considered. Table 4.4 considers the case of individual Alumina particles colliding with each other, or an agglomerate of Alumina colliding with another agglomerate during the fibrous cellulose coating.

**Table 4.1:** Various forces and energies involved in the collision of host and guest particles during PMMA/Alumina Coating.

| Case                          | PMMA-Agglomerated Alumina<br>(Agglomerate size) |   |   | PMMA- Individual<br>Alumina | PMMA<br>Alone                            |
|-------------------------------|---|---|---|-----------------------------|--|
|                               | 200 $\mu\text{m}$ -<br>10 $\mu\text{m}$         | 200 $\mu\text{m}$ -<br>20 $\mu\text{m}$ | 200 $\mu\text{m}$ -<br>30 $\mu\text{m}$ | 200 $\mu\text{m}$ – 700 nm  | 200 $\mu\text{m}$ -<br>200 $\mu\text{m}$ |
| Drag Force                    | 3.15E-08  | 8.31E-08                                | 9.46E-08                                | 2.48E-09                    | 6.31E-07                                 |
| Collision Force               | 5.19E-06  | 2.05E-05                                | 4.55E-05                                | 2.56E-07                    | 4.45E-02                                 |
| Centrifugal Force             | 7.42E-10  | 5.94E-09                                | 2.00E-08                                | 2.55E-13                    | 1.78 E-06                                |
| Van der Waal Force            | 5.39E-07  | 1.03E-06                                | 1.48E-06                                | 3.95E-08                    | 4.4 E-06                                 |
| Impact Force                  | 5.70E-07  | 1.09E-06                                | 1.55E-06                                | 4.17E-08                    | 3.25E-02                                 |
| Impact Velocity               | 0.107   | 0.105                                   | 0.105                                   | 0.2405                      | 0.104                                    |
| Limiting Velocity             | 0.002083  | 0.002083                                | 0.002083                                | 0.002083                    | 0.002083                                 |
| Impact Energy                 | 1.16E-14  | 9.20E-14                                | 3.09E-13                                | 2.06E-17                    | 2.74E-11                                 |
| Plastic Deformation<br>Energy | 1.12E-14  | 8.85E-14                                | 2.98E-13                                | 2.03E-17                    | 2.35E-11                                 |
| Rebound Energy                | 4.00 E-16                                       | 3.50E-15                                | 1.18E-14                                | 3.44E-19                    | 3.98E-12                                 |
| Adhesive Energy               | 8.03 E-15                                       | 1.90E-14                                | 3.09E-14                                | 2.45E-16                    | 3.54E-13                                 |

**Table 4.2:** Various forces and energy involved in collision of guest particle with another guest particle during PMMA/Alumina Coating.

| Case: Collision<br>between particles | Alumina alone | Agglomerated<br>alumina of 20 $\mu\text{m}$ |
|--------------------------------------|---------------|---|
| Drag Force                           | 2.48 E-09     | 6.31 E-08                                   |
| Collision Force                      | 6.01 E-08     | 5.39 E-05                                   |
| Centrifugal Force                    | 2.55 E-13     | 5.94 E-09                                   |
| Van der Waal Force                   | 2.55 E-08     | 7.29 E-07                                   |
| Impact Force                         | 2.77 E-08     | 7.86 E-07                                   |
| Impact Velocity                      | 0.205         | 0.105                                       |
| Limiting Velocity                    | 2.96 E-05     | 2.96 E-05                                   |
| Impact Energy                        | 1.50 E-17     | 9.19 E-14                                   |
| Plastic Deformation<br>Energy        | 1.50 E-17     | 9.19 E-14                                   |
| Rebound Energy                       | 4.25 E-21     | 5.01 E-17                                   |
| Adhesive Energy                      | 1.33 E-17     | 1.17 E-15                                   |

**Table 4.3:** Various forces and energy involved in the collision of host and guest particles during Fibrous Cellulose/Alumina Coating.

| Case                                  | Cell-Agglomerated Alumina<br>(Agglomerate size) |   |   | Cell- Individual<br>Alumina |
|---------------------------------------|---|---|---|-----------------------------|
|                                       | 180 $\mu\text{m}$ -<br>10 $\mu\text{m}$         | 180 $\mu\text{m}$ -<br>20 $\mu\text{m}$ | 200 $\mu\text{m}$ -<br>30 $\mu\text{m}$ |                             |
| Drag Force                            | 2.61E-08  | 4.01E-08                                | 6.02E-08                                | 1.47 E-09                   |
| Collision Force                       | 2.33E-06  | 9.18E-06                                | 2.02E-05                                | 1.55 E-08                   |
| Centrifugal Force                     | 7.42 E-10                                       | 5.94 E-09                               | 2.00 E-08                               | 2.55 E-13                   |
| Van der Waal Force                    | 5.39 E-07                                       | 7.84 E-07                               | 1.12 E-06                               | 3.04 E-08                   |
| Force acting at the<br>time of Impact | 4.33 E-07                                       | 8.20 E-07                               | 1.16 E-06                               | 3.19 E-08                   |
| Impact Velocity                       | 0.071   | 0.070                                   | 0.070                                   | 0.201                       |
| Limiting Velocity                     | 0.150679  | 0.150679                                | 0.150679                                | 0.150679                    |
| Impact Energy                         |   |   |   | 1.44E-17                    |
| Plastic Deformation<br>Energy         |   |   |   | 9.71E-19                    |
| Rebound Energy                        |   |   |   | 1.35 E-17                   |
| Adhesive Energy                       |   |   |   | 2.44 E-16                   |

**Table 4.4:** Various forces and energy involved in collision of guest particle with another guest particle during Fibrous Cellulose/Alumina Coating.

| Case: Collision<br>between particles  | Alumina alone | Agglomerated<br>alumina of 20 $\mu\text{m}$ |
|---------------------------------------|---------------|---|
| Drag Force                            | 1.59E-09      | 4.20E-08                                    |
| Collision Force                       | 4.06E-08      | 3.32E-05                                    |
| Centrifugal Force                     | 2.55 E-13     | 5.94 E-09                                   |
| Van der Waal Force                    | 2.55 E-08     | 7.29 E-07                                   |
| Force acting at the<br>time of impact | 2.70 E-08     | 7.65 E-07                                   |
| Impact Velocity                       | 0.1876        | 0.070                                       |
| Limiting Velocity                     | 2.96E-05      | 2.96E-05                                    |
| Impact Energy                         | 1.254E-17     | 4.1E-14                                     |
| Plastic Deformation<br>Energy         | 1.250 E-17    | 4.1E-14                                     |
| Rebound Energy                        | 3.84 E-21     | 3.35 E-17                                   |
| Adhesive Energy                       | 1.33 E-17     | 1.17 E-15                                   |

From the above tables, it is clear that the forces responsible for impaction are the collision and van der Waal forces and the other forces are negligible. For PMMA/Alumina, all types of collisions result in colliding particles sticking together. But with fibrous cellulose, when the agglomerate collides with the cellulose the particles separate after collision.

Appendix 4 shows the graphs of difference in adhesive energy and rebound energy versus the agglomerate size and impact velocity for PMMA and fibrous cellulose. Figure A1 in Appendix 4 also proves that in the case of PMMA, all types of collision will result in adherence of the particles. Figure A2 shows that in case of fibrous cellulose, for any agglomerate above 3.6 microns colliding with cellulose particle, the difference becomes negative, i.e. the adhesive energy is less than the rebound energy and the particles will separate. Figure A3 to Figure A5 shows a plot of coating criteria versus the impact velocity range and the results are tabulated below.

**Table 4.5:** Interpretation of the plots of coating criteria versus impact velocity given in Appendix 4.

| System  | Impact velocity range which satisfies the coating criteria |
|---|--|
| PMMA-Alumina agglomerate: Size (20 $\mu\text{m}$ )          | $v > 0.002083$ and $v < 0.5678$ m/s                        |
| PMMA-Alumina agglomerate: Size (10 $\mu\text{m}$ )          | $v > 0.002083$ and $v < 1.9102$ m/s                        |
| Fib Cellulose-Alumina agglomerate: Size (1 $\mu\text{m}$ )  | $v > 0.150679$ and $v < 1.3621$ m/s                        |
| Fib Cellulose-Alumina agglomerate: Size (5 $\mu\text{m}$ )  | Coating not possible                                       |
| Fib Cellulose-Alumina agglomerate: Size (10 $\mu\text{m}$ ) | Coating not possible                                       |
| Fib Cellulose-Alumina agglomerate: Size (20 $\mu\text{m}$ ) | Coating not possible                                       |

Table 4.1-4.4 shows that all collisions between alumina particle results in the particles adhering together. Hence with fibrous cellulose, a poor coating and significant

agglomeration was observed. During PMMA coating, even if the agglomeration is taking place, when the agglomerate collides with PMMA it gets coated onto the PMMA and further redistributes between hosts. Hence, a good coating and little agglomeration was observed with PMMA.

### **4.3 Discussion of Rotating Fluidized Bed as a Granulator (RFBG)**

The phenomenon of granulation has been depicted in Figure 2.11. The phenomenon suggested has been based on the results of past studies with conventional fluidized beds [17]. A rotating fluidized bed granulator has been built which incorporates the above phenomenon as the basic principle. The schematic diagram of this granulator is shown in Figure 3.6. Unfortunately, the RFBG has not been operational during the most of this research but a brief study with this equipment has shown that granulation is possible using the RFBG. Alumina particles (size: 10 nm and 25  $\mu\text{m}$ ) were run in the RFBG at a rotating speed of 1520 rpm and fluidization velocity of 2 times the minimum fluidization velocity. The cyclic fluidization cycle was 15 sec forward run and 1 sec reverse run with a dead time of 1 sec in between. This cycle was chosen because it was the minimum time cycle possible with the equipment. The preliminary results are in the form of photographs taken using an optical microscope and shown in Figure 4.14.1 to 4.14.5. These figures clearly show that the 10 nm size alumina was granulated in the RFBG but the 25  $\mu\text{m}$  size alumina did not, although few granulates were seen here and there.

It is very difficult to draw conclusion based on the present results. However, it is conjectured that the micron size alumina granulates break after forming, under the present operating conditions. In other words the operating conditions have to be varied in order to get good granulation results. Therefore an extensive study of the rotating fluidized bed granulator is recommended for future studies.

**ALUMINA GRANULATION PHOTOGRAPHS TAKEN**  
**UNDER OPTICAL MICROSCOPE AT THE**  
**MAGNIFICATION OF 10**

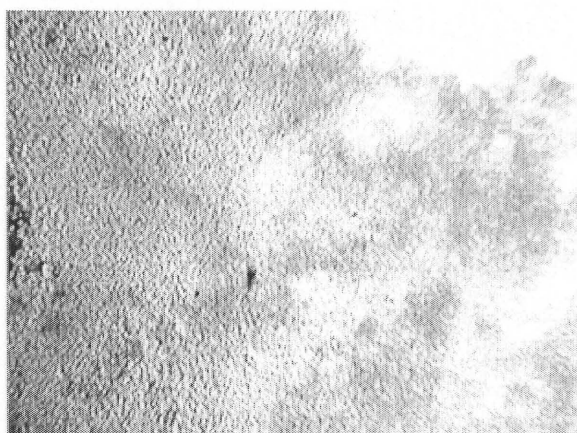


**Figure 4.14.1: Picture showing agglomerates of 10 nm size alumina before running in RFBG.**

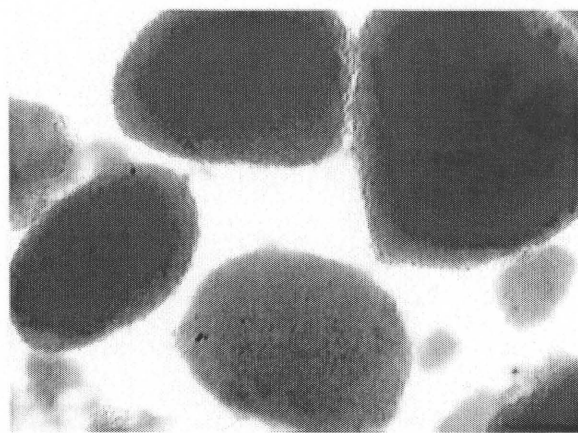


**Figure 4.14.2: Picture showing granulates of 10 nm size alumina formed after running in RFBG.**

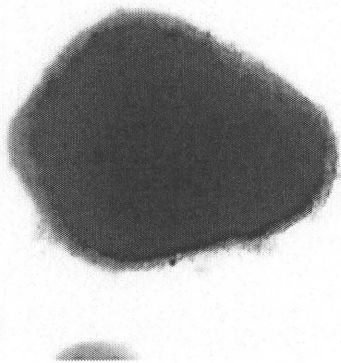


**Figure 4.14.3: Picture showing a single granulate of 10 nm size alumina formed after running in RFBG.**

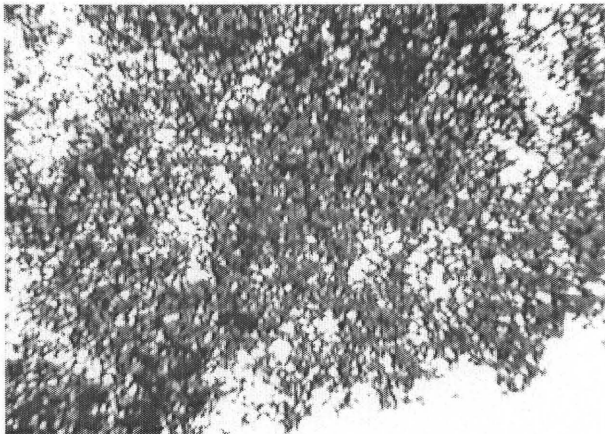


**Figure 4.14.4: Picture showing particles of 25 μm size alumina before running in RFBG.**

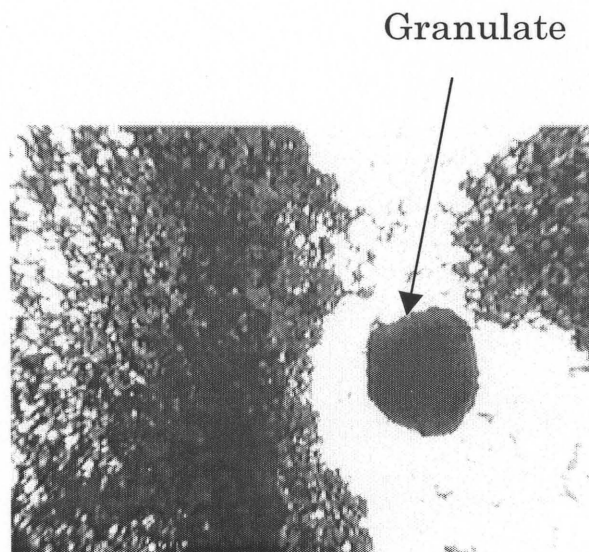


**Figure 4.14.5: Picture showing particles of 25 μm size alumina after running in RFBG, with one granulate also present.**

## **CHAPTER 5**

### **CONCLUSION AND RECOMMENDATION FOR FUTURE RESEARCH**

This thesis was mainly devoted to study of fluidization and dry coating of particles in rotating fluidized bed, both quantitatively and qualitatively. A brief qualitative study was also done on the phenomena of dry granulation using a rotating fluidized. A kinetic model was developed to explain the phenomena of coating in rotating fluidized bed. The possible phenomenon for granulation is also shown schematically.

#### **5.1 Conclusions**

The main results of this work can be summarized as follows:

- 1) It has been found experimentally that the minimum fluidization velocity and pressure drop is 20 % lower than the theoretical pressure drop obtained using equation 3.8. This loss has been accounted to loss of particles, gravity factor, non-uniform distribution of powder along the axis and also on the type of powder and its size distribution. Also sintered metal distributors were found to be better distributors than slotted distributors.



- 2) In our studies, since the guest particles or particles used in granulation are Geldart Group C particles, they are highly cohesive so it is very difficult to deagglomerate them in the RFB.
- 3) The forces involved in the rotating fluidized bed are more than in a conventional fluidized bed, so it is more suitable for coating and granulation purposes. This stems from the fact that the only force, which influences the impact force is the collision force and the collision force, is proportional to relative velocity of the particle, which in turn is proportional to minimum fluidization velocity.
- 4) A good coating result was achieved in the rotating fluidized bed with some particles and not with others. An attempt to develop a kinetic theory has been made which can help to define the type of particles, which can be coated in the rotating fluidized bed. The possible particle interaction phenomenon was also discussed in light of experimental observations. The conclusion made from this phenomenon is that the process of coating and agglomeration is taking place simultaneously. If the coating results are not good than agglomeration is significant. However in some cases, the agglomerates formed can get coated onto the host and then redistribute giving a uniform coating.
- 5) The equipment for the granulation studies, i.e., RFBG, has been built and the initial studies shows the granulation is possible with this equipment. An extensive study could not be done because the equipment was not operational until the last week of this study. Hence it has been recommended as future study.

## 5.2 Recommendation for Future Research

During the process of coating, the particle loss was significant. This loss prevented us from making a quantitative analysis of the coating since it was unknown, whether the particle loss was due to guest or host particles. This loss also prevented us from running the bed at a superficial air velocity higher than 1.5 times the minimum fluidization velocity. The powder loss can be curtailed by using a filter at the outlet of distributor, to catch the particle and redisperse them. Also some additional particle systems can be used to elaborate on the kinetic model for coating proposed in this thesis. Also the phenomenon can be studied in greater depth by varying operating parameters.

The equipment for the granulation studies has been built an extensive study of granulation in the rotating fluidized has been left for the future. An extensive study involving particle size analysis, measurement of the strength of granulates and its analysis and defining the parameters, which can give the best, granulates has to be done. Also the rotating fluidized bed built is at its first stage of design and will require lot of improvement, which also has to be studied in totality.

Thus a start has been made with this new equipment built at NJIT. But it still awaits an extensive and in depth research study for both coating and granulation purposes. And this research has to be fundamental as well as application oriented, to realize the usefulness of this equipment to its maximum extent.

## APPENDIX 1

### PROGRAM TO COMPUTE THE MINIMUM FLUIDIZATION VELOCITY

**Program to compute the minimum fluidization velocity and to plot a graph between pressure drop and superficial velocity (written in c++):**

/\* This program takes the input as rotating speed in rpm and compute the minimum fluidization velocity. It also computes the pressure drop at various superficial velocities and output is send to an excel file where a graph can be drawn to see the pattern of Pressure Drop Vs Superficial Velocity. Since input is only rotating speed, to use this program for different particles, change the value of density, particle size, weight of particles used. Compare the output thus received with experimental results to find the packed bed voidage. Based on voidage value of 0.4-0.44, the value of sphericity can accordingly used. After optimizing all the values, this program is ready for doing any calculations for that powder\*\*\*\*\*/

```
# include <iostream.h>           // for input from key board
# include <fstream.h>           // for input output operations from file streams
# include <math.h>               // for math functions like sqrt etc
# include <stdlib.h>
# include <iomanip.h>            // for output formatting

void main()

{

    ofstream ostream;
```

```

ostream.open ("fluid1.xls");           // Opening the output excel file

long double umf=0;                     // Avg. minimum fluidization velocity

long double umfs=0;                    // Surface minimum fluidization velocity

long double umfc=0;                    // Critical minimum fluidization velocity

double rpm, dg, df, dp, w, zi, phi_s, W, r0, l;

/* dg= bulk density, df = density of fluidization air, dp= particle density, w =
angular velocity, zi = voidage, phi_s = sphericity, W = Weight of particles used,
r0 = outer radius of the packed bed which is taken equal to radius of distributor,
l = length of distributor *****/

long double phi_zi;

long double phizi;

long double c1, c2, c3, phi_1, phi_2;

long double rpf,ri,u0,dP ;

/* rpf = radius of interface of packed bed and fluidized bed, ri = inner radius of
packed bed, u0 = superficial velocity, dP = pressure drop *****/

dg=850;

df=1.2;

double size = 0.000200;                // Particle size of Host

double visc = 1.81e-05;                // Viscosity of the fluid

zi=0.43;

phi_s=1;

```

```

cout<<" The rpm is ";

cin>>rpm;

dp=dg/(1-zi);

w= 2*3.14*rpm/60;

//cout<< "The wt. of the material is ";

//cin>>W;

float F = 0.8; // The F factor for pressure drop

W=0.030*F;

r0=0.029;

l=0.087;

ri= sqrt((pow(r0,2)-(W/(dg*3.14*l))));

phi_zi=1/(phi_s*pow(zi,3));

phizi=(1-zi)/(pow(phi_s,2)*pow(zi,3));

cout<<"The Inner radius          = "<<ri;

cout<<"\nThe phi_zi(phi_s*zi^3)      = "<<phi_zi;

cout<<"\nThe phizi(1/phi_s^2*zi^3)    = "<<phizi;

cout<<"\nThe Voidage is              = "<<zi<<endl;

cout<<"The sphericity is             = "<<phi_s<<endl;

c1= pow(r0,2)*(1/ri-1/r0);

c2=r0*log(r0/ri);

c3=(pow(r0,2)-pow(ri,2))/2;

phi_1=(150*(1-zi)*phi_zi*visc)/(pow(size,2));

```

```

phi_2=(1.75*(1-zi)*phizi*df)/size;

//cout<<"\nThe phi_1 is          = "<<phi_1;

//cout<<"\nThe phi_2 is          = "<<phi_2<<endl;

/* The equation for average min fluidization velocity */

umf=(sqrt(pow((phi_1*c2),2)+4*phi_2*c1*(dp-df)*pow(w,2)*c3*(1-zi))-
phi_1*c2)/(2*phi_2*c1);

/* The equation for surface min fluidization velocity */

umfs=(sqrt(pow(phi_1,2)+4*phi_2*(dp-df)*(1-zi)*ri*pow(w,2))-
phi_1)/(2*phi_2*r0/ri);

/* The equation for critical min fluidization velocity */

umfc=(sqrt(pow(phi_1,2)+4*phi_2*(dp-df)*(1-zi)*r0*pow(w,2))-
phi_1)/(2*phi_2);

cout<<"The avg Fluidization velocity    = "<<umf;

cout<<"\nThe min. Fluidization velocity    = "<<umfs;

cout<<"\nThe critical Fluidization velocity = "<<umfc<<endl;

ostream<<"    U0 "<<"    Del P"<<endl;

for (uo=0 ;uo<umfs;)

{

    /*For velocity less than surface minimum fluidization velocity, pressure
    drop is given by the equation below *****/

    dP=phi_1*uo*c2+phi_2*pow(uo,2)*c1;

    ostream<<setw(10)<<setprecision(6)<<uo<<setw(10)<<setprecision(6)<<
    dP<<endl;

```

```

uo=uo+0.01028 ;

/*0.01028=20 SCFH i.e. incremental air flow rate for experimental setup*/
}
for (;uo<umfc;)
{
    /* For velocity greater than surface minimum velocity, radius is not fixed
    and calculated using the equation below which is put into the equation of
    pressure drop below*****/

    rpf=sqrt((phi_1*uo*r0 + (phi_2*pow(uo,2)*pow(r0,2)/((ri+r0)/2)))/((dp-
    df)*(1-zi)*pow(w,2)));

    dP=(1-zi)*(dp-df)*pow(w,2)*(pow(rpf,2)-pow(ri,2))/2+
    phi_1*uo*r0*logl(r0/rpf) + phi_2*pow(uo,2)*pow(r0,2)*(1/rpf-1/r0);

    ostream<<setw(10)<<setprecision(6)<<uo<<setw(10)<<setprecision(6)<<
    dP<<endl;

    uo=uo+0.01028 ;
}

/*For velocity greater than critical fluidization velocity, the pressure drop
equation is given below, which shows it is dependent only on weight of powder
used*****/

```

```

for(;uo<=0.4626;)
{
    dP=(1-zi)*(dp-df)*pow(w,2)*(pow(r0,2)-pow(ri,2))/2 ;

ostream<<setw(10)<<setprecision(6)<<uo<<setw(10)<<setprecision(6)<<dP<<endl;

    uo=uo+0.01028 ;

}

ostream.close();
}

```



## APPENDIX 2

### PHYSICAL PROPERTIES OF POWDERS

**Table A1:** Physical properties for PMMA [12], Fibrous Cellulose [23], Spherical Cellulose [23], Alumina [12] and Air.

| Material Properties                  | PMMA  | Fibrous Cellulose | Spherical Cellulose | Alumina | Air   |
|--------------------------------------|-------|-------------------|---------------------|---------|-------|
| Particle Density(Kg/m <sup>3</sup> ) | 1190  | 700               | 1400                | 3970    | 1.2   |
| Particle size(μm)                    | 200   | 180               | 230                 | 0.7     |       |
| Viscosity(Kg/m. sec)                 |       |                   |                     |         | 1.204 |
| Hamaker constant                     | 8.442 | 5.0               |                     | 14.0    |       |
| Young's Modulus (GPa)                | 3.3   | 1.5               |                     | 345     |       |
| Poisson ratio                        | 0.5   | 0.35              |                     | 0.26    |       |
| Yield Strength (MPa)                 | 15    | 40                |                     | 70      |       |
| Voidage during fluidized stage       | 0.5   | 0.5               | 0.5                 | 0.5     |       |

## APPENDIX 3

### SAMPLE CALCULATION

#### Example (PMMA: 200 $\mu\text{m}$ , Alumina agglomerate: 20 $\mu\text{m}$ )

Particle 1 = PMMA (host)

Particle 2 = Alumina (guest)

Air density  $\rho_f = 1.2 \text{ kg/m}^3$

Air viscosity  $\mu = 1.784 \times 10^{-5} \text{ Poise}$

Diameter of host  $d_1 = 2 \times 10^{-4} \text{ m}$

Diameter of guest  $d_2 = 2 \times 10^{-5} \text{ m}$

Particle density (host)  $\rho_{p1} = 1190 \text{ Kg/m}^3$

Particle density (guest)  $\rho_{p2} = 3970 \text{ Kg/m}^3$

Young's modulus (host)  $E_1 = 3300 \text{ MPa}$

Young's modulus (guest)  $E_2 = 345 \text{ GPa}$

Poisson ratio (host)  $\nu_1 = 0.5$

Poisson ratio (guest)  $\nu_2 = 0.26$

Distributor radius  $r = 0.029 \text{ m}$

Length of distributor = 0.089 m

Voidage in fluidized state  $\varepsilon = 0.5$

Rotation speed rpm = 1500

Hamaker constants:  $A_1 = 8.442 \times 10^{-20} \text{ J}$

$A_2 = 14 \times 10^{-20} \text{ J}$

Min fluidization velocity  $u_{mf} = 0.45 \text{ m/s}$

Superficial velocity  $u = 1.5 \times u_{mf} = 0.675 \text{ m/s}$

Hamaker interaction constant  $A_{12} = \sqrt{A_1 A_2} = 10.9 \times 10^{-20} \text{ J}$

The equation for k is given as  $k = \frac{1 - \nu^2}{\pi E}$

$$k_1 = \frac{1 - 0.5^2}{\pi \times 3.3 \times 10^9} = 7.23 \times 10^{-11}$$

$$k_2 = \frac{1 - 0.26^2}{\pi \times 3.45 \times 10^{11}} = 8.61 \times 10^{-13}$$

$$\text{And K is given as } K = \frac{4}{[3\pi(k_1 + k_2)]} = \frac{4}{[3\pi(7.23 \times 10^{-11} + 8.61 \times 10^{-13})]} = 5.8 \times 10^9$$

The mass of the particle is given by  $m = \frac{\pi}{6} d^3 \rho_p$

$$m_1 = \frac{\pi}{6} (2 \times 10^{-4})^3 \times 1190 = 4.98 \times 10^{-9} \text{ kg} \quad m_2 = \frac{\pi}{6} (2 \times 10^{-5})^3 \times 3970 = 1.66 \times 10^{-11} \text{ kg}$$

The Angular Velocity  $\omega = \frac{2\pi n_r}{60} = \frac{2\pi * 1500}{60} = 157 \text{ rad/sec.}$

The distance between two particle [8]  $s = 4 A^0 = 4 * 10^{-10} \text{ m}$

The van der Waal force is given by  $F_v = \frac{A_{12}}{12s^2} \frac{d_1 d_2}{d_1 + d_2}$

$$= \frac{10.9 * 10^{-20}}{12(4 * 10^{-10})^2} \frac{2 * 10^{-4} * 2 * 10^{-5}}{(2 + 0.2) * 10^{-4}} = 1.03 * 10^{-6} \text{ N}$$

The Reynolds Number  $Re = \frac{\rho_f u d_2}{\mu} = \frac{1.2 * 0.675 * 2 * 10^{-5}}{1.78 * 10^{-5}} = 0.9$

And Galileo Number Ga is given as  $Ga = \frac{(\rho_p - \rho_f) \rho_f d_2^3 r \omega^2}{\mu^2}$

$$= \frac{(3970 - 1.2) * 1.2 (2 * 10^{-5})^3 * 0.029 * 157^2}{(1.78 * 10^{-5})^2}$$

$$= 86$$

n for drag force is given as  $n = \frac{2.4(2 + 0.043 * Ga^{0.57})}{1 + 0.043 * Ga^{0.57}} = 3.95$

The drag force is given by  $F_y = \left[ 2.25 + 0.36(Re \epsilon^{-n})^{0.37} \right]^{3.45} \frac{\pi}{8} \rho u^2 d_1^2 \epsilon^{-2n}$

$$= \left[ 2.25 + 0.36(0.91 * 0.5^{-3.95})^{0.37} \right]^{3.45} \frac{\pi}{8} * 1.2 * 0.675^2 (2 * 10^{-5})^2 0.5^{-0.79} = 6.31 * 10^{-8} \text{ N}$$

The force due to centrifugal force acting towards the distributor wall is given by

$$F_g = \frac{\pi}{6} (\rho_p - \rho_f) d_2^3 r \omega^2 \epsilon = \frac{3.14}{6} (3970 - 1.2) (2 * 10^{-5})^3 * 0.029 * 157^2 * 0.5$$

$$= 5.94 * 10^{-9} \text{ N}$$

The approach velocity is given as  $V = (1.5P_{s,n}D_b r \omega^2 \varepsilon)^{1/2}$

$$\text{where } D_b = \frac{3.77}{r\omega^2} [(u - u_{mf})]^2 = \frac{3.77}{0.029 * 157^2} [(0.5 * 0.45)]^2 = 0.000267 \text{ m}$$

$$\text{So } V = (1.5 * 0.077 * 0.000267 * 0.029 * 157^2 * 0.5)^{1/2} = 0.105 \text{ m/s}$$

The collision force is given as  $F_c = n\alpha^{3/2}$

$$\text{Where } \alpha \text{ is given as } \alpha = \left( \frac{5V^2}{4nn_1} \right)^{2/5}$$

Here

$$n = \sqrt{\frac{8}{9\pi^2(k_1 + k_2)^2} \frac{d_1 d_2}{d_1 + d_2}} = \sqrt{\frac{8}{9\pi^2((723.79 + 8.61) * 10^{-13})^2} \frac{2 * 10^{-4} * 2 * 10^{-5}}{(2 + 0.2) * 10^{-4}}}$$

$$= 1.74 * 10^7$$

and

$$n_1 = \frac{m_1 + m_2}{m_1 m_2} = \frac{(498 + 1.66) * 10^{-11}}{4.98 * 10^{-9} * 1.66 * 10^{-11}} = 6.04 * 10^{10}$$

$$\text{Thus } \alpha = \left( \frac{5 * 0.105^2}{4 * 1.74 * 10^7 * 6.04 * 10^{10}} \right)^{2/5} = 1.11 * 10^{-8} \text{ m}$$

$$\text{Hence } F_c = 1.74 * 10^7 (1.11 * 10^{-8})^{3/2} = 2.05 * 10^{-5} \text{ N}$$

Since the collision force is of the order of magnitude 3 to 4 of that of drag and centrifugal-buoyant force, hence these forces have negligible effect on the velocity of the particle. Hence for all practical purposes, the initial velocity at the annulus distance i.e.  $A^0$  is equal to approach velocity  $V$ .

The resultant force acting on the particle at the time of impact is

$$F_I = F_y + F_v - F_g = 1.09 * 10^{-6} \text{ N}$$

To calculate the final impact velocity  $v$ , following equation is used.

$$\text{The impact velocity } v = \sqrt{\frac{2 * F_I * d}{m_2} + V^2}$$

$$\text{where } d = 4 \text{ \AA} = 4 * 10^{-10} \text{ m}$$

$$\text{Hence } v = \sqrt{\frac{2 * 1.09 * 10^{-6} * 4 * 10^{-10}}{1.66 * 10^{-11}} + 0.105^2} = 0.1052 \text{ m/s}$$

$$\text{The limiting elastic velocity is given by } \phi = \left( \frac{2\pi}{3K} \right)^2 \left( \frac{2}{5\rho} \right)^{\frac{1}{2}} y^{\frac{5}{2}}$$

where  $y$  is the yield limit and for value for PMMA (Appendix 2) is =15 MPa

$$\text{Hence } \phi = \left( \frac{2\pi}{3 * 5.8 * 10^9} \right)^2 \left( \frac{2}{5 * 3970} \right)^{\frac{1}{2}} (15 * 10^6)^{\frac{5}{2}} = 0.002083 \text{ m/s}$$

$$\text{Impact Energy is given as } Q_I = \frac{1}{2} m_2 v^2 = \frac{1}{2} * 1.66 * 10^{-11} * (0.1052)^2 = 9.20 * 10^{-14} \text{ J}$$

$$\text{The Plastic deformation energy is given by } Q_p = \left( \frac{\left( 2mv^2 - \frac{1}{8} m\phi^2 \right)^{\frac{1}{2}} - \left( \frac{15}{8} m\phi^2 \right)^{\frac{1}{2}}}{2} \right)^2$$

$$= \left( \frac{1.66 * 10^{-11} \left[ \left( 2 * 0.105^2 - \frac{1}{8} * 0.002083^2 \right)^{\frac{1}{2}} - \left( \frac{15}{8} * 0.002083^2 \right)^{\frac{1}{2}} \right]}{2} \right)^2 = 8.85 * 10^{-14} \text{ J}$$

$$\text{The rebound energy is given as } Q_R = Q_I - Q_p = 9.20 * 10^{-14} - 8.85 * 10^{-14} = 3.5 * 10^{-15} \text{ J}$$

The total surface adhesive energy is given by  $Q_A = U_M + U_S$

$$U_M = P_0 \frac{\left( P_1^{2/3} + 2P_0 P_1^{-1/3} \right)}{3K^{2/3} R_c^{1/3}} \quad U_S = \Delta\gamma\pi \left( \frac{R_c P_1}{K} \right)^{2/3}$$

The external load applied on a particle is centrifugal force due to mass of particle [18]

and is given as  $P_0 = m r \omega^2 = 1.66 * 10^{-11} * 0.029 * 157^2 = 1.19 * 10^{-8} \text{ N}$

The force  $P_1 = P_0 + 3\Delta\gamma\pi R_c + \left[ (P_0 + 3\Delta\gamma\pi R_c)^2 - P_0^2 \right]^{1/2}$

Here  $\frac{1}{R_c} = \frac{1}{R_1} + \frac{1}{R_2}$  and  $R_c = 9.09 * 10^{-9} \text{ m}$

$\Delta\gamma = A/2.1 * 10^{-18}$  where A is in J and  $\Delta\gamma$  in  $\text{J/m}^2$ .

$\Delta\gamma = 10.9 * 10^{-20} / 2.1 * 10^{-18} = 0.0402 \text{ J/m}^2$ .

$P_1 = 3.71 * 10^{-5} \text{ N}$ .

$U_M = 6.53 * 10^{-17} \text{ J}$

$U_S = 1.89 * 10^{-14} \text{ J}$

$Q_A = 1.9 * 10^{-14} \text{ J}$

Now, the value of  $Q_R$  is  $3.5 * 10^{-15} \text{ J}$  and the value of  $Q_A$  is  $1.9 * 10^{-14} \text{ J}$  i.e.  $Q_R < Q_A$ .

Since the rebound energy is not enough, hence particles will not separate and will stick together.

## APPENDIX 4

### COATING CRITERIA

#### Plots of Coating Criteria:

Criterion for coating- Difference of Adhesion Energy and Rebound Energy Vs Agglomerate Size for PMMA particles

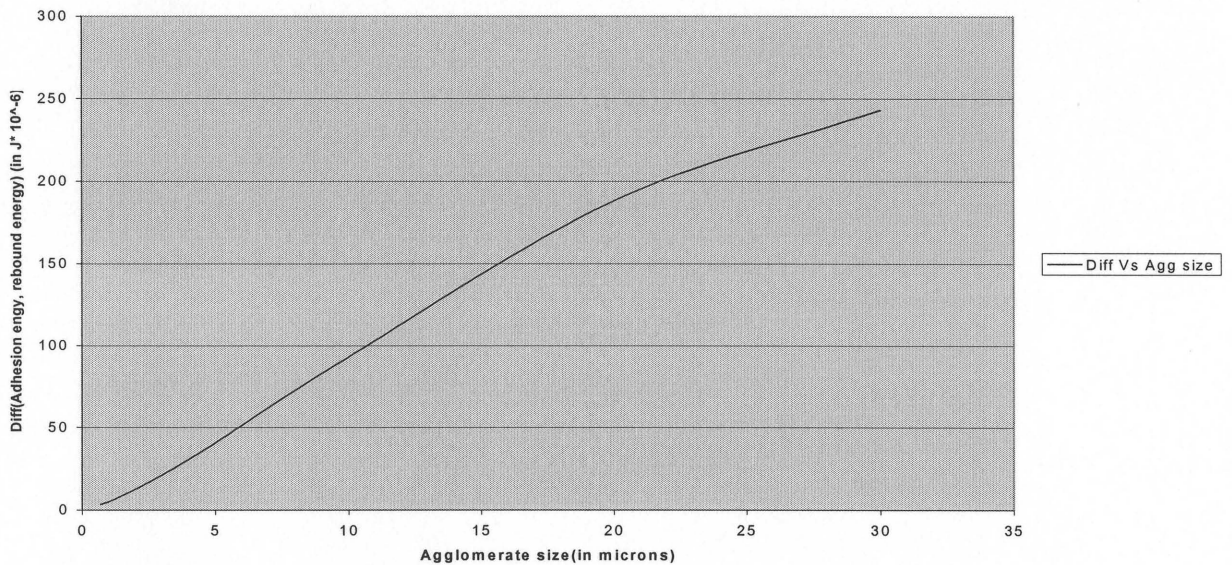


**Figure A1:** Plot of difference in Adhesion Energy and Rebound Energy Vs Agglomerate Size for PMMA particles

Criterion for Coating - Difference of Adhesion and Rebound Energy versus the Agglomerate Size for Fibrous Cellulose

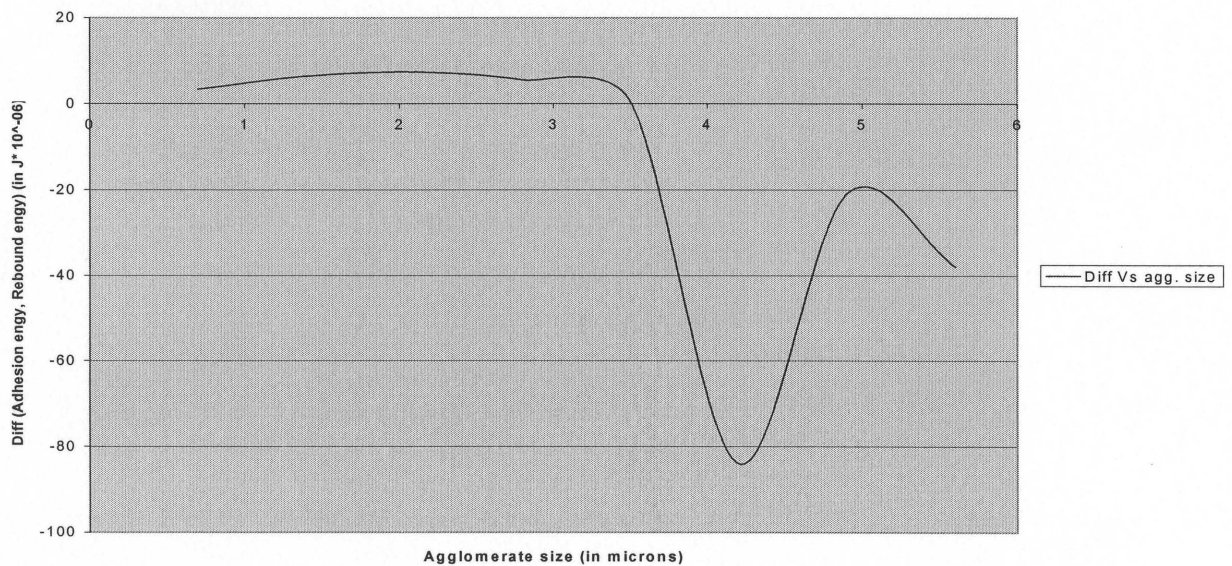


**Figure A2:** Plot of difference in Adhesion and Rebound Energy versus the Agglomerate Size

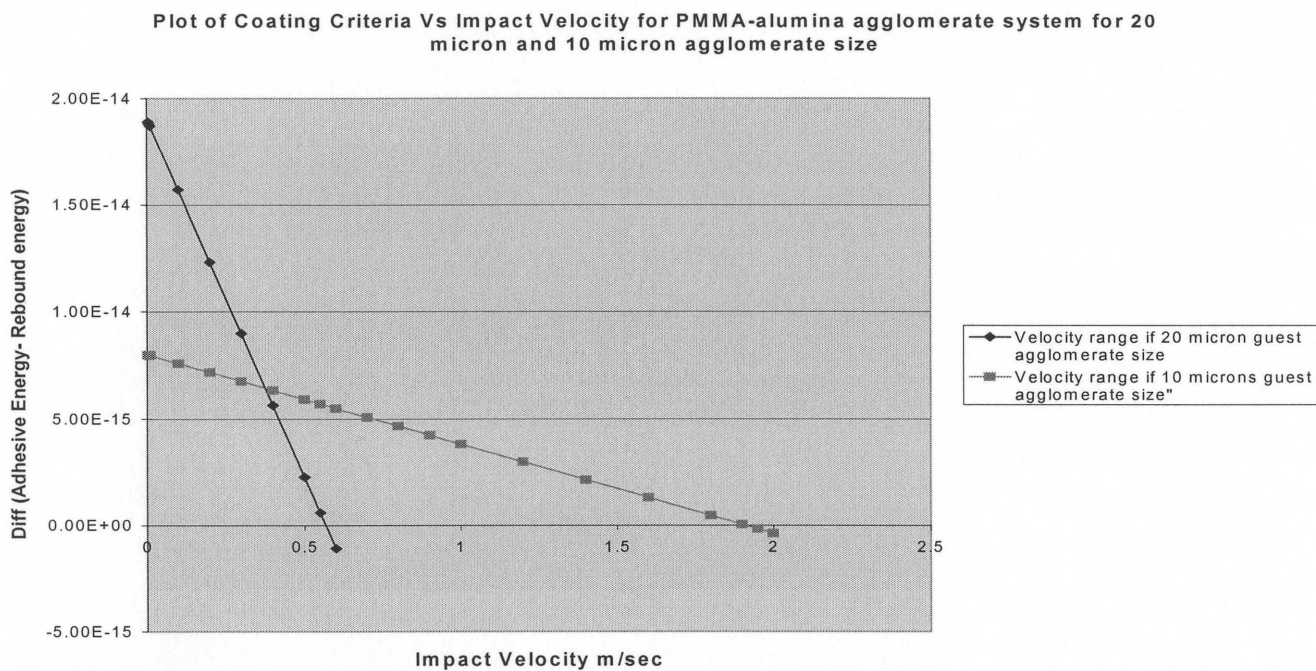


**Figure A3:** Plot of difference in Adhesion and Rebound Energy versus the Impact Velocity for PMMA-Alumina agglomerate of agglomerate sizes 10  $\mu\text{m}$  and 20  $\mu\text{m}$ .

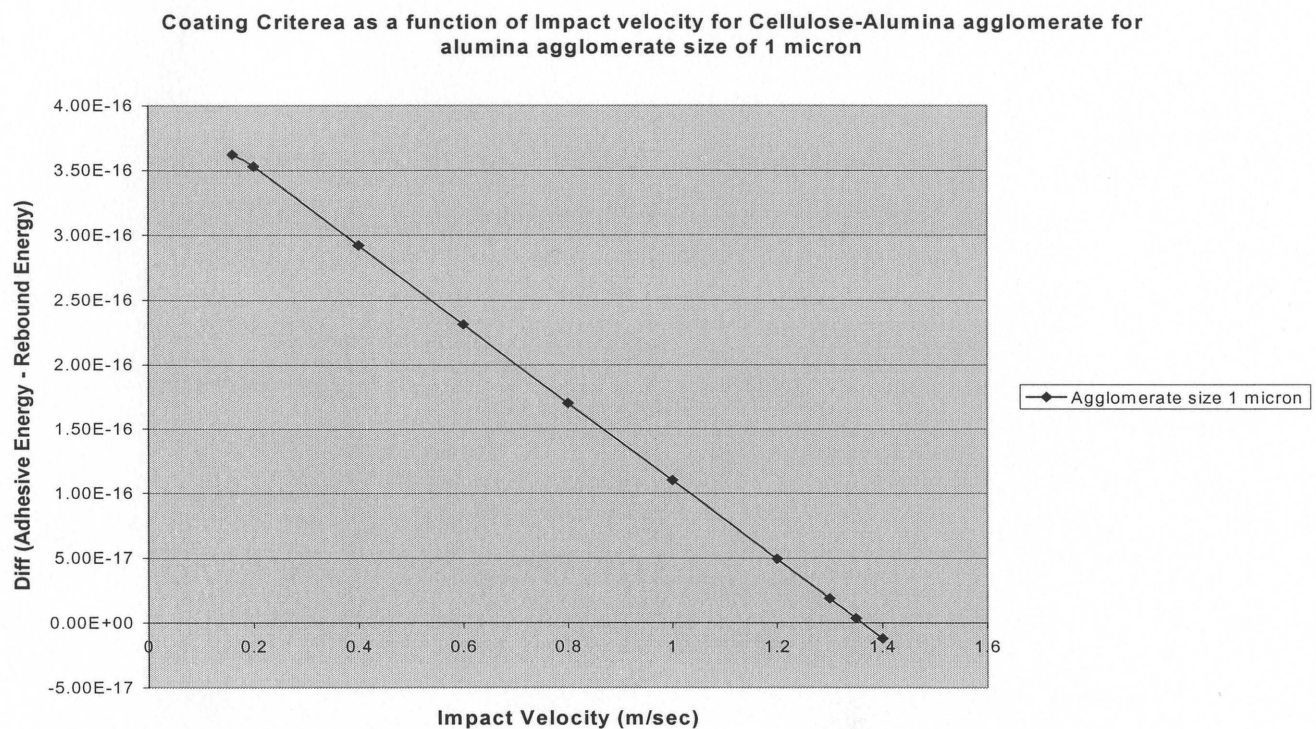


**Figure A4:** Plot of difference in Adhesion and Rebound Energy versus the Impact Velocity for Fibrous Cellulose-Alumina agglomerate of agglomerate size 1  $\mu\text{m}$ .



Coating Criteria as a function of impact velocity for Cellulose-Alumina agglomerate for alumina agglomerate size 5, 10 and 20 microns

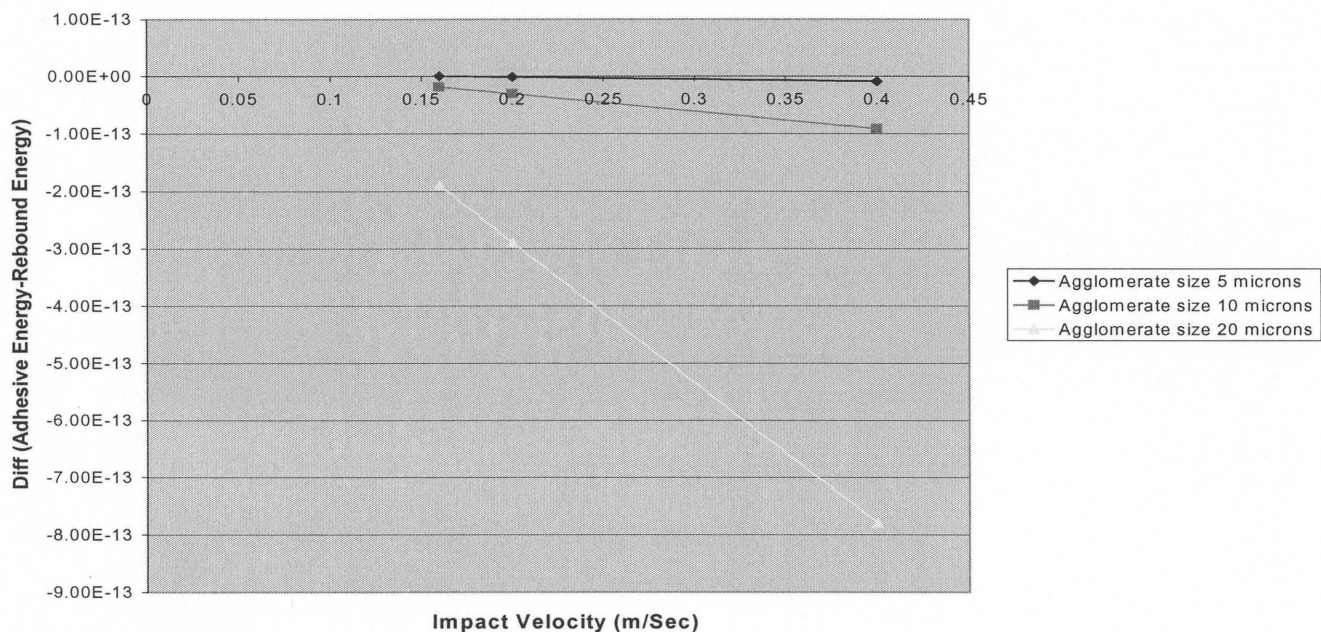


**Figure A5:** Plot of difference in Adhesion and Rebound Energy versus the Impact Velocity for Fibrous Cellulose-Alumina agglomerate of agglomerate sizes 5  $\mu\text{m}$ , 10  $\mu\text{m}$  and 20  $\mu\text{m}$

Coating Criteria as a function of Yield limit, Hamakar constant and Young's Modulus

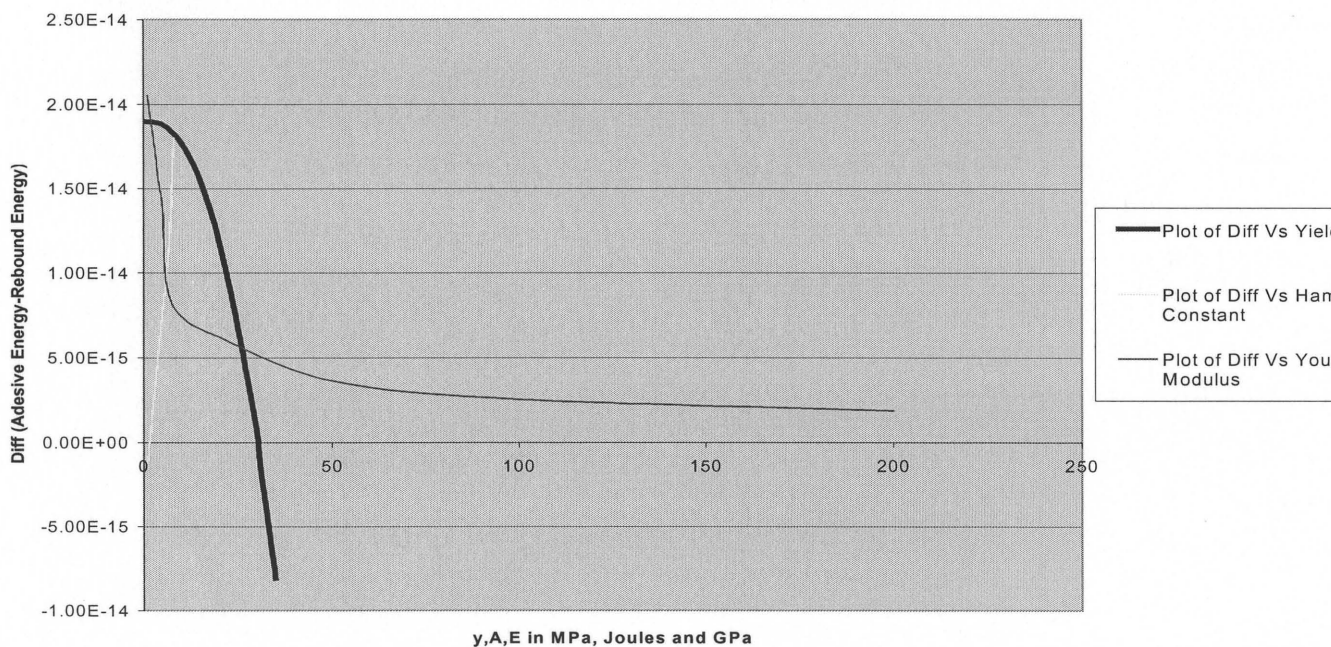


**Figure A6:** Plot of difference in Adhesive and Rebound Energy as a function of Yield limit, Hamakar constant and Young's Modulus

## REFERENCES

1. **Chen Y.M.**, *Fundamentals of Centrifugal Fluidized bed*. AIChE Journal, 1986.
2. **Kao J., Pfeffer R. and Tardos G.I.**, *On Partial Fluidization of Rotating Fluidized Beds*. AIChE Journal, May 1987.
3. **Qian G.H., Bagyi I., Pfeffer R., Shaw H. and Stevens G.H.**, *A Parametric Study of a Horizontal Rotating Fluidized Bed Using Slotted and Sintered Metal Cylindrical Gas Distributors*. Powder Technology 100(1998) 190-199.
4. **Qian G.H., Bagyi I., Pfeffer R., Shaw H. and Stevens G.H.**, *Particle Mixing in Rotating Fluidized Bed: Inferences about Fluidized State*. AIChE Journal, Vol. 45, No. 7, July 1999.
5. **Wen C.Y. and Yu Y.H.**, *A Generalized Method for Predicting Minimum Fluidization Velocity*. AIChE Symposium, 1966.
6. **Fan L.H. and Zhu C.**, *Principles of Gas Solid Flows*, Cambridge University Press, 1998.
7. **Geldart D.**, *Gas Fluidization Technology*, John Wiley and Sons Ltd, 1986.
8. **Israelachvili J.**, *Interfaces and Surface forces, Second Edition*, Academic Press, 1997.
9. **Visser J.**, *Invited Review, van der Waals and Other Cohesive Forces Affecting Powder Fluidization*. Powder Technology, 58, 1-10, 1989.
10. **Zhou T. and Li H.**, *Estimation of Agglomerate Size for Cohesive Particles during Fluidization*. Powder Technology 101, 57-62, 1999.
11. **Iyer. R.**, *Master's Thesis*, New Jersey Institute of Technology, May 1999.
12. **Bodhisatwa Choudhry**, *PhD Dissertation*, New Jersey Institute of Technology, January 2000.
13. **Honda H., Kimaru M., Honda F., Matsuno T. and Koishu M.**, *Preparation of Monolayer Coated Powder by Dry Impact Blending Process Utilizing Mechanochemical Treatment*. Colloid and Surfaces, 82 (1994), 117-128.
14. **Khan A.R. and Richardson J.F.**, *Pressure Gradient and Friction Factor for Sedimentation and Fluidization of Uniform Spheres in Liquids*. Chemical Engineering Science, 45(1), 255, 1990.

## REFERENCES (Continued)

15. **Timoshenko S.P. and Goodier J.N.**, *Theory of Elasticity, Third Edition*, Mc-Graw Hill Book Company, 1970.
16. **Watano S., Pfeffer R., Dave R.N. and Dunphy W.**, *Dry Particle Coating by a Newly Developed Rotating Fluidized Bed Coater*. AIChE Annual Meeting, Miami Beach, FL, Nov 15-20, 1998.
17. **Nishii K., Itoh Y. and Noburu K.**, *Pressure Swing Granulation, a Novel Binderless Granulation by Cyclic Fluidization and Gas Flow Compaction*. Powder Technology, 74, 1-6, 1993.
18. **Rogers L.N. and Reed J.**, *The Adhesion of Particles Undergoing an Elastic-Plastic Impact with a Surface*. Journal of Physics D: Appl. Physics, Printed in Great Britain, 17, 677-689, 1984.
19. **Khan F. and Pilpil N.**, *An Investigation of Moisture Sorption in Microcrystalline Cellulose using Sorption Isotherms and Dielectric Response*. Powder Technology, 50, 237-241, 1987.
20. **Abe E., Yamada N., Hirose H. and Nakamura H.**, *Coating Mass Distribution of Seed Particles in a Tumbling Fluidized Bed Coater*. Powder Technology 97(1998), 85-90.
21. **Hamaker H.C.**, *The London-van der Waals Attraction between Spherical Particles*. Physica 1V, 10, 1058, 1937.
22. **Iwadate Y and Horio M.**, *The Prediction of Sizes Formed in Fluidized Beds*. Proceedings of the 5<sup>th</sup> World Congress of Chemical Engineering, 2<sup>nd</sup> International Particle Technology Forum, Vol. V, 1996, 571.
23. **www.avicel.com**, *The website for the cellulose products from FMC corporation*.